

Simulation of Wave Climate for the Arabian Sea and Bay of Bengal

*Thesis submitted in partial fulfilment of
the requirements for the degree of*

DOCTOR OF PHILOSOPHY
in
PHYSICAL OCEANOGRAPHY




J. SWAIN
Naval Physical and Oceanographic Laboratory
Cochin-682021

Cochin University of Science and Technology
Cochin-682021

August 1997

Certificate

This is to certify that this thesis entitled "Simulation of Wave Climate for the Arabian Sea and Bay of Bengal" is an authentic record of research work carried out by Mr. Jaganath Swain (M.Sc., M.Phil.), Scientist-D of Naval Physical and Oceanographic Laboratory, Cochin-21 under my supervision and guidance for the Ph.D. degree of Cochin University of Science and Technology, Cochin-22 and no part of this has previously formed the basis for the award of any other degree in any other university.



Place: Trivandrum,
Date: August 1997.

Dr. M. Baba
Head, Marine Science Division
Centre for Earth Science Studies
Akkulam, Thuruvikal P.O.
Trivandrum, Kerala.

PREFACE

One of the well known ocean environmental disturbances is the wind-induced surface gravity waves which are important in the air-sea interaction process of the coupled ocean-atmosphere system. The wave information or the sea state is essential for efficient management and use of our coastal and offshore environment. In the absence of routine operational wave forecasts and long-term wave measurements for the Arabian Sea and Bay of Bengal, visually observed wave data are being used for several applications. Visual observations are routinely made from weather ships, land-based stations and ocean going vessels. They are available over longer periods and cover the shipping routes. However, visual observations are only the first estimates and can't be considered as reliable. The next alternative is the establishment of a climatic database through model hindcasting. For the Indian Seas (Arabian Sea and Bay of Bengal) there is a limitation for conducting a long-term wave hindcast due to the scarcity of barotropic data used for the preparation of synoptic weather charts. Therefore, an attempt is made to conduct a simulation experiment for the establishment of deep water wave climate for the Indian Seas using available historical data as input to the wave model. The results of this simulation experiment are presented in this thesis.

The thesis consists of seven chapters. The introductory chapter presents some general terminologies and definitions in "Kymatology" (the science of ocean waves) related with the present study and a brief discussion on various sources of data for wave climate establishment. It describes the requirement and availability of visually observed wave data, measured wave data, hindcast wave data, and operational wave forecast data for establishment of a long-term regional wave climate. It also gives a qualitative assessment of these data from the climatic point of view. The significance of wave climate simulation and the scope of the present work are discussed.

Wave prediction techniques which are presently in use are discussed in the second chapter. Brief outline of the numerical wave prediction models including the model used in this study for wave climate simulation are given. It is found that the third generation wave model (WAM) which was developed and demonstrated by the WAMDI group is quite suitable for this study. It represents the physics of the wave evolution in accordance with our present day knowledge, for the full degrees of freedom for the two dimensional wave spectrum. The fundamental equations, numerical scheme, model grid structure, and the input and output options of the model are described in brief. It also describes the model performance and the intercomparisons with various other models.

The source of input wind and surface current data used in this study for simulation of regional wave climate is discussed in the third chapter. It provides information on the quality of input data and the methods of estimation of mean monthly fields. It also includes a brief discussion on the summer and winter monsoon wind variability and the monsoonal surface circulation. The most important part of this chapter is the specification of input data to the model.

The fourth chapter discusses the wave model implementation for the regional grid system. The input and output specifications to the model are explained. Model execution using "the mean climatic year of winds" and the compilations of various model outputs are also presented. Wave model is executed for the regional grid system (50-100 deg. east, 0-25 deg. north, 1x1 deg. resolution) assuming appropriate boundary conditions. Representative model runs are carried out for all the months from January to December. The model outputs are stored for all grid points at each time step while the spectral outputs are stored for selected grids. The monthly, seasonal and annual distributions of significant wave height, period and mean direction for total sea and swell are estimated after post processing of model outputs.

Validation of simulated wave climate is presented in the fifth chapter. The simulation experiment has been carried out in spite of limited measurements available for the Indian Seas. Hence, a complete validation of the simulation results is not possible with the available measurements. However, a qualitative validation of the height and period parameters are carried out using available ship-borne wave recorder data and ship-reported visually observed data. The wave height data are compared with the Geosat altimeter data for two selected locations.

The results and discussion on the regional wave climate based on the simulation experiment are presented in the sixth chapter. The spatial distributions of significant wave parameters are discussed (monthly, seasonal and annual) in detail. The bivariate and cumulative distributions of significant wave height and period have been analysed for the Arabian Sea and Bay of Bengal during rough weather (May-September) and fair weather (October-April) seasons. Secondly, a comparative study of the wave climate between (1) the Arabian Sea and Bay of Bengal and (2) East and west coast of India are presented in this chapter. The spectral characteristics for a selected site are also discussed. Finally, the limitations of the simulated wave climate are explained. The last chapter summarises the important results of the simulation experiment. The study suggests that the model could successfully simulate the wave climate for the Indian Seas based on the mean climatic year of winds and the simulated database can be utilized for several applications.

CONTENTS

	Page
LIST OF FIGURES	vi
LIST OF TABLES	ix
CHAPTER I. INTRODUCTION	1-11
I.1 General terminologies	1
I.2 Definition of wave climate	3
I.3 Data source for wave climate	4
I.3.1 Quality and duration of wave data	4
I.3.2 Visually observed wave data	5
I.3.3 Measured wave data	6
I.3.4 Hindcast wave data	7
I.3.5 Operational wave forecast data	8
I.4 Significance of wave climate simulation	8
I.4.1 Concept of "mean climatic year of winds"	9
I.4.2 The simulation process	9
I.5 Scope of the present work	10
CHAPTER II. SELECTION OF WAVE MODEL	12-29
II.1 Introduction	12
II.2 Early wave prediction techniques	12
II.3 Numerical wave prediction models	13
II.4 Wave model intercomparison study	14
II.5 The present model	16
II.5.1 Background of the model	17
II.5.2 Fundamental equations	18
II.5.3 Numerical scheme	21
II.5.4 Model grid structure	24
II.5.5 Model system	25
II.5.6 Model options and user inputs	25

II.5.7	<i>Model outputs</i>	27
II.6	Performance of the model	28
CHAPTER III.	INPUT DATA FOR SIMULATION OF WAVE CLIMATE	30-41
III.1	Introduction	30
III.2	Source of wind and surface current data	30
III.3	Assessment of data quality	31
III.4	Estimation of mean monthly wind fields	33
III.5	Discussion on the Indian monsoon and surface circulation	35
III.5.1	<i>Summer and winter monsoon winds</i>	35
III.5.2	<i>Monsoonal surface circulation</i>	36
III.6	Input data specification for the present study	37
CHAPTER IV.	SIMULATION OF WAVE CLIMATE	42-46
IV.1	Introduction	42
IV.2	Wave model implementation	42
IV.2.1	<i>Regional grid system</i>	43
IV.2.2	<i>Input and output specifications</i>	43
IV.3	Wave model execution	44
IV.4	Compilation of model outputs	46
CHAPTER V.	VALIDATION OF SIMULATED WAVE CLIMATE	47-51
V.1	Introduction	47
V.2	Validation using visually observed wave data	47
V.3	Validation using measured wave data	50
CHAPTER VI.	SIMULATED WAVE CLIMATE FOR THE INDIAN SEAS	52-67
VI.1	Introduction	52
VI.2	Spatial distribution of wave parameters	52
VI.2.1	<i>Monthly distribution</i>	52
VI.2.2	<i>Seasonal distribution</i>	60
VI.2.3	<i>Annual distribution</i>	61

VI.3	Statistical distribution of wave height and period	62
VI.3.1	<i>Bivariate distribution</i>	62
VI.3.2	<i>Cumulative distribution</i>	62
VI.4	Spectral characteristics	63
VI.5	A comparative study of wave climate	63
VI.5.1	<i>Arabian Sea and Bay of Bengal</i>	64
VI.5.2	<i>East and West coast of India</i>	64
VI.6	Limitations of simulated wave climate	65
VI.7	Future outlook	66
CHAPTER VII.	SUMMARY AND CONCLUSIONS	68-71
APENDIX-A	3g-WAM FLOW CHARTS	72-77
APENDIX-B	3g-WAM PROGRAMS, SUBROUTINES AND FUNCTIONS	78-82
APENDIX-C	INCLUDE FILES (PARAMETERS FOR ARRAY DIMENSITIONS)	83-85
APENDIX-D	USER INPUT FILES	86-98
REFERENCES	99-106
AUTHOR'S PUBLICATIONS ON OCEAN WAVES	107-109

LIST OF FIGURES

		Next to Page
Fig.1	Location map for Indian Seas.	11
Fig.2A	Wind data distribution for Indian Seas (IMD, 1961-70). ...	30
Fig.2B	Wind data distribution for Indian Seas (H&L, 1911-70). ...	31
Fig.2C	Surface current data distribution for Indian Seas (1954-94).	31
Fig.3A	Mean surface wind fields for Indian Seas (January to April).	35
Fig.3B	Same as Fig.3A for May to August.	35
Fig.3C	Same as Fig.3A for September to December.	35
Fig.4A	Observed joint probability distribution for u and v components of winds (January to March).	35
Fig.4B	Same as Fig.4A for April to June.	35
Fig.4C	Same as Fig.4A for July to September.	35
Fig.4D	Same as Fig.4A for October to December.	35
Fig.5A	Mean surface current fields for Indian Seas (January to .. April).	36
Fig.5B	Same as Fig.5A for May to August.	36
Fig.5C	Same as Fig.5A for September to December.	36
Fig.6	Observed joint probability density for u and v components of wind during July.	39
Fig.7	Schematic representation for wind estimation from observed joint probability distribution of u and v components.	39
Fig.8A	The mean climatic year of winds (67.5°E , 12.5°).	40
Fig.8B	Same as Fig.8A (87.5°E , 12.5°).	40
Fig.9	Model grid system for Indian Seas.	43
Fig.10	Evolution of wave spectrum for 72 hours of model run using estimated mean climatic wind fields for the month of July.	46

Fig.11A	Visually observed windsea data distribution for Indian Seas (1961-70).	... 47
Fig.11B	Visually observed swell data distribution for Indian Seas (1961-70).	47
Fig.12	Visually observed significant wave height versus swell wave height in the Indian Seas.	48
Fig.13A	Comparison between simulated and visually observed Hs for Arabian Sea and Bay of Bengal during rough weather and fair weather seasons respectively.	49
Fig.13B	Same as Fig.13A for Ts.	49
Fig.14A	Same as Fig.13A for Hsw.	49
Fig.14B	Same as Fig.13A for Tsw.	49
Fig.15A	Measured wave data distribution for Indian Seas using ship-borne wave recorder (1976-93, rough weather season).	50
Fig.15B	Same as Fig.15A for fair weather season.	50
Fig.16A	Comparison between simulated and measured (SBWR) Hs for the Arabian Sea and Bay of Bengal during rough and fair weather seasons respectively.	50
Fig.16B	Same as Fig.16A for Ts.	50
Fig.17	Comparisons of results obtained from wave climate simulation and GEOSAT satellite mission for two selected sites.	51
Fig.18A	[a] The significant wave height, [b] Significant wave period and windsea direction (January).	53
Fig.18B	[a] The swell wave height, [b] swell wave period and direction (January).	53
Fig.19A	Same as Fig.18A for February.	53
Fig.19B	Same as Fig.18B for February.	53
Fig.20A	Same as Fig.18A for March.	53
Fig.20B	Same as Fig.18B for March.	53
Fig.21A	Same as Fig.18A for April.	53
Fig.21B	Same as Fig.18B for April.	53
Fig.22A	Same as Fig.18A for May.	53

Fig. 22B	Same as Fig. 18B for May.	53
Fig. 23A	Same as Fig. 18A for June.	53
Fig. 23B	Same as Fig. 18B for June.	53
Fig. 24A	Same as Fig. 18A for July.	53
Fig. 24B	Same as Fig. 18B for July.	53
Fig. 25A	Same as Fig. 18A for August.	53
Fig. 25B	Same as Fig. 18B for August.	53
Fig. 26A	Same as Fig. 18A for September.	53
Fig. 26B	Same as Fig. 18B for September.	53
Fig. 27A	Same as Fig. 18A for October.	53
Fig. 27B	Same as Fig. 18B for October.	53
Fig. 28A	Same as Fig. 18A for November.	53
Fig. 28B	Same as Fig. 18B for November.	53
Fig. 29A	Same as Fig. 18A for December.	53
Fig. 29B	Same as Fig. 18B for December.	53
Fig. 30	Same as Fig. 18A for May-September.	61
Fig. 31	Same as Fig. 18A for October-April.	61
Fig. 32	Same as Fig. 18A for January-December.	61
Fig. 33	Bivariate distribution for Hs and Ts for the Arabian Sea and Bay of Bengal during rough weather and fair weather seasons.	62
Fig. 34A	Cumulative distribution of Hs for the Arabian Sea and Bay of Bengal during rough weather and fair weather seasons.	62
Fig. 34B	Same as Fig. 34A for Ts.	62
Fig. 35A	Average wave spectrum for a selected site in the Arabian Sea during rough weather season.	63
Fig. 35B	Same as Fig. 35A during fair weather season.	63

LIST OF TABLES

	Page
1. Indian Institutions involved in wave data collection.	7
2. Numerical wave models.	15
3. Number of data points used for the analysis of wave model input data.	33
4. Number of visually observed windsea and swell observations ... obtained from IMD for the period 1961-70.	48
5. Monthly wave height and period ranges for windsea and swell. ..	54

CHAPTER I. INTRODUCTION

I.1 GENERAL TERMINOLOGIES

There are five basic types of waves namely sound, capillary, gravity, inertial, and planetary waves which have been identified in the oceans with five basic restoring forces all acting simultaneously to produce more complicated mixed type of waves and oscillations (Khandekar, 1989). The present study deals with the *wind-induced surface gravity waves* of periods 1 to 30s which are most common and have maximum impact on human activity. Therefore, knowledge of the surface waves is essential for efficient management and appropriate utilization of our coastal as well as deep sea environment. Since long, scientists and engineers have recognized the fact that these waves are dominating and influential factors to be considered in various applications. They influence considerably the air-sea interaction processes of the coupled ocean-atmosphere system. Hence the requirement of establishing a climatic wave database cannot be overemphasized. Wave information acquired over several years from any given region forms a basis for updating the currently used wave prediction models and for the development of models for future. Moreover, an evaluation of the long-term representativity of any of the ocean environmental variabilities including the surface waves becomes essential from climatic considerations.

Ursell (1956) in his well known paper entitled "Wave generation by wind" stated that, *wind blowing over the water surface generates waves in the water by physical processes which can not be regarded as completely known at present*. Despite several theoretical and observational advances which took place subsequently over the last 40 years, Ursell's statement is still applicable. One of the most fascinating features of the surface of the sea is the innumerable waves of different sizes and shapes present at any given time. The sea surface remains calm very rarely. With a light breeze, an intricate pattern of capillary waves are formed. As the wind continues to blow, the capillary waves grow in size and become surface gravity waves in which gravity is the most dominating restoring force. These gravity waves continue to grow as long as the incoming energy from all sources is greater than the energy dissipated by all possible means such as wave breaking and turbulent water motions etc.

Growth of waves depends on the *wind speed* normally referred to 10m above the sea surface, *wind duration* and *fetch*. Fetch is the length of water surface over which wind blows. Waves are also influenced by the presence of surface currents and get modified when they propagate to shallow waters. However, the present study deals with only the deep water waves. Sea surface waves are special type of oscillatory water waves which propagate along the air-water interface. In the deep water, their speed depends on wavelength or period as they are dispersive. Hence the longer waves move ahead of the shorter ones and can be observed first at a distant point from the generating area. Wind waves are classified into *sea* and *swell*. Waves are known as seas (or windseas) as long as they are under the influence of prevailing wind in the local generating area. When these waves move out of the generating area and are no longer subject to significant wind input, they are known as swells.

A common statistical representation of the sea-state or the wave field containing innumerable waves of different heights and periods is by means of *significant wave height* (H_s) and *significant wave period* (T_s) that satisfy most practical applications. Sverdrup and Munk (1947) define H_s as *the average height of the one-third highest waves* which is equal to the average height of the waves estimated by an experienced observer. The value of T_s obtained by visual observations is likely to be the average of 10 to 15 successive prominent waves. If we examine a typical wave record, T_s is apt to be the average period of all waves whose troughs are below and crests are above the mean water level (CERC, 1984). The most commonly used method of estimating height (H_s) and period (T_z) from a wave record is known as zero-up-crossing method as suggested by Tucker (1963) and Draper (1967). T_z is known as zero-up-crossing period which can be replaced by T_s (CERC, 1984). The corresponding wave parameters for H_s and T_s are H_{m0} and T_p obtained through spectral analysis by computing Fast Fourier Transform (Bendat and Piersol, 1971) of the digital wave record where H_{m0} is defined as four times the square root of the area under the wave variance spectrum and T_p is the inverse of the frequency at its peak. In deep water, it is commonly found that $H_{m0} \cong H_s$ (Longuet-Higgins, 1952; Goda, 1974) and $T_p \cong 1.05 T_s$ (Goda, 1974 and 1985). For many engineering applications, T_p can be directly used in the place of T_s (Bishop et al., 1989).

As wave information is needed for various applications, it is generally predicted following two different methods namely *significant wave method* and *wave spectrum method*. In the case of significant wave method,

the statistical parameters of the sea-state such as H_s and T_s are estimated using constant wind speed, wind duration, and fetch. In reality, the wind system is often associated with variable wind speed, duration, and fetch. The significant wave concept does not take into account the spectral character of the sea-state. The wave spectrum method predicts the spectrum of the waves from which various wave parameters can be derived. During the last forty years, several spectral forms have been proposed which provide a sound basis for describing the sea-state using a prescribed analytical form (Khandekar, 1989). This has led to the development of modern spectral wave models to predict the sea-state. The wave prediction is called as *hindcasting* when it is based on the past winds and *forecasting* when predicted winds are used. Sometimes, the prediction is made on real-time basis based on the observed and/or analyzed winds which is referred to as *nowcasting*.

1.2 DEFINITION OF WAVE CLIMATE

Wave climate is a fairly new concept introduced with an analogy to the atmospheric weather climate (Goda, 1990). It can be expressed in terms of several long-term *wave statistics* which are formulated depending on the type of application. In simple terms, wave climate refers to the general condition of the sea-state of a specific location or over a coastal or offshore region. The principal elements that are associated with wave climate are the significant wave parameters such as H_s , T_s and direction. As in the atmospheric climate, the wave climate is also described in terms of months, seasons, and years.

Wave statistics as such can be classified into *short-term* and *long-term*. Short-term wave statistics deals with the statistical properties of individual waves which belong to a short time-duration, say 20 minutes (one typical wave record). It may sometimes be considered as a representative statistics for a duration of 1 to 3 hours around the time of the wave recording. Long-term wave statistics is associated with the wave climate as defined previously or with the lifetime of a coastal or offshore structure and is subdivided accordingly. It means that, long-term wave statistics are generally formulated for a specified time interval considering the type of requirement.

I.3 DATA SOURCE FOR WAVE CLIMATE

Various data sources for establishment of wave climate are visually observed data, instrumentally measured wave data, wave hindcast data and operational wave forecast data. The quality, duration, and limitations of these data sources are discussed below.

I.3.1 Quality and duration of wave data

The fundamental requirements for the generation of a suitable wave climate or the extreme wave statistics of any given region are quality and duration of the wave data acquired from one or more sources as indicated above. Visually observed wave data involve a significant degree of estimation variability. Measured wave data using the latest available equipment is most reliable compared to all other sources. Accelerometer (heave) buoys and their directional counterparts (heave-pitch-roll buoys) have become the wave measurement standards of today. The buoy measurements are generally restricted to specific sites of interest where they are deployed. However, the modern remote sensing methods of observing waves have a greater potential in future as it can provide a spatial coverage in time. The accuracy of remote sensing data has to be established with real-time measurements obtained using standard equipment. As the availability of remote sensing data is limited and their accuracies are not yet fully established, either measured or visually observed wave data are currently in use for most applications. Visually observed data can be replaced by hindcast or operational forecast data after validation using the sea truth measurements.

From the wave climate point of view, accuracy and duration of the wave data without significant gaps are considered to be of equal importance. In some cases, wave measurements over a minimum period of one year is being used for coastal engineering applications. But it is too short a duration to yield reliable information on wave climate or extreme wave statistics. Goda (1984) has demonstrated that the annual mean of H_s in a single year may deviate up to 15% from the average value obtained over long durations. The deviation may be still more for regions where seasonal wind reversal and year-to-year variations are predominant.

In the present case, wave conditions in the Arabian Sea and Bay of Bengal (hereinafter referred to as the Indian Seas) solely depend on the

strength of the monsoon. During a weak monsoon year, the annual mean of H_s can vary significantly from the mean for several years. Therefore, the duration of wave data should be sufficiently long for a reliable estimate on wave climate. A time period of minimum five to twenty years may be considered for this purpose (Bishop and Donelan, 1989).

I.3.2 Visually observed wave data

Visual wave observations are routinely made from weather ships, land based stations like lighthouses, and ocean going vessels who voluntarily comply with the request of meteorological agencies. Therefore, these observations are available over long durations covering a large area of the ocean where ships routinely cruise. The most famous compilation of ship reported visual wave observations is *Ocean wave statistics* by Hogben and Lumb (1967) which was revised later by Hogben et al. (1986). The U.S. Navy has also published a worldwide marine climatic atlas (1981). A number of publications either on wave climate or long-term wave statistics are available on regional basis for different parts of the world oceans. For the Indian Seas, excepting some port and harbor authorities who routinely estimate the prevailing wave condition visually, the *Indian Daily Weather Reports (IDWR)* published by *India Meteorological Department (IMD)* are the main source of visual wave data. The Naval Physical and Oceanographic Laboratory, Cochin has published *Wave statistics of the Arabian Sea* based on IDWR charts (NPOL, 1978). Similarly, the National Institute of Oceanography, Goa has also published *Wave (Swell) atlas for Arabian Sea and Bay of Bengal* and *Wave tables/atlas for the Indian coast based on ship observations* (1982, 1989a, 1989b).

Visually observed wave data may not be of good quality as its accuracy is wholly dependent on the experience and skill of the observer. Even the observations made by experienced observers of ocean weather ships are said to have bias. Attempts have been made to establish correlation between visual and measured wave heights (Sores, 1986). In most cases, visual wave heights are reported to the nearest 0.5m and wave periods to the nearest 1s. Compared to wave heights, the wave periods reported by experienced observers are less accurate. Hence, the correlation on visual and measured wave periods is not well established (Goda, 1990). The possible reason may be that the windsea and swell periods are reported separately for visual data as opposed to a single average or significant wave period provided by instrument measurements. The wave periods published in IDWR charts range

from 5 to 14s while the actual periods measured by instruments can vary from 2 to about 30s. There is another major drawback for visual wave data that the ships have a tendency to avoid rough weather. In spite of all these limitations, visual wave information still remains the major source of data that covers the most of the ocean areas and for longer durations.

I.3.3 Measured wave data

A few governmental research institutions (Table 1) in India have been conducting short-term as well as long-term wave measurement programmes using pressure and/or accelerometer sensors. Most of them use wave-rider and wave directional buoys. There are a few Indian research vessels and some of them are fitted with ship-borne wave recorders. These vessels collect wave data during their scientific cruises. During some field experiments using these vessels, time-series wave measurements of short durations have been conducted by deploying wave buoys in the shelf waters. Information on the observed wave characteristics or short-term wave climate of some specific regions has appeared in various research papers (Swamy et al., 1976; Das et al., 1979; Fernandez et al., 1981; Gouveia et al., 1981; Dattatri, 1983; Vethamony et al., 1984; Baba and Harish, 1985; Baba and Joseph, 1988; Nayak et al., 1989; Swain and Ananth, 1992; Swain et al., 1993). However, considering all the available measurements, the amount of measured wave data in the Indian Seas is very limited. A comprehensive catalog of the measured wave data (deep and shallow) collected up to 1985 from the Indian Seas was published by Baba (1985). Similar comprehensive reports are not available beyond 1985. Recently, based on GEOSAT radar altimeter data of about three years (November 1986 to January 1990) Young and Holland (1996) have published the *Atlas of the Oceans: Wind and wave climate*. It presents the monthly charts of average wind speed, wind direction, and wave height over 4x4 degree resolution covering the entire globe.

The quality of measured wave data using standard instruments depend on the type of the sensor. The duration of measurement varies from site to site. One of the drawbacks of measured wave data using pressure sensors, ship-borne wave recorders and wave-rider buoys is the lack of directional information. In some cases, the visually observed wave direction is used to supplement these measurements. By and large, out of the available wave measurements found in the literature, the directional measurements using heave-pitch-roll buoys are very limited in the Indian Seas.

Table 1. Indian Institutions involved in wave data collection

	Name of the agency	Place
1.	CESS Centre for Earth Science Studies	Trivandrum
2.	CMFRI Central Marine Fisheries Research Institute	Cochin
3.	CWPRS Central Water and Power Research Station	Pune
4.	IIT Indian Institute of Technology	Madras
5.	NIO National Institute of Oceanography	Goa
6.	NPOL Naval Physical and Oceanographic Laboratory	Cochin

I.3.4 Hindcast wave data

Wave hindcasts are generally carried out for generating major storm wave data over longer durations. The duration is chosen over a period of known storm activity and hindcast is performed for that period. Another type of wave hindcast is the daily generation of wave data over several years for wave climate analysis in the areas where measured wave information is either limited or not available. Wind data covering the region of interest for the whole duration is constructed using synoptic weather charts and used as input to the wave model for hindcasting. Hindcast wave data should be preferably calibrated with instrument measurements before any statistical analysis is made. However, the accuracy of the hindcast depends on the accuracy of the derived wind field information and the adequacy of suitable wave growth models. There cannot be any remedy for the former problem if the weather maps are constructed with sparse barotropic data. The latter problem is being resolved gradually in the recent years. However, presently no such hindcast studies have been carried out for the Indian Seas for longer periods using state-of-the-art wave models. The main advantage of hindcast method is that wind data is more abundant and generally reliable than visual observations of sea surface waves. A few wave forecast and hindcast case studies are reported by Srivastava (1964), Dattatri and Renukaradhya (1971), Reddy et al. (1980), Prasada Rao and Durga Prasad (1982), Joseph (1988) and Swain et al. (1989). All of them used empirical models except Joseph (1982) who used a second generation wave model. These studies were more of an academic nature. Similarly, Gadre et al. (1981) and Nayak (1983) attempted for estimating the extreme wave conditions required for coastal and offshore

designs. Although there are a few other studies not cited here, the results obtained from all these studies are not adequate for the establishment of wave climate for the Indian Seas.

I.3.5 Operational wave forecast data

Several countries like France, Germany, Japan, and Norway have been providing routine regional wave forecasts which are being used for various operational applications. Similar routine operational wave forecasts are not available for the Indian Seas. The U.S. Navy Fleet Numerical Oceanography Centre at Monterey gives routine global wave forecasts. The European Centre for Medium-Range Weather Forecasts (ECMWF), U.K. also provides both global as well as regional wave forecasts for the North Atlantic and the Gulf of Mexico. Such forecasts over the entire globe is mainly used for ship routing to avoid storm areas.

There are several shortcomings in operational wave forecasts. The first is the reliability or the accuracy of the forecasts. The second is the scarcity of data points or low resolution of the models used which results in lack of information in coastal waters and near storm centres. The third is the delay in compilation of the forecast data into workable wave climate database. However, operational wave forecast data has a greater potential of becoming an important data source over several parts of the world oceans in the near future.

I.4. SIGNIFICANCE OF WAVE CLIMATE SIMULATION

In the absence of both long-term hindcast and routine operational forecast data for the Indian Seas, visually observed wave data is being used for several applications. However, as already mentioned, visual wave data cannot be considered as reliable. The main drawback for conducting a long-term wave hindcast for the Indian Seas is the limited wind as well as barotropic data used for the preparation of IDWR charts (0830 and 1730 hrs). As the atmospheric pressure is more accurately measured compared to winds, wind fields are usually estimated based on the pressure values. However, if the available measurements are limited, the estimation of winds for the whole of the Indian Seas (proposed grid size 1x1 degree) based on these synoptic charts will involve greater uncertainty. For a long-term wave hindcast, winds should be estimated at regular intervals of, say, 3 or 6 hours. If the wind input to the wave model has a bias, the hindcast based

on these estimates will have further bias. To overcome the above problem, an altogether different approach has to be adopted.

I.4.1 Concept of "mean climatic year of winds"

Considering the scarcity of barotropic data over the Indian Seas, the observed winds can be directly used to estimate a "*mean climatic year of winds*" based on the data gathered over several years. Mean climatic year of winds consists of estimated mean wind fields for the region of interest over a selected time interval (say 1 to 6 hours) for all the 365 days. Hence, the wind data is averaged for the synoptic hours corresponding to the time of observation as indicated earlier in the case of IDWR charts or at least for each day of the year covering 365 days. Hence, the historical data over all the years for which the hindcast has to be made is ultimately reduced to one year. Further, if the data strength is found to be still insufficient, a mean climatic year of winds may be established following statistical and probabilistic approaches which will be discussed in Chapter-III. It would be appropriate to do so because it helps in removing the uncertainties involved in the widely scattered (both space and time) individual wind estimates. Hence, if a mean climatic year of winds is used as the input to generate a mean climatic year of waves in a way similar to the long-term wave hindcast, it can be treated as a simplified approach provided that the results agree with the mean wave fields computed from the observed wave variability. There is a basic difference between the long-term hindcast and the method explained above. In the former case, wave fields are generated for a period of, say, 5 to 20 years and then averaged over the months, seasons, and years whereas in the latter case, wave fields will be generated only for a period of one year using directly the mean climatic year of winds. Although the wave model has to run for one full year of wind input (termed as the mean climatic year of winds) representing the most general pattern of wind variations, the method cannot be considered as hindcasting as it does not try to predict the actual wave conditions of the past. It only tries to simulate the wave field for an assumed mean wind field variation. Therefore it would be a right choice to name it as a process of simulation.

I.4.2 The simulation process

From theoretical and applied literature on the simulation process, it is apparent that the various disciplines apply the same basic set of

fundamental rules to understand and predict the real world systems that are very complex in nature. The present simulation process will be formulated based on our experience of wind and wave variability over the region. Here it is not aimed at simulating very complex wind and wave conditions which are normally encountered during severe weather conditions such as cyclones. Moreover, the input wind which will be estimated from historical data and used by the model shall not involve such complex wind conditions which are observed during severe weather conditions. Hence the wind specification for the wave model based on available historical data will be carried out so as to simulate only the mean wave conditions representing several years. The main objective here is to simulate and study the wave climate for the Indian Seas in the absence of sufficient input data which would generate wind fields at regular time intervals as required for long-term wave hindcasting.

Wave climate simulation using a suitable wave model is attempted in this study as the available wind measurements are limited and widely scattered in space and time. However, the method which is adopted here will be able to take care of the input wind specification for the wave model to a large extent. Secondly, it is realized that the present day numerical models are quite capable of providing accurate and detailed spatial and temporal representations of the ocean compared to the existing climatologies, real-time oceanographic measurements and a simple combination of the two (Clancy, 1992; Clancy and Sadler, 1992). In fact, the models are also capable of augmenting the extremely sparse in situ oceanographic data in a substantial way by inferring oceanographic information from other sources by employing sophisticated physical and statistical methods (Michael Clancy, 1979). Hence, the present simulation experiment can be more advantageous as it aims at inferring the sea-state variability only from a climatic consideration.

1.5. SCOPE OF THE PRESENT WORK

Day-by-day, there is an increasing emphasis on the sea-state information. Hence, the ocean wave modelling community, coastal engineers, marine forecasters, and meteorologists are very much concerned for the establishment of a reliable and up-to-date wave database for sufficiently longer duration. A long-term wave database of a region can be utilized effectively for many practical applications including planning of various coastal and offshore activities. Wave data is very useful for the modern

shipping industry for safe and optimum ship routing. It can also help in the computation of wave induced ship motions which is required for design of ships. The same is the case with offshore structures. A long-term wave climatology is essential in identifying the areas of maximum wave power potential along the coastal belt.

In addition to civilian applications, wave climate has a variety of applications in Naval defence. Some of the important areas are navigation, landing and take off operations at sea, mine laying/sweeping, towing of hydrophones, missile launching, torpedo firing, search/rescue operations, and amphibious warfare. As on today, underwater acoustic detection is the principal means of locating subsurface vehicles and targets. Sound propagation in the sea is often affected by the surface disturbances. The surface waves scatter the sound and produce Doppler shifts. The presence of near-surface bubbles in a rough sea results in absorption and scattering of sound. Rough seas are also a major source of locally generated ambient noise in the sea.

In the absence of reliable and up-to-date wave climate information for the Indian Seas, simulation appears to be the only alternative. The present simulation experiment is planned for the seas around India (Fig.1) which extend from 50° to 100° E and 0° to 25° N. India has a long coast line of about 7000 Km bordering the Arabian Sea (West coast) and Bay of Bengal (East Coast). The assumed boundary separating the Arabian Sea and Bay of Bengal is the 80° longitude. The area covered in this study has only one open sea boundary to the south (0° latitude). The other three sides are almost enclosed by land. Wave conditions which prevail in this region show both temporal and spatial variability along with the wind. Although the data available for this region is limited, we have some qualitative picture of the problem addressed here. In this study, attempts are made for a clear understanding and quantification of the same from a climatic point of view. Long-term winds representing a mean climatic year and the monthly mean surface current fields will be utilized as the inputs. The wave model outputs are to be generated over 1×1 degree resolution and the same shall be the basis for establishment of wave climate of this region.

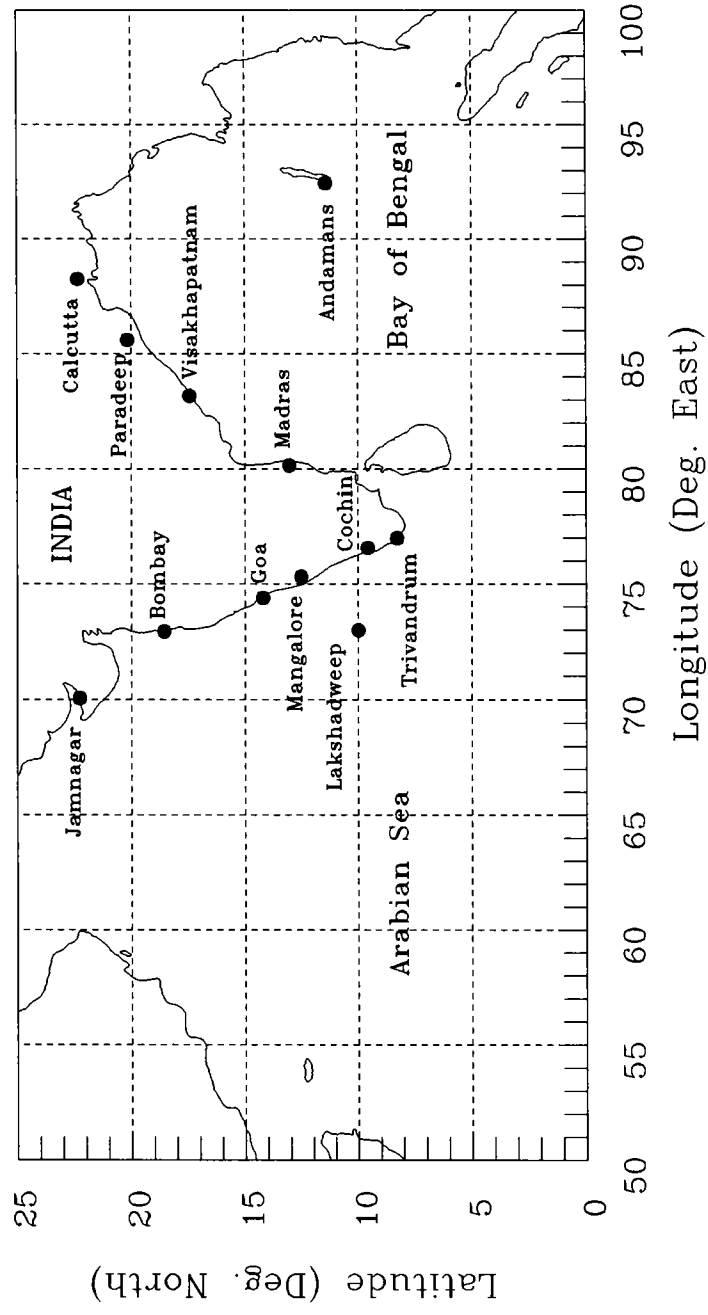


Fig.1 Location map for Indian Seas.

CHAPTER II. SELECTION OF WAVE MODEL

II.1 INTRODUCTION

In the early days of navigation, mariners and sailors were using different wind-scales for describing the sea-state. Based on these descriptive wind-scales, a numbering system known as *Beaufort scale* was suggested by British Rear-Admiral Sir Francis Beaufort in 1805. The Beaufort scale with its associated wave-height values was the only operational procedure available for describing sea-state in the early 1900s. However, the description of sea-state in terms of a numbering system was not considered as satisfactory since the requirement of wave information was increasingly felt both for defence and well as civilian applications. There were serious efforts towards the development of simple operational wave prediction procedures. Hence, following the simple empirical relationships which were developed during the early phases of wave modelling and prediction, there have been several theoretical developments leading to the use of present day third generation wave model for routine forecasts. The following two sections will discuss the development, classification, and the limitations of the models which are extensively used.

II.2 EARLY WAVE PREDICTION TECHNIQUES

Simple empirical wave prediction models were developed during the Second World War in response to a crucial need for operational wave forecasting for the Allied Forces's amphibious invasion at Normandy and France (Bishop et al., 1989). Sverdrup and Munk (1947) developed the first semi-empirical method to predict the significant wave height and period. It was mainly used for forecasting the sea-state conditions over the North Sea. After Sverdrup and Munk, several other models were developed. The models which are widely used are SMB (Bretschneider, 1970) and JONSWAP (Hasselmann et al., 1973). Some other available models are Darbyshire and Draper (1963), Kruseman (1976), Toba (1978), Mitsuyasu et al. (1980), and Donelan (1980). However, these models can only be applied to such conditions where the advection of swells into the forecast area remains insignificant. The main assumption in these models is that the wind field over the generating area at any given time can be represented by a mean value. These models yield estimates of wave height and period as empirical functions of wind speed, fetch, duration of wind, and water depth.

II.3 NUMERICAL WAVE PREDICTION MODELS

Since the pioneering paper of Gelci et al. (1957), a number of numerical wave models have been developed. They are grouped into first, second, and third generation wave models. The first generation models were developed during sixties and early seventies. These models avoided the problem of explicitly modelling the complete energy balance. The details regarding how the wave spectrum attained its equilibrium form were not specified as it was assumed that the wave components suddenly stop growing when they reach a universal saturation level (Phillips, 1958). However, it is generally recognized today that universal high frequency equilibrium spectrum originally proposed by Phillips does not exist (The WAMDI group, 1988). By and large, first generation models exhibit basic quantitative shortcomings by overestimating the wind input and underestimating the strength of nonlinear transfer by almost an order of magnitude. Later, with the aid of extensive wave growth experiments (Mitsuyasu, 1968, 1969; Hasselmann et al., 1986) and direct measurements of wind input to the waves, fundamental changes in the basic concept of spectral energy balance took place leading to the development of second generation wave models during late seventies. However, these models too had restrictions resulting from the simplified nonlinear transfer parameterization effectively required for the spectral shape of the windsea spectrum to be prescribed for frequencies higher than the peak frequency. The specification of the spectral shape was introduced either at the outset in the formulation of transport equation for parametric and hybrid models or as a side condition in the computation of spectrum for discrete models. Although the adjustment to a quasi-universal spectral shape could be justified theoretically, the second generation models were unable to simulate the complex wave field generated by the rapidly changing wind fields. The problems of these models remained largely numerical than physical. Some techniques to overcome such difficulties are discussed in SWAMP (1985). Subsequently, it was proposed that, third generation model should be developed in which the wave spectrum can be computed alone by integration of the basic transport equation without any prior assumption on the spectral shape. Hence, during late eighties, a major thrust towards the development and implementation of the third generation wave model was achieved by The WAMDI group (1988). The model involves improved physics and includes the exact specification of non-linear transfer of wave energy due to resonant wave-wave interactions.

The numerical wave models available so far are classified into three broad categories depending on the way they are formulated. These are decoupled propagation wave models, parametric and hybrid wave models, and coupled discrete wave models. The decoupled propagation wave models involve representation of directional wave spectrum by a discrete number of finite band widths, the spectral components travelling in a specified number of directions along the ray paths. Parametric description of wave field in case of parametric wave models is suitable only for the windsea region of the spectrum in which the non-linear energy transfer is dominant. Normally, parametric wave models are combined as hybrid models with standard discrete spectral representations for the swell components and referred as parametric and hybrid or coupled hybrid wave models. These models encounter difficulties in the windsea-swell transition regime of wave spectrum in which non-linear energy redistribution is neither negligible nor dominant. Such a transition regime arises whenever wind speed decreases or wind changes its direction. To avoid this difficulty, some models tried to forego the basic informational economy offered by the parametric approach and retained the traditional representation for the entire spectrum, including both windsea and swell region. These models are referred to as coupled discrete models. However, the uniform representation of windsea-swell transition regime could not be properly exploited by most of the coupled discrete models (except the third generation wave model) as long as the parametric representation of the nonlinear energy transfer remains limited to relatively few degrees of freedom. The wave models which belong to the above mentioned model classes are listed in Table 2 (Khandekar, 1989; SWAMP, 1985). Most of those listed are participants of SWAMP wave model intercomparison study.

II.4 WAVE MODEL INTERCOMPARISON STUDY

A group of researchers on wave models had proposed for a wave model intercomparison study to understand the interrelations existing among the various wave models developed in the past. The results of the study are discussed extensively in SWAMP (1985). Some salient features of the SWAMP study, highlighting the model used in the present simulation experiment, are discussed below.

During the SWAMP intercomparison study, ten spectral wave models were tested using several idealized wind fields representative of typical atmospheric flow patterns like uniform wind blowing orthogonally off a

Table 2. Numerical wave models

Model	Institution	Model Class	Application
a) DSA	Central d'Océanographie et d'Etude, France.	DP (1g)	Routine wave forecast for Atlantic.
b) GSOWM	U. S. Navy.	DP (1g)	Global operational wave forecast.
c) ODGP	Oceanweather Inc., USA.	DP (1g)	Operational forecast, Western North Atlantic.
d) MRI	Meteorological Research Institute, Japan.	DP (2g)	Operational wave forecast, North Pacific regional wave statistics.
e) VENICE	Istituto per lo Studio della Dinamica delle, Venice, Italy.	DP (2g)	Regional wave statistics.
f) NOWAMO	Norwegian Meteorological Institute, Norway.	CH (2g)	Operational wave forecast for north-east Atlantic.
g) GONO	Royal Netherlands Meteorological Institute, The Netherlands.	CH (2g)	Operational wave forecast for North Sea.
h) TOHOKU	Geophysical Institute, Tohoku University, Japan.	CH (2g)	Regional wave statistics, Japan Sea.
i) HYP A	Institut fur Meereskunde, Federal Republic of Germany.	CH (2g)	Regional wave statistics, Operational forecast for North Atlantic and North Sea.
j) BMO	British Meteorological Office, UK.	CD (2g)	Operational forecast, Atlantic, North Pacific, North Sea, Mediterranean; Regional wave statistics.
k) SAIL	Atlantic Oceanographic & Meteorological Lab., NOAA, USA.	CD (2g)	Regional wave statistics.
l) DNS	Scripps Institution of Oceanography, USA.	CD (2g)	Regional wave statistics.
m) WAM	European Centre for Medium-Range Weather Forecasts (ECMWF), UK, (& several other users).	CD (3g)	Global wave forecast, Regional wave forecast for North Atlantic and Gulf of Mexico.

Note: DP -> Decoupled Propagation model.
 CH -> Coupled Hybrid model.
 CD -> Coupled Discrete model.
 1g -> First generation wave model.
 2g -> Second generation wave model.
 3g -> Third generation wave model.

straight coast line, wind field with sudden change in wind direction, stationary and moving hurricanes etc. Ideally, for a prescribed wind field and boundary conditions, a numerical wave prediction model should compute the two dimensional wave spectrum starting from a postulated functional form of the three basic source functions of the spectral energy balance (see equation 2.3). However, the first generation of decoupled propagation models compute the initial growth rate from prescribed source functions and presume a given limiting form for the equilibrium spectrum. The second generation of coupled hybrid models assume a given quasi-equilibrium shape for the entire windsea spectrum while the coupled discrete models integrate the full transport equation using simple parameterization of non-linear transfer leading to spectral instabilities at frequencies beyond the peak frequency. Therefore, the second generation coupled discrete models too have to assume a prescribed spectral shape over much of the windsea spectrum. Unlike these models, the third generation of coupled discrete model (EXACT-NL, present name WAM) employs a discretised continuous-operator parameterization of non-linear transfer containing an equal number of degrees of freedom as used in the discrete representation of the wave spectrum. All the 10 models were executed for seven different type of wind fields and the results were compared. The comparisons revealed that the first and the second generation wave models performed reasonably well in most of the test cases but they did not provide a proper description of the sea-state during rapidly varying wind conditions. For the same hurricane wind fields, it was demonstrated that the maximum wave height computed by these models varied from 8 to 25m. The short-comings of first and second generation wave models are available in SWAMP (1985) and Komen et al. (1994). The difficulties faced by first and second generation models in dealing with the problem of rapidly changing wind fields were not encountered by the third generation wave model. However, the SWAMP study fails to provide any insight into the performance of the wave models under operational environments.

II.5 THE PRESENT MODEL

Selection of a model is an important task while dealing with the problem of wave climate simulation. Several empirical models are used to hindcast wave climate using hourly values of wind input. These models are termed as *wave climate models*. They use a pragmatic backstepping procedure to handle varying wind speeds from a constant direction but the treatment of variation in wind direction is too complex (Bishop and Donelan, 1989).

The averaging procedure for input wind speed is continued as long as the wind direction remains within a practicable range and the duration of average does not exceed a prescribed limit. These problems are not encountered if one uses a numerical wave model by neglecting the computational economy offered by the empirical models. The empirical models normally compute the significant wave parameters of the regions for which the winds are assumed to be more or less uniform while numerical models are capable of providing two dimensional wave spectra at each grid point of the model. Moreover, the present task being a simulation experiment, it involves a special procedure for specifying the wind input which is not similar to hindcast methods. Therefore, the use of an empirical model cannot yield the expected results. However, several other aspects should also be considered before selection of a numerical model. The important ones are the following:

- i) *type of input data for the model*
- ii) *model capability and performance*
- iii) *computational requirements*
- iv) *validation of the model output*

From these considerations, the third generation wave model 3g-WAM (The WAMDI Group, 1988) appears to be the most appropriate in the present study because, it is capable of simulating wave fields for a variety of wind conditions. However, the model is computation-intensive. The total computation requirement may be minimized by following certain specified procedures. The following sections contain detailed discussions on the above model including its capabilities and performance.

II.5.1 Background of the model

Integration of the basic transport equation without any additional constraints on the spectral shape requires an explicit prescription of the three components of the source function (wind input, non-linear interaction, and dissipation). This was first realized in 3g-WAM. The model represents the physics of wave evolution in accordance with our knowledge today for the full set of degrees of freedom of the two dimensional wave spectrum and solves the wave transport equation explicitly without any prior assumption on the shape of the wave spectrum. The global version of the model is implemented in an operational setup at ECMWF. The analyzed and forecast wind fields from a high resolution atmospheric model are being

used as the inputs for wave hindcast studies and 10-day wave forecasts respectively. The 3g-WAM is currently used by the Naval Meteorology and Oceanography Command of the U.S. Navy for issuing routine operational forecasts (Michael Clancy and Johnson, 1997; Wittmann and Farrar, 1997).

II.5.2 Fundamental equations

The model used in this study is the revised version of the model called WAMODEL, Cycle-4 (Gunther et al., 1992). In contrast to first and second generation wave models, 3g-WAM computes the 2d-wave variance spectrum through integration of the basic transport equation

$$\frac{\partial F}{\partial t} + \frac{\partial}{\partial \phi} (\dot{\phi} F) + \frac{\partial}{\partial \lambda} (\dot{\lambda} F) + \frac{\partial}{\partial \theta} (\dot{\theta} F) = S \quad (2.1)$$

where: F - represents the spectral density with respect to (f,θ,φ,λ)
 f - denotes frequencies
 θ - directions
 φ - latitudes and
 λ - longitudes.

$\dot{\phi}$, $\dot{\lambda}$ and $\dot{\theta}$ are the rates of changes of position and propagation direction of wave packets travelling along the great circle path.

$$\begin{aligned} \dot{\phi} &= \frac{d\phi}{dt} = v R^{-1} \cos \theta \\ \dot{\lambda} &= \frac{d\lambda}{dt} = v \sin \theta (R \cos \phi)^{-1} \\ \dot{\theta} &= \frac{d\theta}{dt} = v \sin \theta \tan \phi R^{-1} \end{aligned} \quad (2.2)$$

where $v = g/4\pi f$ denotes the group velocity, g is acceleration due to gravity, and R is the radius of the earth.

The time and space evolution of ocean surface wave field or the source function S in equation 2.1 may be represented by

$$\frac{\partial F}{\partial t} + \mathbf{v} \cdot \nabla F = S = S_{in} + S_{nl} + S_{ds} \quad (2.3)$$

where $\mathbf{v} = v(f, \theta)$ is the deep water group velocity and the net source function S is represented as the sum of the input S_{in} by the wind, the non-linear transfer S_{nl} by resonant wave-wave interactions, and dissipation S_{ds} .

As momentum is transferred from the air flow to the waves, the stress in the surface layer depends both on the wind speed and the wave induced stress τ_w . The growth rate of waves then depends on the friction velocity U_* and the roughness length Z_0 .

The wind input term is given by

$$S_{in} = \gamma \cdot F \quad (2.4)$$

where F is the two-dimensional spectrum and γ is the growth rate of waves. For a logarithmic wind profile γ depends on the following two parameters

$$X = U_* \cos(\Theta - \varphi) / C \quad \text{and} \quad \Omega = \frac{g Z_0}{U_*^2} \quad (2.5)$$

where U_* is the friction wind speed, Θ is the direction of wave propagation, φ is the wind direction, and C is the phase speed of waves. Thus, through Ω , the growth rate of waves depends on the sea surface roughness which on its turn depends on sea-state.

The growth rate normalized by angular frequency ω is represented by

$$\frac{\gamma}{\omega} = \beta \quad (2.6)$$

where

$$\beta = \frac{\beta_m}{k^2} \mu \ln^4(\mu), \quad \mu < 1$$

k is the von Karman constant, $\beta_m = 1.2$, and μ is the dimensionless critical height, $\mu = k \cdot Z_c$ where k is wave number, Z_c the critical height defined by $U_0(Z = Z_c) = C$.

The stress τ of the air flow over sea waves depends on the sea-state and from the consideration of momentum balance of air, it is found that

$$\tau = C_d U^2(L) \quad (2.7)$$

where C_d is the drag coefficient given by

$$C_d = \left\{ k / (\ln(L/Z_0)) \right\}^2 \quad (2.8)$$

$$\text{and} \quad Z_0 = \frac{\alpha \tau}{g} \left[(1 - (\tau_w / \tau)) \right]^{-1} \quad (2.9)$$

The constant α is chosen in such a way that for old wind seas the usual Charnock relation for the drag over sea waves is used.

L is the mean height above the waves and τ_w , the wave-induced stress are given by

$$\tau_w = \rho_w \int \omega \gamma (F \cdot \cos(\theta - \varphi)) df d\theta \quad (2.10)$$

In practice, the wave stress τ_w is in the direction of the wind.

The nonlinear source function S_{nl} is represented by the discrete interaction operator parameterization which retains the basic form of the exact nonlinear transfer expression given by

$$\begin{aligned} S_{nl}^{\text{exact}}(k_4) &= \int \omega_4 \sigma \delta \left[k_1 + k_2 + k_3 + k_4 \right] \\ &\quad \times \delta \left[\omega_1 + \omega_2 - \omega_3 - \omega_4 \right] \left[n_1 n_2 (n_3 + n_4) \right. \\ &\quad \left. - n_3 n_4 (n_1 + n_2) \right] dk_1 dk_2 dk_3 \end{aligned} \quad (2.11)$$

where $n_j = F(k_j) / \omega_j$ denotes the action spectrum and the coefficients $\sigma(k_1, k_2, k_3, k_4)$ describes the coupling strength of a resonantly interacting wave number quadruplets k_1, k_2, k_3 and k_4 . However, the five

dimensional continuum of all resonant quadruplets (three integration and two for k_4) is reduced to two-dimensional continuum by considering only a mirror symmetrical pair of discrete interaction configurations. Two continuous dimensions are still needed to define the magnitude and direction of the reference wave number vector, scaling the interaction configuration.

In order to obtain proper energy balance at high frequencies the dissipation by white capping is extended by adding a k^2 term. Thus

$$S_{dis} = (-\gamma_d) F \quad (2.12)$$

$$\text{where } \gamma_d = \frac{1}{2} c_{dis} \langle \omega \rangle \left[\langle k \rangle^2 E \right]^2 \left[\frac{k}{\langle k \rangle} + \left[\frac{k}{\langle k \rangle} \right]^2 \right]$$

The value of $c_{dis} = 4.5$, E is the total wave variance, k is the wave number, and $\langle \omega \rangle$ and $\langle k \rangle$ are mean angular frequency and mean wave number respectively are given by

$$\langle \omega \rangle = \left[E^{-1} \cdot \int \int F(f, \theta) \cdot \omega^{-1} df d\theta \right]^{-1} \quad (2.13)$$

$$\langle k \rangle = \left[E^{-1} \cdot \int \int F(f, \theta) \cdot k^{-1/2} df d\theta \right]^{-1} \quad (2.14)$$

$$\text{where } E = \int \int F(f, \theta) df d\theta \quad (2.15)$$

The dependence of the proportionality factor on the square of the frequency is consistent with the white capping dissipation function.

II.5.3 Numerical scheme

The source function integration is carried out using an implicit scheme which enables the use of an integration time step greater than the dynamic adjustment time of the highest frequencies of wave spectrum, still treated prognostically in the model. The high frequency adjustment time scales are considerably shorter than the evolution time scales of the energy-containing frequency bands near the peak of the spectrum. Hence, in

high frequency region, it is sufficient to determine the quasi-equilibrium level to which the spectrum adjusts in response to more slowly changing low-frequency waves. The implicit second order, centered difference equations excluding the advection terms are given by

$$F_{n+1} = F_n + \frac{\Delta t}{2} \left(S_{n+1} + S_n \right) \quad (2.16)$$

where Δt is the time step and the index n refers to the time level. If S_{n+1} depends linearly on F_{n+1} , equation 2.16 could be solved directly for the spectrum F_{n+1} at the new time step. However, S_{in} is the only term which is linear. It may be written as

$$S_{n+1} = \beta_{n+1} + F_{n+1} = \beta_{n+1} \Delta F + \beta_{n+1} F_n \quad (2.17)$$

where
$$\beta_{n+1} = \beta \left[u_*^{n+1} \right] \quad (2.18)$$

and
$$\Delta F = F_{n+1} - F_n \quad (2.19)$$

For the remaining source function

$$S_{n+1}^{rest} = S_{n+1}^{nl} + S_{n+1}^{ds} \quad (2.20)$$

By introducing the Taylor expansion

$$S_{n+1}^{rest} = S_n^{rest} + \frac{\partial S_{n+1}^{rest}}{\partial F} \Delta F + \dots \quad (2.21)$$

The functional derivative in equation 2.21 is numerically a discrete matrix which is divided into a diagonal matrix Λ_n and a nondiagonal residual N_n . That is

$$\frac{\partial S_{n+1}^{rest}}{\partial F} \equiv M_n = \Lambda_n + N_n \quad (2.22)$$

Substituting equations 2.17, 2.20 and 2.22 in 2.16:

$$\begin{aligned} & \left[1 - \frac{\Delta t}{2} \left(\Lambda_n + N_n + \beta_{n+1} \right) \right] \Delta F \\ & = \Delta t \left[\left(\frac{\beta_n + \beta_{n+1}}{2} \right) F_n + S_n^{\text{rest}} \right] \dots \quad (2.23) \end{aligned}$$

If nondiagonal terms are not too large, the matrix on the left hand side can be inverted by expanding with respect to the nondiagonal contributions, leading to

$$\Delta F(f, \theta) = A(f, \theta) + \sum_{f', \theta'} B(f, \theta; f', \theta') A(f', \theta') + \dots \quad (2.23)$$

where

$$A(f, \theta) = \left\{ \left[\Delta t \frac{(\beta_n + \beta_{n+1})}{2} F_n + S_n^{\text{rest}} \right] \times \left[1 - \frac{\Delta t}{2} \left(\Lambda_n + \beta_{n+1} \right) \right]^{-1} \right\}_{(f, \theta)} \quad (2.24)$$

and the first diagonal matrix in the expansion takes the form

$$B(f, \theta; f', \theta') = \frac{N_n(f, \theta; f', \theta') \frac{\Delta t}{2}}{\left\{ 1 - \frac{\Delta t}{2} \left(\Lambda_n + \beta_{n+1} \right) \right\}_{(f, \theta)}} \quad (2.25)$$

The matrix M_n can be readily determined in the course of computing the two source functions S_n^{nl} and S_n^{ds} . The inclusions of the diagonal contributions require slightly more computation time than the explicit scheme.

Two alternate propagation schemes were originally included in the model (The WAMDI Group, 1988).

a) a first order upwind scheme

$$F_j^{n+1} = F_j^n - \sum_k \frac{\Delta t}{\Delta x_k \cos \theta_j} \left[(u \cos \theta F)_j^n - (u \cos \theta F)_{k-}^n \right] \dots (2.26)$$

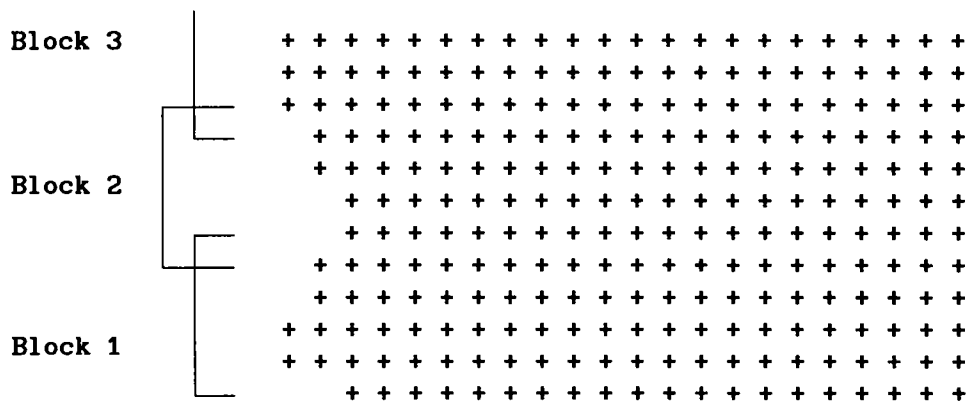
and b) a second order leapfrog scheme

$$F_j^{n+1} = F_j^{n-1} - \sum_k \frac{\Delta t}{2 \Delta x_k \cos \theta_j} \left[(u \cos \theta F)_{k+}^n - (u \cos \theta F)_{k-}^n \right] + \text{diffusion} \dots (2.27)$$

In the above two equations, the index n refers to the time level and the indices $k-$, $k+$ to the neighboring grid points in the upstream and downstream propagation directions respectively (relative to the reference grid point j). The index k runs over the three propagation directions λ , ϕ and θ ; and u_k , Δx_k denotes the velocity components and grid spacing respectively in the relevant directions. In general, the difference between the model results using both the propagation methods was found to be small. The present version of the model uses the former method.

II.5.4 Model grid structure

The grid system considers only the sea grids as model grids in contrast to the earlier versions of this model which include both sea and land grids. The grids are arranged into blocks of say 512 grids each. The grids in a block run from west to east and south to north always. As the computation of the nonlinear source function is not vectorizable, the grid points are placed into the innermost loop running from south to north in the form of one dimensional blocks. To account for the wave propagation across the north or south boundaries of the block, the blocks overlap by two latitudes. So, computations are done from second southern-most latitude to one before the northern most-latitude. The schematic diagram shown below gives an idea about the arrangement of model blocks.



II.5.5 Model system

The model system consists of 1) pre-processing programs, 2) processing programs and 3) post-processing programs. The flow charts for all the programs (total eight program modules) are shown in Appendix-A and the purpose of individual main programs, subroutines and functions are given briefly in Appendix-B. All the program modules have the standard extension "FOR" and their include files are shown in Appendix-C. The programs PREPROC and PRESET are the pre-processing modules. PREPROC generates all the time independent information for the wave model. The initial wave field is generated by PRESET for wave model cold start. Outputs from PREPROC and PRESET are used by the stand alone version of the wave model or the shell program CHIEF. Both CHIEF and BOUINT are the processing programs. CHIEF carries out the model integration for chosen propagation, source term, wind input and output time steps. Program BOUINT interpolates the boundary output spectra from a coarse grid model run in time for the fine grid boundary input. This program is required only when nested grids are used. The post processing programs are PGRID, PSWGRID, PSPEC and PSWSPEC. PGRID and PSWGRID print the gridded output and gridded swell output files while PSPEC and PSWSPEC print the spectral output and swell spectral output files (at selected grids) respectively. It may be noted that the routines which are placed inside dashed boxes in Appendix-A are supporting routines which do not take part in model computation.

II.5.6 Model options and user inputs

The 3g-WAM wave model has various options which can be set by the user before execution. Brief details of the model options are given below:

- i. Model runs for any given regional or global grid system (grid resolution is arbitrary in space and time);
- ii. Wave propagation can be either in spherical or cartesian coordinate grid system;
- iii. User can opt for either deep water run or for shallow water including current refraction;
- iv. Model runs for coarse and/or fine grids (infinite levels of nesting can be done). Nested grids consist of a coarse grid model and time interpolation of the boundary spectrum is done for fine grid model;
- v. The wind input can be interpolated in space and/or time;
- vi. All model time steps and output options can be set as per the specifications of the model;
- vii. The source integration can be interrupted and restarted at arbitrary times.

. The user can control a range of model options through the user input files. Each main program as described under model system has a user input file which has the name with extension "DAT" (Example: CHIEF.DAT). A list of all the user input files are given in Appendix-D. These files contain information regarding each input to be specified before execution of the different program modules of 3g-WAM. However, there are certain restrictions for some of the user inputs and the important ones are given below:

- i. Nested grids consist of a coarse grid model and a fine grid model. Fine grid model should have rectangular grids inside the coarse grid and all corner points of the fine grid system should be coarse grid points;
- ii. All model time steps should be specified as integers in seconds or hours. They have to be multiples of one minute;
- iii. The wind input time step should be the time difference between two wind fields in the sequential input file;

iv. The source function time step should not be greater than 1200s for deep water run and 600s for shallow water;

v. All model output time steps (spectra as well as gridded outputs) should be multiples of the propagation time step;

vi. The time increment to save result and restart files should be a multiple of the wind input time step.

The model requires the following data at all the grid points at each time step:

- i. Topographic data in meters (-ve for sea & +ve for land grids);
- ii. Surface current speed in meters/second and direction in degree;
- iii. Wind speed in meters/second and direction in degrees at 10m from sea surface.

II.5.7 Model outputs

The gridded outputs of various parameters are available at selected time steps of the model. However, the two dimensional spectral outputs will be only for selected grids and time steps. A list of all the model outputs are given below.

- I. Significant wave height
- II. Mean wave direction
- III. Mean wave frequency
- IV. Friction wind speed
- V. Friction wind direction
- VI. Peak wave frequency
- VII. Sea-state dependent drag coefficient
- VIII. Normalized wave stress
- IX. Swell wave height
- X. Mean swell direction
- XI. Mean sea direction
- XII. Mean swell frequency
- XIII. 2-dimensional wave spectra
- XIV. 2-dimensional swell spectra

II.6 PERFORMANCE OF THE MODEL

The 3g-WAM model is being used operationally for global as well as regional forecasts, validation/interpretation of satellite measurements and finally as a research tool by various users (Janssen et al., 1996). The capabilities of this model have been studied in detail by the WAMDI group (1988) and Komen et al. (1994). However, a systematic verification study of the model has not been achieved except by Zambresky (1989) using conventional buoy data and Romeiser (1993) using Geosat altimeter data. Romeiser (1993) carried out global validation of 3g-WAM using Geosat wave height data for a period of one year. Both these authors concluded that the model wave heights using ECMWF winds showed good agreement with the observed data in general. However, Zambresky (1989) also noticed that, 3g-WAM often has a tendency to under-predict extreme sea-states and Romeiser (1993) found a significant regional as well as seasonal disagreement between model output and satellite data. Wave heights were underestimated by about 20% during southern hemisphere winter in large parts of southern hemisphere and the tropical regions, while the agreement was fairly good for the rest of the year.

The verification studies mentioned above used modelled wave heights for 1988 obtained from Cycle-2 of the 3g-WAM wave model. Since 1988, a few important changes have been introduced in the wind as well as wave forecasting systems at ECMWF. In September 1991, the resolution of ECMWF's atmospheric model was doubled in the horizontal and nearly doubled in the vertical. First of all, the increased resolution of the atmospheric model is expected to improve the predictions of sea-state along the storm tracks especially in the southern oceans. Secondly, the new version of 3g-WAM (Cycle-4) was launched in November 1991 which has improved physics regarding wind input and dissipation of wave energy compared to the previous versions. Thirdly, the assimilation of ERS-1 altimeter wave height data started in August 1993. Finally, the horizontal resolution of the wave model was increased from 3 degrees to 1.5 degrees which has a beneficial impact on the prediction of extreme sea-states as more details of generating wind fields are considered. Hence the model is expected to have better prediction capability than before. Janssen et al. (1996) have reviewed the present status of the 3g-WAM, Cycle-4 at ECMWF. Recently, ECMWF has also upgraded the data assimilation technique to three-dimensional variational approach and the authors have verified the

wave forecasts against the verifying analysis and found that the model performs reasonably well up to a period of five and a half day while the forecast skill in the southern hemisphere is comparatively less. They are hopeful that further progress in wave forecasting is expected to come in near future since the variational assimilation is only a beginning now.

CHAPTER III. INPUT DATA FOR SIMULATION OF WAVE CLIMATE

III.1 INTRODUCTION

Wind drives the wave models whether it is for forecasting, hindcasting, or climate simulation. In early days, appropriate wind information were extracted from synoptic weather charts published at regular intervals. Weather charts are normally prepared using mostly ship observations and assuming continuity in the weather pattern over the oceanic regions. Later, with the advent of high speed computers and numerical weather prediction models, regional and hemispheric weather charts have been prepared using objective analysis schemes (Cressman, 1959). These schemes provide winds over a grid mesh using the available information in a given area. While computing winds, the effect of atmospheric stability which is a measure of temperature difference between the sea surface and the overlying air is also considered since it is identified as an important factor influencing the growth of waves (Cardone, 1969).

In addition to wind, wave models also use surface current information if current refraction is to be considered in the prediction. When waves moving through still water encounter a current at an angle with the wave direction, they get refracted and undergo changes in their length, steepness and direction. The effect of a following or opposing uniform current on surface gravity waves was first introduced by Unna (1942). Since 1960, theoretical and experimental aspects of the interaction between gravity waves and currents are receiving increased attention. The problem of waves propagating through a known slowly varying horizontal current is reviewed by Craik (1985). Baddour and Song (1990) have illustrated changes in wave height and length due to the interaction between waves and currents.

III.2 SOURCE OF WIND AND SURFACE CURRENT DATA

The IDWR wind data from 1961 to 1970 was obtained from IMD, New Delhi and utilized in the present study. Fig.2A shows the wind data distribution for the Indian Seas (IMD, 1961-70) over one degree square grids. The mean monthly wind fields of Indian Seas published in the "Climatic atlas of the Indian Ocean, Part-I: Surface climate and atmospheric circulation" by Hastenrath and Lamb (H&L, 1979) are also utilized in this study. The digital wind data used in this atlas was obtained from the Department of

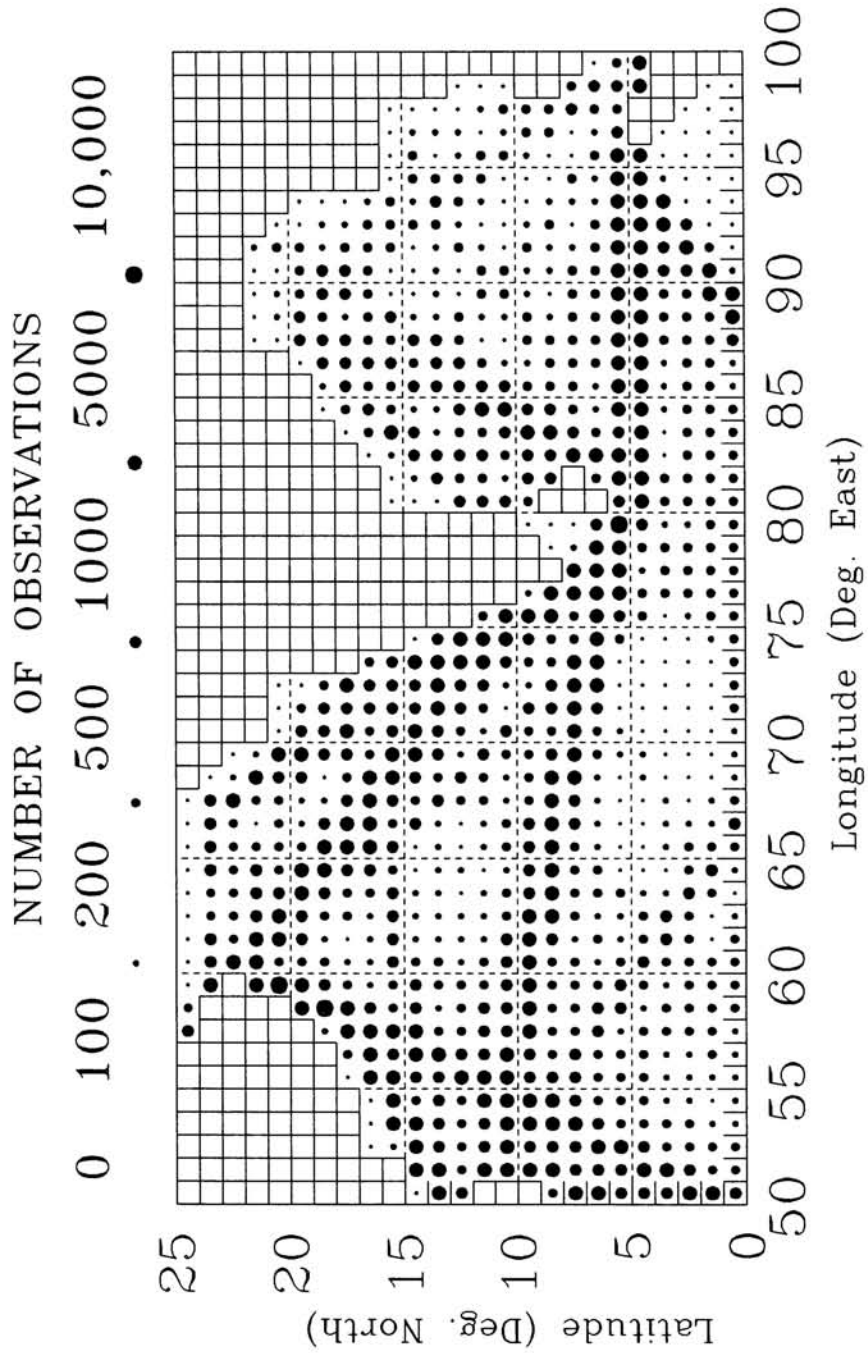


Fig.2A Wind data distribution for Indian Seas (IMD, 1961-70).

Atmospheric and Oceanic Sciences, University of Wisconsin, Madison, U.S.A. The monthly estimates of this atlas over one degree grid resolution were computed based on the observations made by ships for a period of sixty years (H&L, 1911-70). The data distribution is shown in Fig.2B. Surface current data distribution as shown in Fig.2C are mostly based on the ship drift measurements from 1954 to 1994. These data are obtained from the Meteorological Office, Berkshire, U.K. in the form of monthly means for two degree square grids. The size of the thick circle for a given grid indicates the number of observations corresponding to one particular range as indicated on top of the above mentioned figures. It may be noticed that, the wind as well as surface current data are concentrated along shipping lanes. In the case of Fig.2A, the number of data points available along the shipping lanes varies between 5,000 to 10,000 while for the rest of the grids the data density is comparatively less. Same is the case with Fig.2B where the data strength along the shipping lanes mostly exceed 10,000 but for the rest of the grids it is always less than 5,000 excluding a few grids. Compared with the wind data shown in Fig.2A and 2B, surface current data strengths are relatively low. As all the above mentioned data are based on ship measurements, they are mostly biased for the shipping lanes.

III.3 ASSESSMENT OF DATA QUALITY

One of the major difficulties in wave prediction is the non-availability of input winds with desirable accuracy. As already mentioned, the wind as well as surface current data utilized in this study are mostly based on ship reports. The wind data supplied by IMD is similar to the ship reported winds acquired elsewhere. Some ships estimate the winds visually by matching the Beaufort scale and the corresponding sea-state. The ships which are provided by anemometers report the measured winds. However, the height at which the anemometers are installed in different ships vary from 10 to 60m above the sea level (Hamilton, 1986). The observations at different levels from the sea surface are corrected to a common height of 10m which is the reference height for wind measurement at sea recommended by World Meteorological Organization (WMO). Dischel and Pierson (1996) discuss about systematic and random errors in ship-reported winds for use in planning and verifying satellite measurements. Earle and Wilkerson (1986) have concluded that winds measured by ships with anemometers installed are slightly better compared with observed winds of ships without anemometers. The basic data used for the estimation of mean monthly currents used in this study also formed the basis of the atlas by

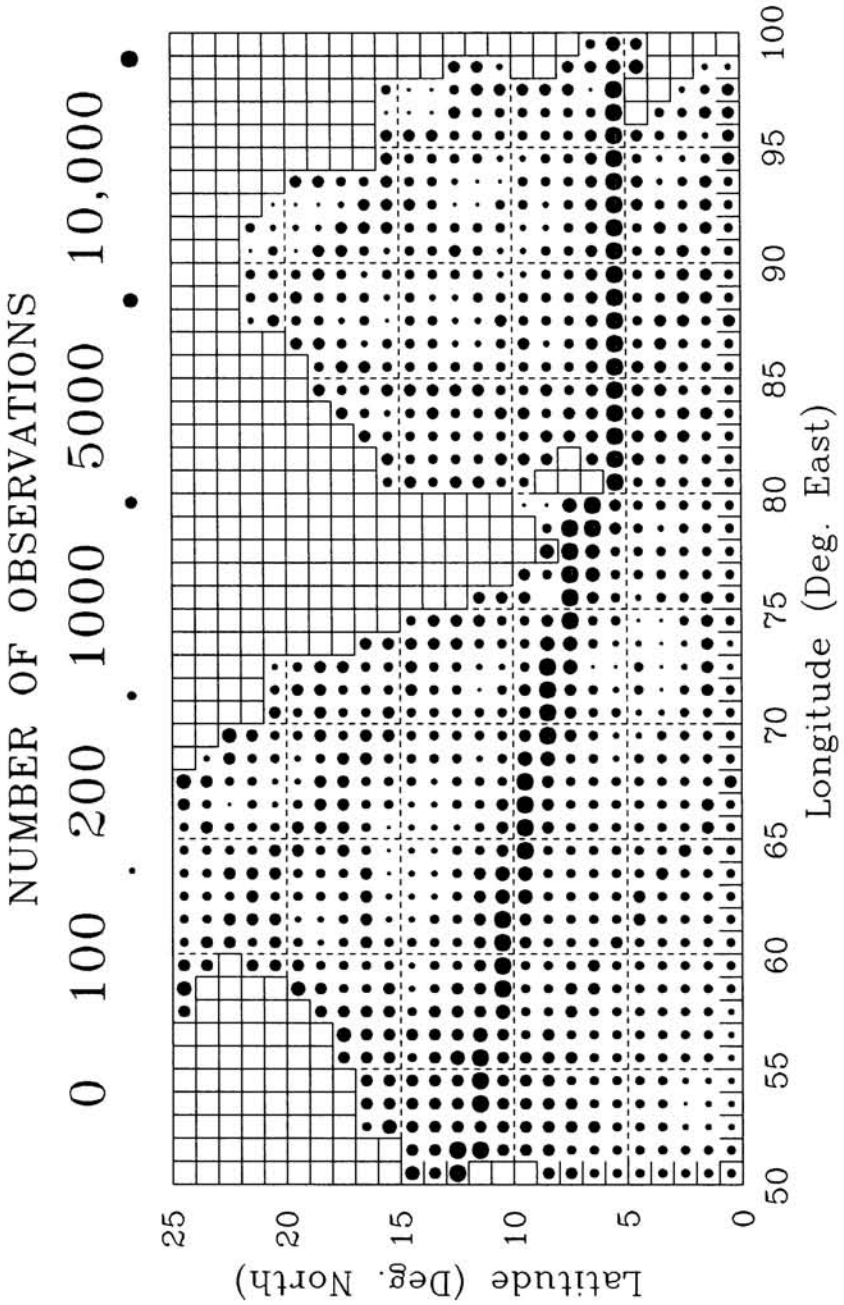


Fig.2B Wind data distribution for Indian Seas (H&L, 1911-70).

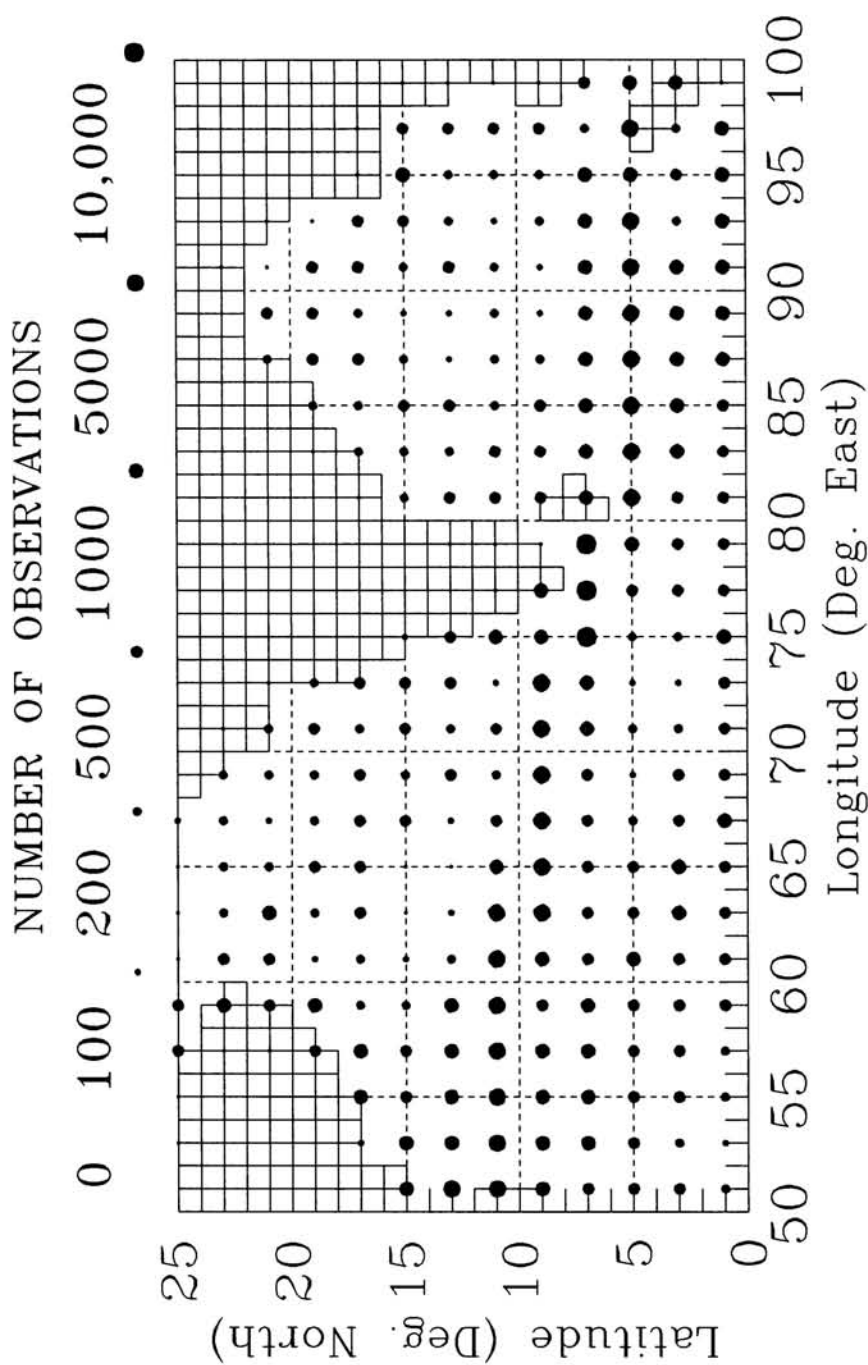


Fig.2C Surface current data distribution for Indian Seas (1954-94).

Cutler and Swallow (1984). However, the present data set is from 1954 to 1994 whereas Cutler and Swallow used the same data from 1954 to 1984. The data summary is available in their atlas.

In this study, monthly variations of wind in space and time are established based on the above mentioned data sets covering 10 to 60 years. Although there are limitations for ship reported data as discussed above and durations of wind and surface currents differ from one another, they can be safely used for the analysis of climatic mean conditions. The data which exceed a decade and more, can be considered as long enough for such studies (Hastenrath and Greischar, 1991). Moreover, errors involved in the individual estimates should not be critical for analysis of long-term mean monthly variations.

A detailed account of the wind (IMD) and surface current data for the individual months is given in Table 3. It may be seen that the wind data for the ten year period (1961-70) varies from about 50,600 to 58,000 observations per month. However, the surface current data (1954-94) is about four times the period of wind data of IMD and the number of observations per month varies from nearly 28,000 to 38,000. The amount of raw data processed by Hastenrath and Lamb (1979) for the estimation of mean monthly fields of wind (H&L, 1911-70) and surface current are 17,13,450 (approx.) and 3,73,264 respectively. Excluding the mean monthly fields of H&L, the total number of IMD wind observations used in this study are 6,47,136 after discarding observations which do not appear to be realistic. For example, wind speeds greater than 40 m/s were rejected. Secondly, observations which contain both the wind speed and wind direction were only considered for analysis as the mean wind fields are computed through vector averaging.

Table 3. Number of data points used for the analysis of wave model input data

	Month	Wind (1961-70)	Surface current (1954-94)
1	January	51,587	36,149
2	February	53,466	27,969
3	March	57,974	37,898
4	April	54,424	28,556
5	May	56,726	32,664
6	June	54,394	30,260
7	July	55,162	29,794
8	August	56,679	30,236
9	September	50,603	32,149
10	October	53,093	28,671
11	November	51,343	28,883
12	December	51,683	30,035
	Total	6,47,136	3,73,264

III.4 ESTIMATION OF MEAN MONTHLY WIND FIELDS

As the IMD wind data (1961-70) density is much higher compared to that of H&L (1911-70), both the data sets are suitably combined to estimate the resultant wind fields. The mean winds using IMD data is computed as given below.

$$\bar{X}_{10} = \frac{\sum_{i=1961}^{1970} N_i X_i}{\sum_{i=1961}^{1970} N_i} \quad \dots 3.1$$

where i denotes the year, X denotes individual monthly mean value of a given parameter, N denotes the number of observations from which individual monthly means are computed and \bar{X}_{10} is the calculated ten-year average of the parameter considered (in this case, u or v component of wind).

The u and v components are computed using the ship reported wind speed (U in m/s) and direction (θ in degrees) using the following equation

$$u = U \cos \theta \text{ and } v = U \sin \theta \quad \dots 3.2$$

While computing the above mentioned individual mean monthly wind components for different years, a simple two way interpolation scheme (Mathews, 1987) is adopted for the grids without any observation. Finally, the ten-year mean components over one degree resolution are smoothed using Laplacian method (Carnahan et al., 1969).

It is ascertained that only a part of the IMD wind data (less than 30%) has formed the basis of the sixty-year mean wind fields of H&L. Therefore, the ten-year average of IMD data and the sixty-year average of H&L (\bar{X}_{60}) are combined as follows:

$$\bar{X}_{60} = \frac{6 \times \bar{X}_{60} + 0.7 \times \bar{X}_{10}}{6 + 0.7} \quad \dots 3.3$$

where \bar{X}_{60} denotes sixty-year monthly average of the wind component and \bar{X}_{60} is the combined wind component.

Finally, the resultant wind speed and direction for the individual months over a one degree grid is estimated as follows:

$$\text{Wind speed} = \sqrt{u^2 + v^2} \quad \text{and}$$

$$\text{Wind direction} = \tan^{-1} \left[\frac{u}{v} \right] \quad \dots 3.4$$

Following equations 3.1 to 3.4, the monthly wind fields for the Indian Seas from January to December averaged over one degree squares are estimated and shown in Fig.3A to 3C. The contours represent wind speed in meters/second and the arrows represent wind direction from true north.

III.5 DISCUSSION ON THE INDIAN MONSOON AND SURFACE CIRCULATION

Seasonal reversal of the surface wind field over the tropical Indian Ocean, known as the Indian monsoon, has profound effects on upper hydrospheric structure and surface current systems. The wind system completely reverses between the boreal winter (November to April) and the boreal summer (May to October) so that a substantial seasonal departure from geostrophic balance is expected for the surface currents (Hastenrath and Greischar, 1991). The following sections summarize characteristic features of the winter and summer monsoon winds and the associated surface circulation in the Indian Seas.

III.5.1 Summer and winter monsoon winds

As already indicated, the wind fields shown in Fig.3A-C are largely characterized by season to season variations. A comprehensive analysis of the same is presented here. Although mean monthly winds are shown in Fig.3A-C, it may be difficult to make a proper analysis based on these figures if one tries to sum up overall basin scale variabilities. Therefore, the observed joint probability density for u and v components of wind at 1 m/s interval is computed (Jenkins and Watts, 1968) for both the Arabian Sea and Bay of Bengal based on the IMD data. Contour diagrams for the joint probability distributions from January to December are shown in Fig.4A-D. The outermost contour has the lowest probability value of 0.002 and the contour interval is also 0.002. Thus, the innermost contour has the maximum probability value which may vary from month to month. Probability density values for the respective u and v components indicate their duration of occurrence in a given month (total probability = 1.0). For example, during the month of April (Fig.4B), the lower wind speed values have the maximum probability. The probability distribution reveal that the winds during April are highly variable in the Arabian Sea as well as the Bay of Bengal. The reverse is the case during July as the maximum probability is associated with higher winds though there is some variation in the wind pattern between the Arabian Sea and Bay of Bengal. Seasonal variations in the winds based on both the mean monthly wind fields (Fig.3A-C) and the monthly joint probability distributions (Fig.4A-D) are discussed below.

During the winter monsoon (November through February), the north-east trade winds blow outwards from the Asiatic high pressure region to the

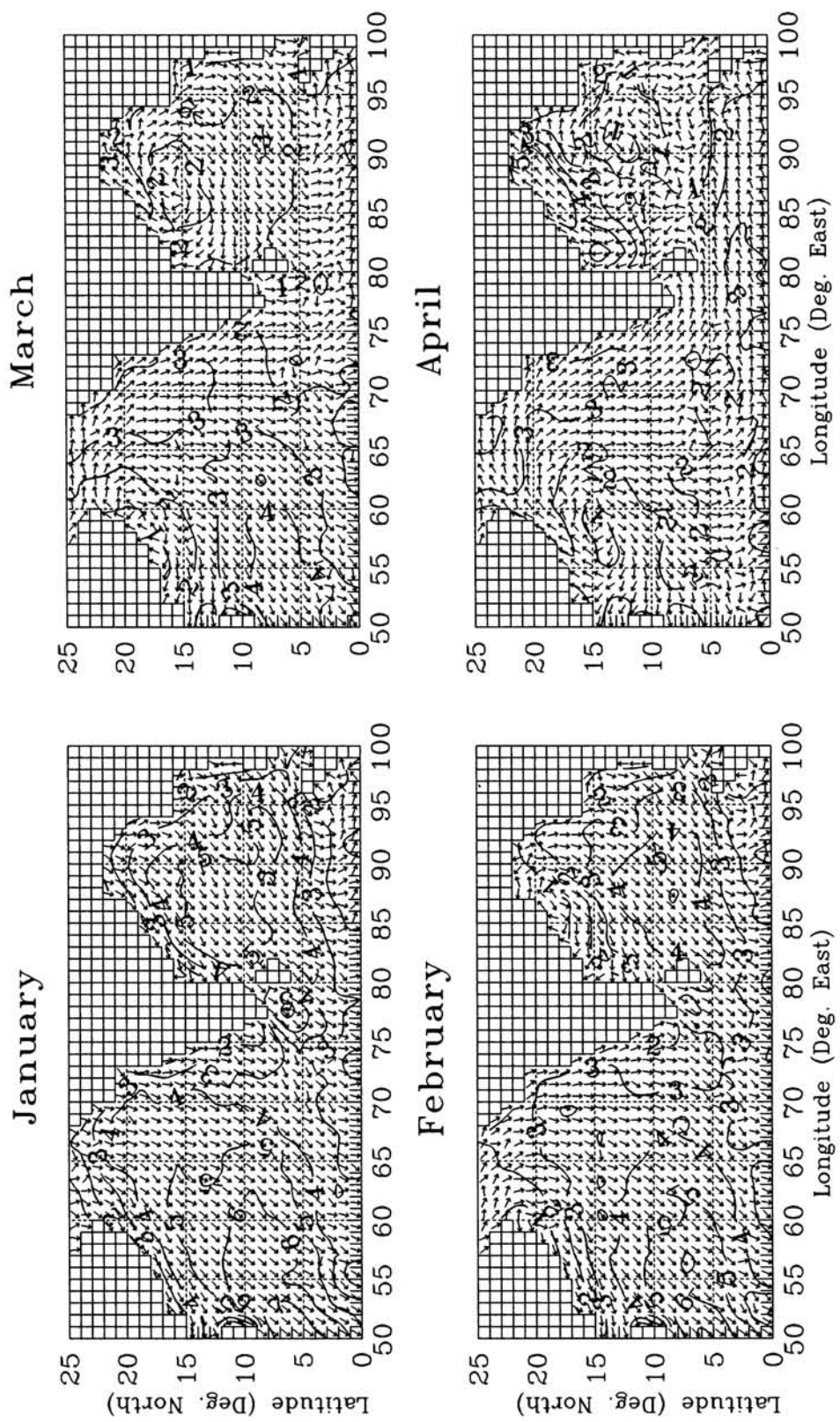


Fig.3A Mean surface wind fields for Indian Seas
(Contour interval 1 m/s).

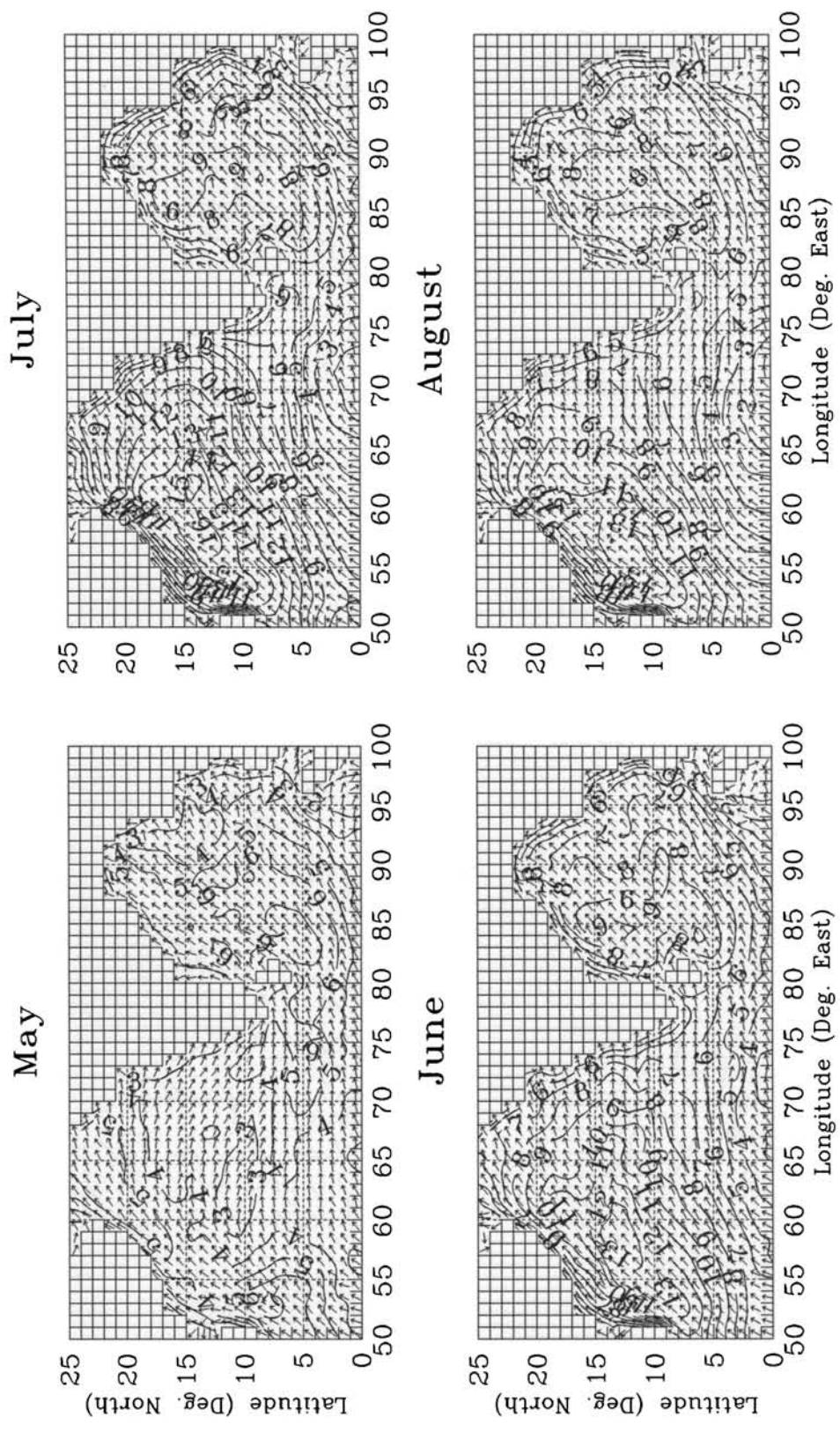


Fig.3B Mean surface wind fields for Indian Seas
(Contour interval 1 m/s).

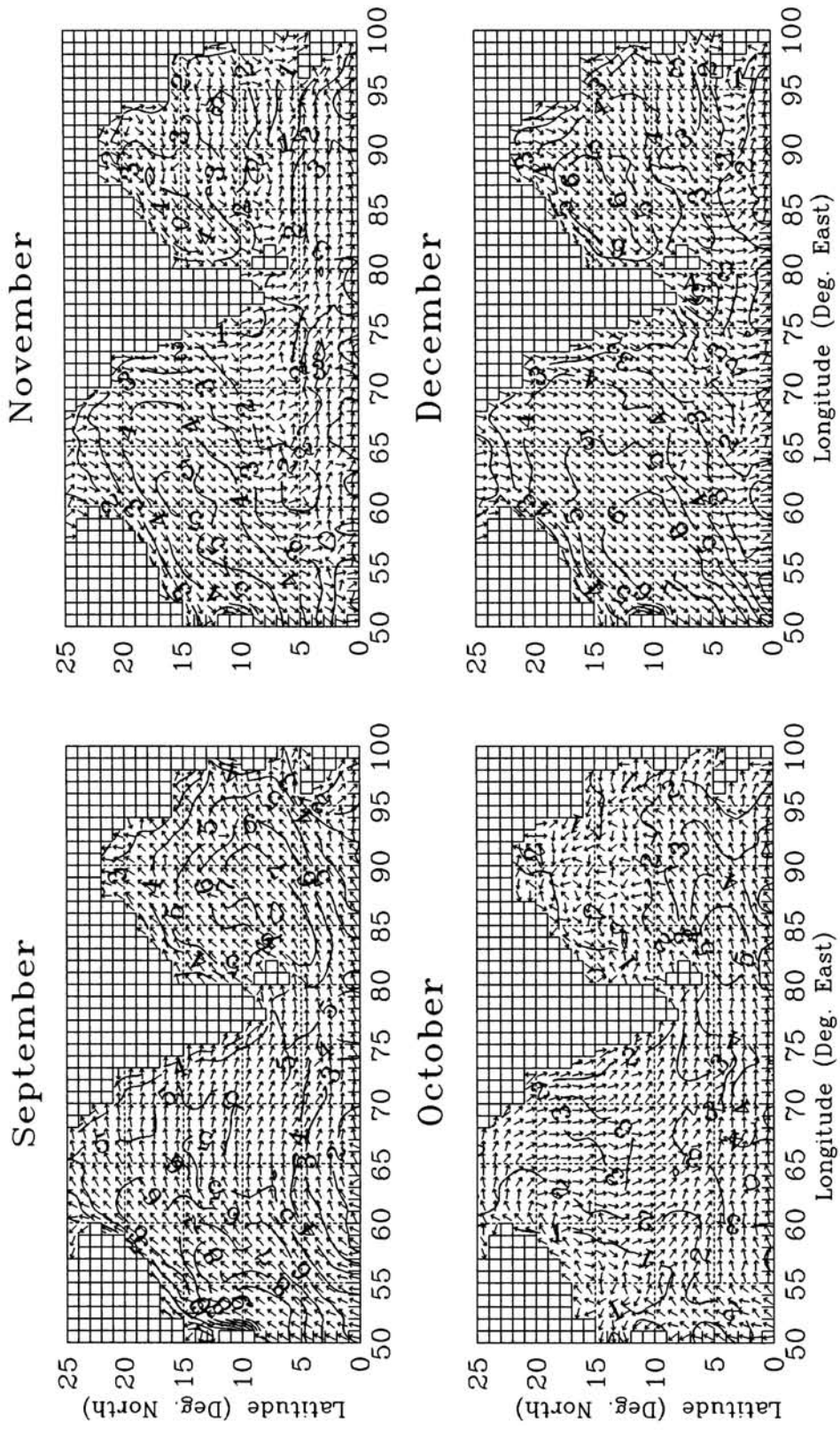


Fig.3C Mean surface wind fields for Indian Seas
(Contour interval 1 m/s).

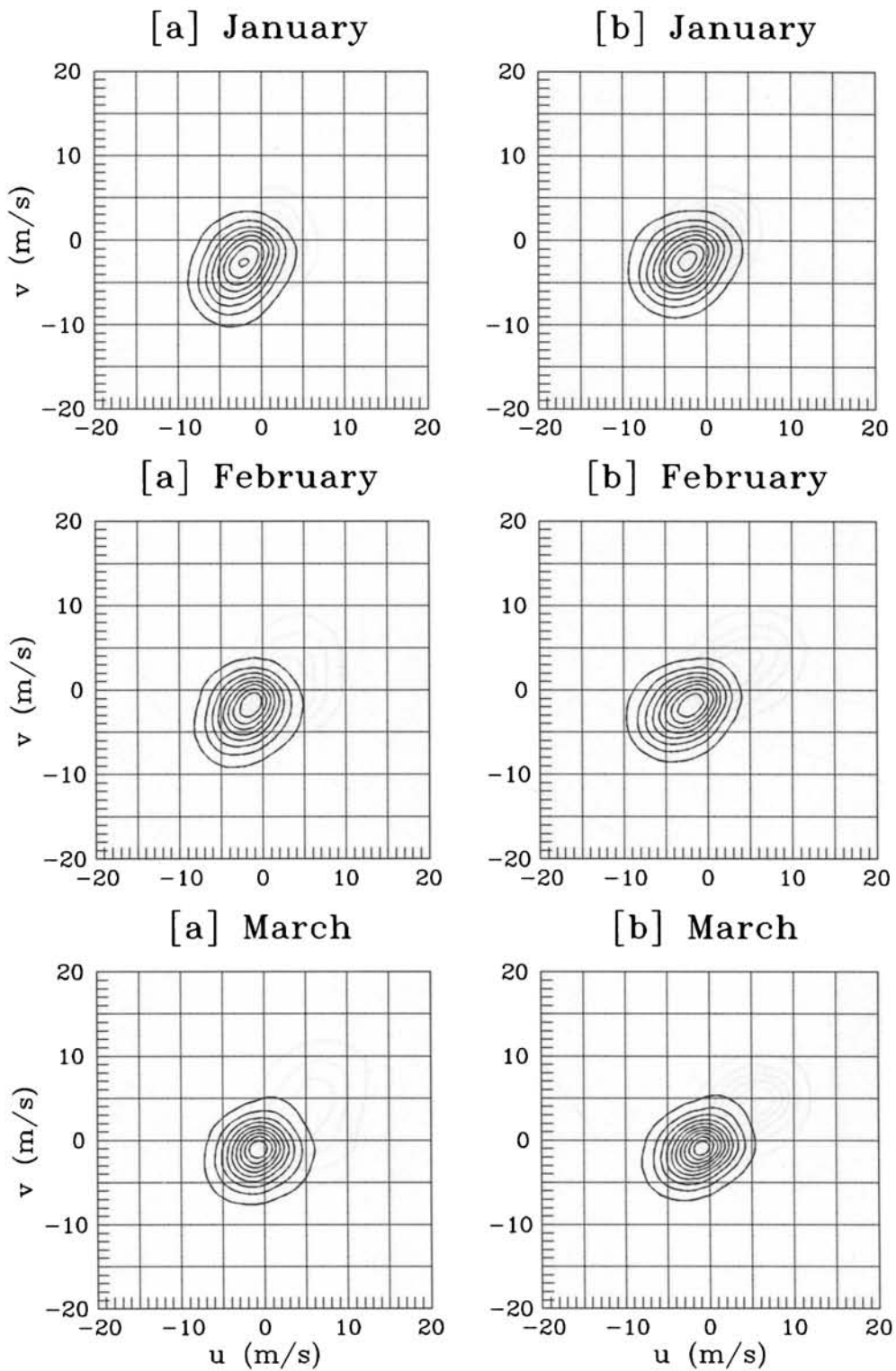


Fig.4A Observed joint probability distribution for u & v components of winds. [a] Arabian Sea, [b] Bay of Bengal. The value of lowest contour (outermost) and contour interval are 0.002.

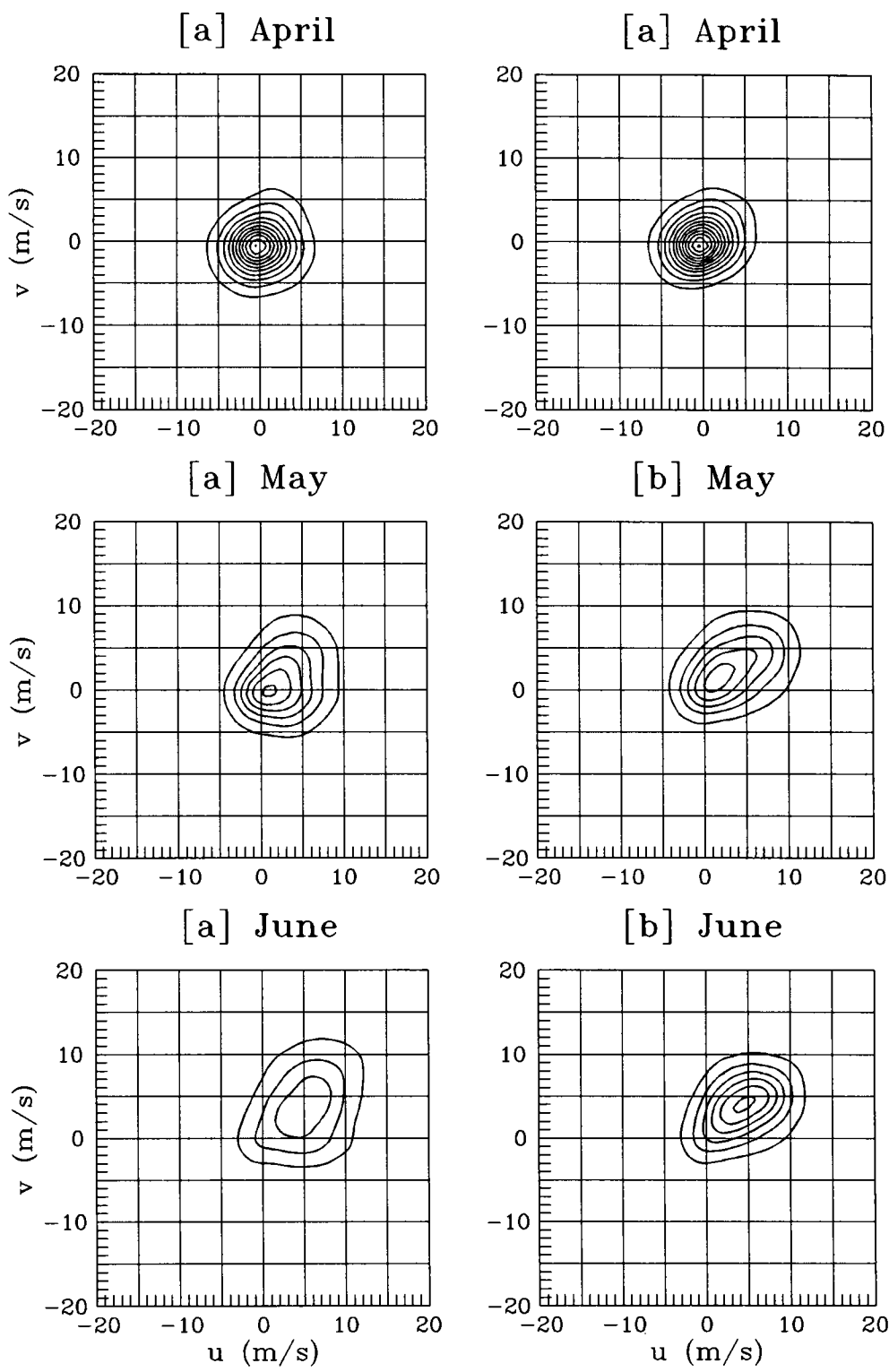


Fig.4B Observed joint probability distribution for u & v components of winds. [a] Arabian Sea, [b] Bay of Bengal. The value of lowest contour (outermost) and contour interval are 0.002.

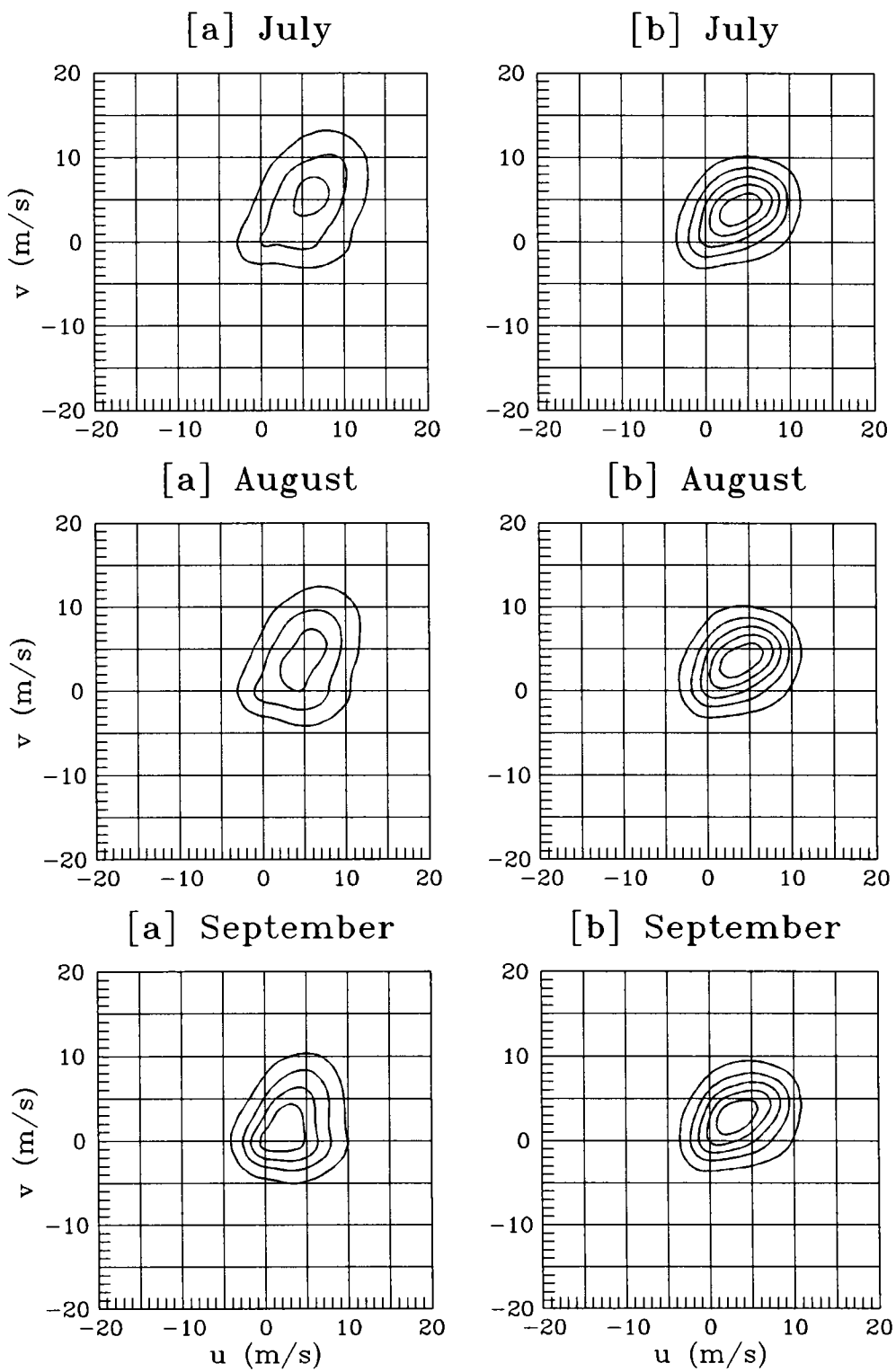


Fig.4C Observed joint probability distribution for u & v components of winds. [a] Arabian Sea, [b] Bay of Bengal. The value of lowest contour (outermost) and contour interval are 0.002.

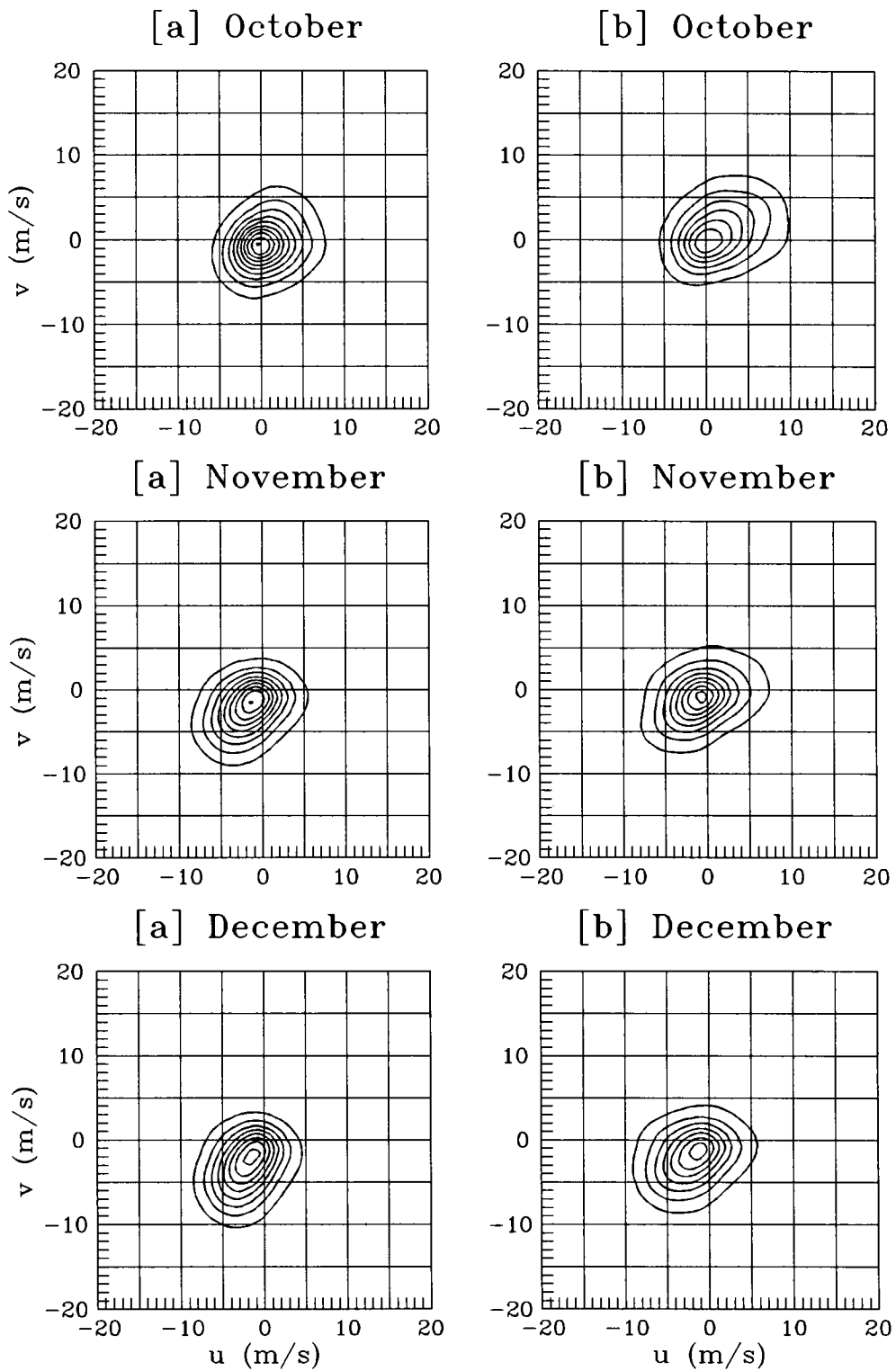


Fig.4D Observed joint probability distribution for u & v components of winds. [a] Arabian Sea, [b] Bay of Bengal. The value of lowest contour (outermost) and contour interval are 0.002.

Arabian Sea and Bay of Bengal (Hastenrath and Lamb, 1979). This is clearly seen from the spatial as well as joint probability distributions (Fig.3C & 3A; Fig.4D & 4A). The southward shifting of wind speed maxima is very prominent in the Arabian Sea compared to that in the Bay of Bengal (Fig.3C & A). The average wind speed over the whole of the Arabian Sea and Bay of Bengal remains higher (about 5.5 m/s) during December and January compared to the rest of the winter monsoon months. Fig.4D & 4A reveal that the overall wind pattern during December to February remains the same for the Arabian Sea and Bay of Bengal. However, during November the northeast component remains stronger in the Arabian Sea compared to the Bay of Bengal. During March and April, the winter monsoon wind patterns gradually weaken and evolve into the characteristic summer monsoon winds. Anticyclonic vortices develop over both the Arabian Sea and Bay of Bengal during April (Fig.3A). The resultant winds over the central Bay of Bengal are of low magnitude as the wind directions show maximum variability.

During the summer monsoon period, southwesterly and westerly winds sweep the Arabian Sea and Bay of Bengal. July is considered as the peak of the southwest monsoon during which mean wind speed reaches up to 16 m/s in the Arabian Sea (Fig.3B). The Bay of Bengal also experiences higher winds compared to the rest of the summer monsoon months. The wind direction during the summer monsoon (May through September) does not show much variations in the Bay of Bengal (predominantly southwesterly). Fig.4B & C show that the Arabian Sea winds gradually change their direction from May to September. The winds approach towards the Indian continent from west and north of northwest. The major reversal to Asian winter monsoon conditions occurs from September to October. The resultant winds in the Bay of Bengal become weak and variable while the Arabian Sea experiences wind blowing with a marked northerly component (Fig.3C). The wind speed minima are again characterized with variable wind directions with the reappearance of strong northeast winds over the Arabian Sea and the western Bay of Bengal by the month of November.

III.5.2 Monsoonal surface circulation

The mean monthly fields of surface currents obtained from the British Meteorological Office over two degree grids are shown in Fig.5A-C for January to December in a way similar to the mean monthly wind fields (Fig.3A-C). A brief outline of the monsoonal surface circulation is presented below.

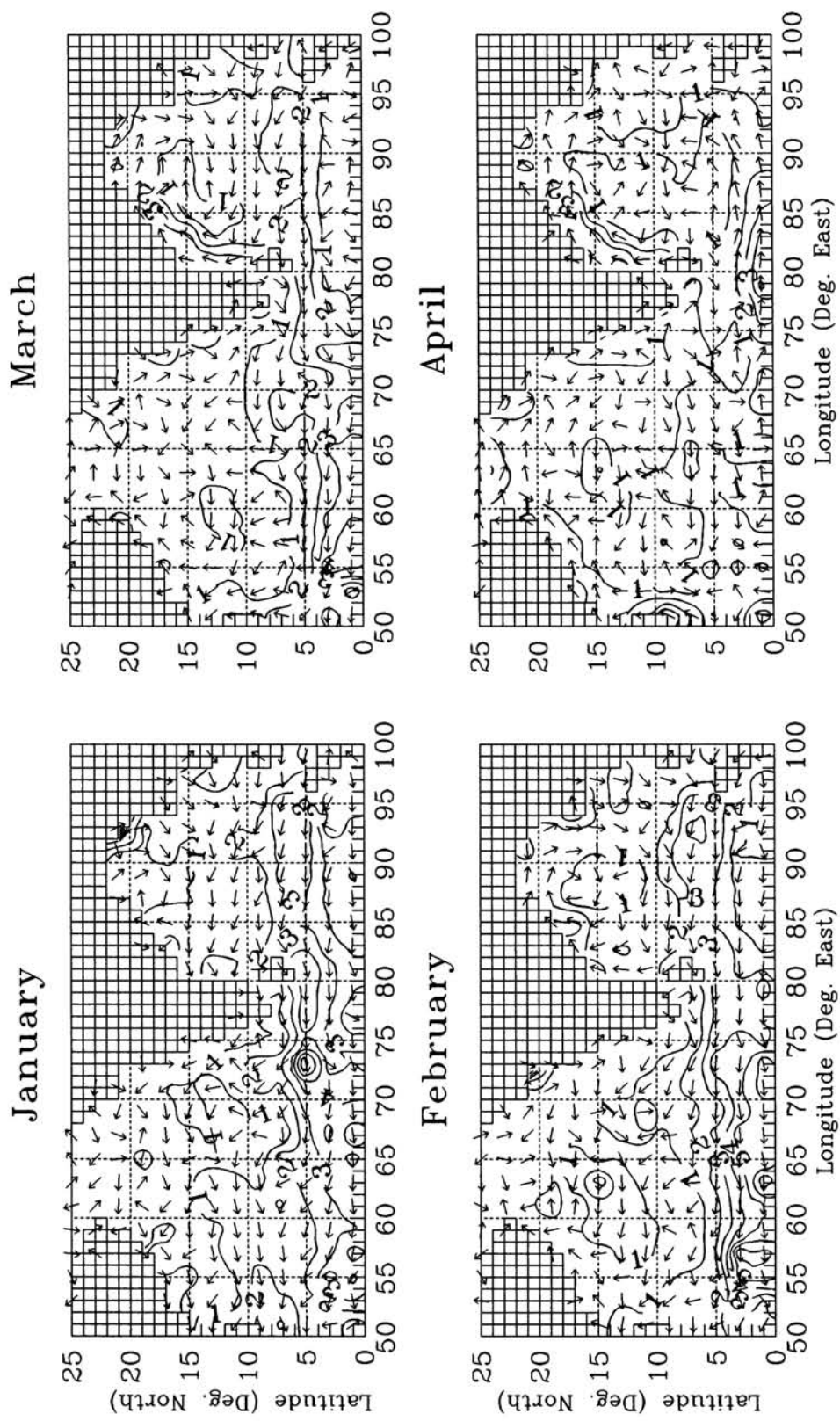


Fig.5A Mean surface current fields for Indian Seas
(Contour interval $\cdot 1$ m/s).

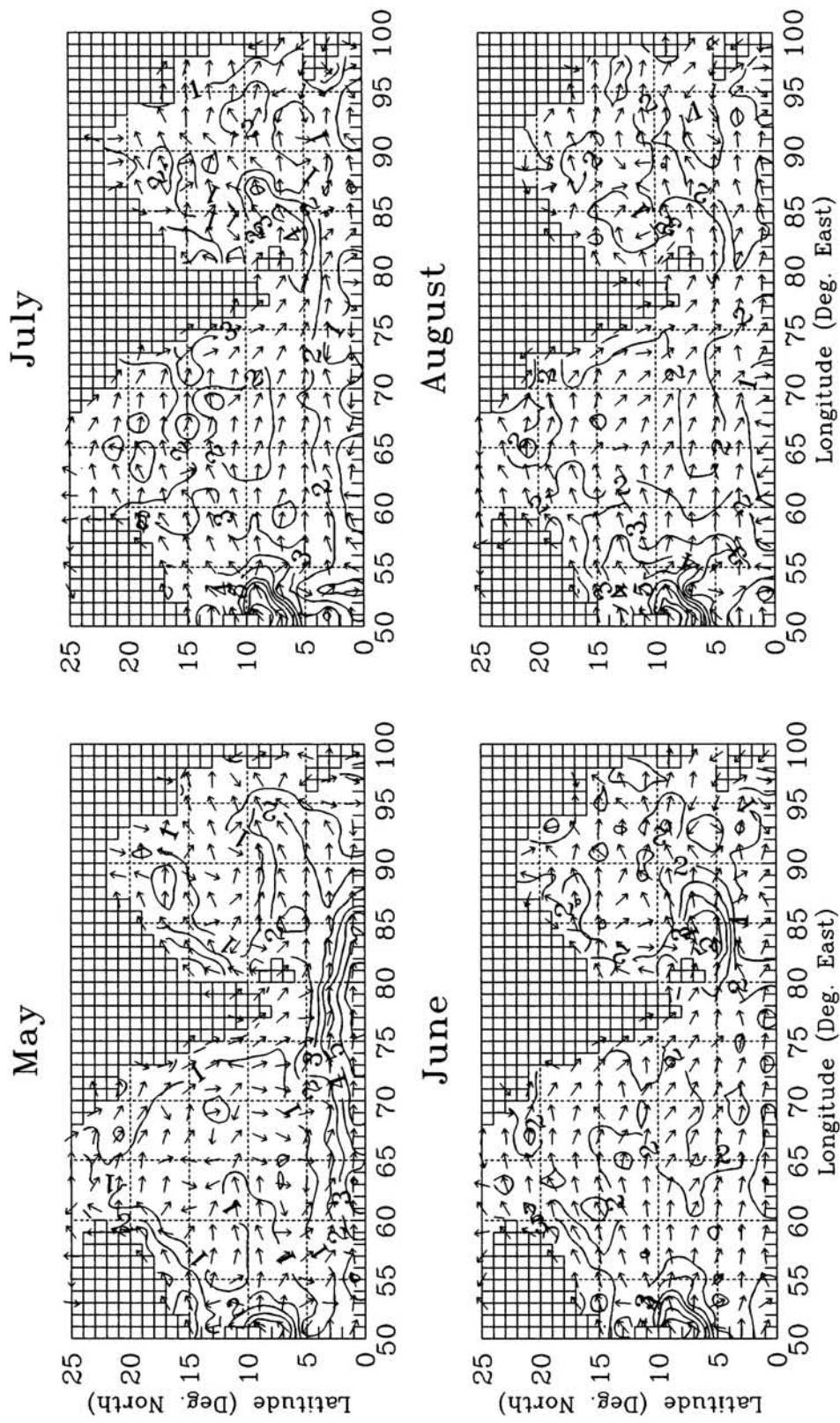


Fig.5B Mean surface current fields for Indian Seas
(Contour interval 1 m/s).

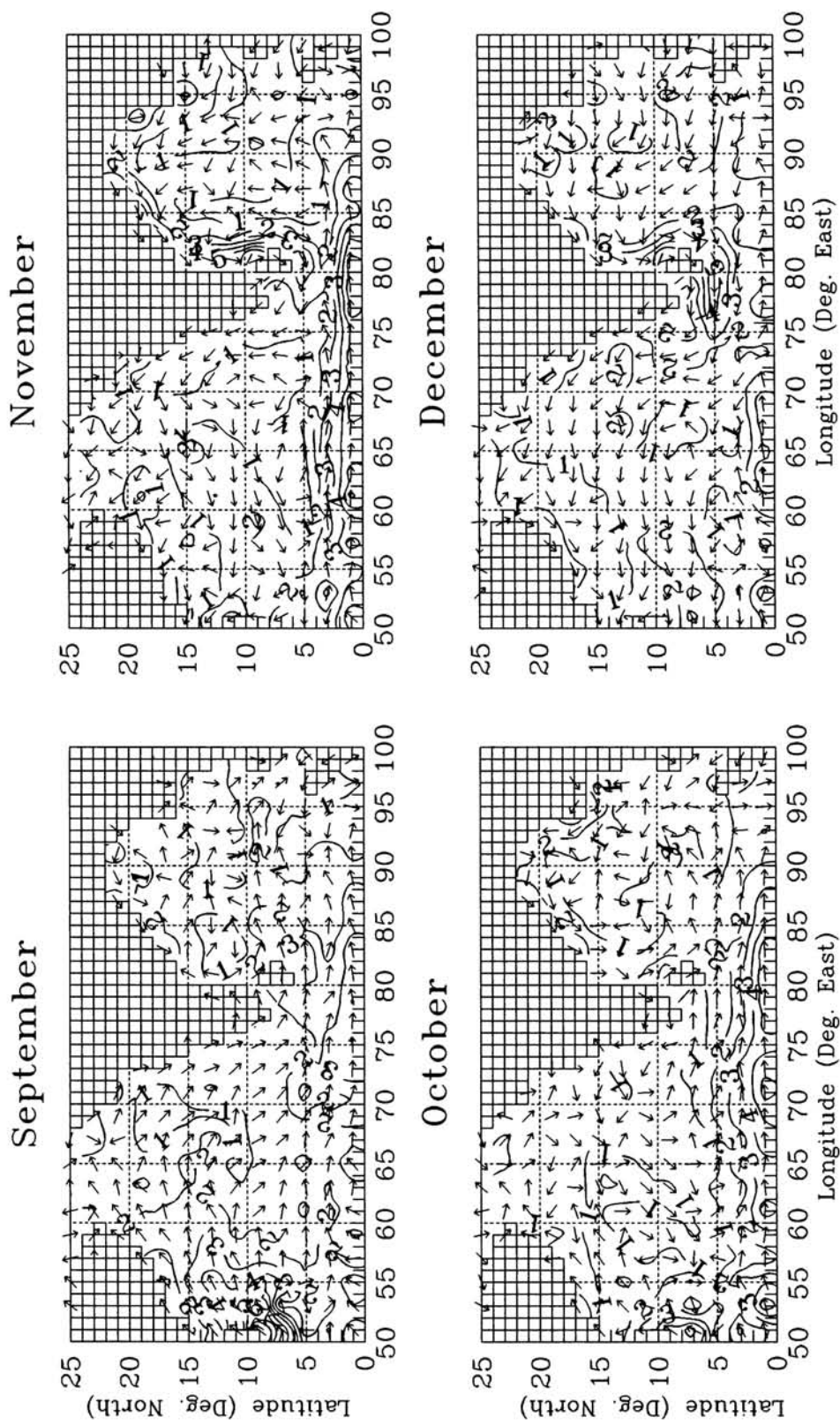


Fig.5C Mean surface current fields for Indian Seas
(Contour interval 1 m/s).

The monthly mean current fields shown in Fig.5A-C reveal that the observed surface circulation of the tropical Indian Ocean undergoes dramatic reversals with the monsoonal reversal of winds. During the northeast monsoon, a westward directed current known as the Northeast Monsoon Current appear to the south of the Indian subcontinent, currents with westward component are confined to the northern part of the Arabian Sea and Bay of Bengal during November and December. The flow is southwestward along the east coast and northwestward along the west coast of India. Eastward flow covers lower latitudes. In March and April, anticyclonic gyres develop in the Arabian Sea and Bay of Bengal in response to the anticyclonic vortices in the surface wind field (Hastenrath and Greischar, 1989). With the onset of the southwest monsoon (May to September), a clockwise gyral circulation dominates the open Arabian Sea. During this period, an eastward surface flow known as the Southwest Monsoon Current appears in the southeastern part of the Arabian Sea. This current is opposite in direction to the Northeast Monsoon Current. An intense surface current known as the Somali Current flows northeastward along the coast of eastern Africa (Hastenrath and Greischar, 1991). From June to September, the Somali current extends eastward and occupies most of the northern parts of the Arabian Sea and hugs the west coast of India with southeastward flow direction.

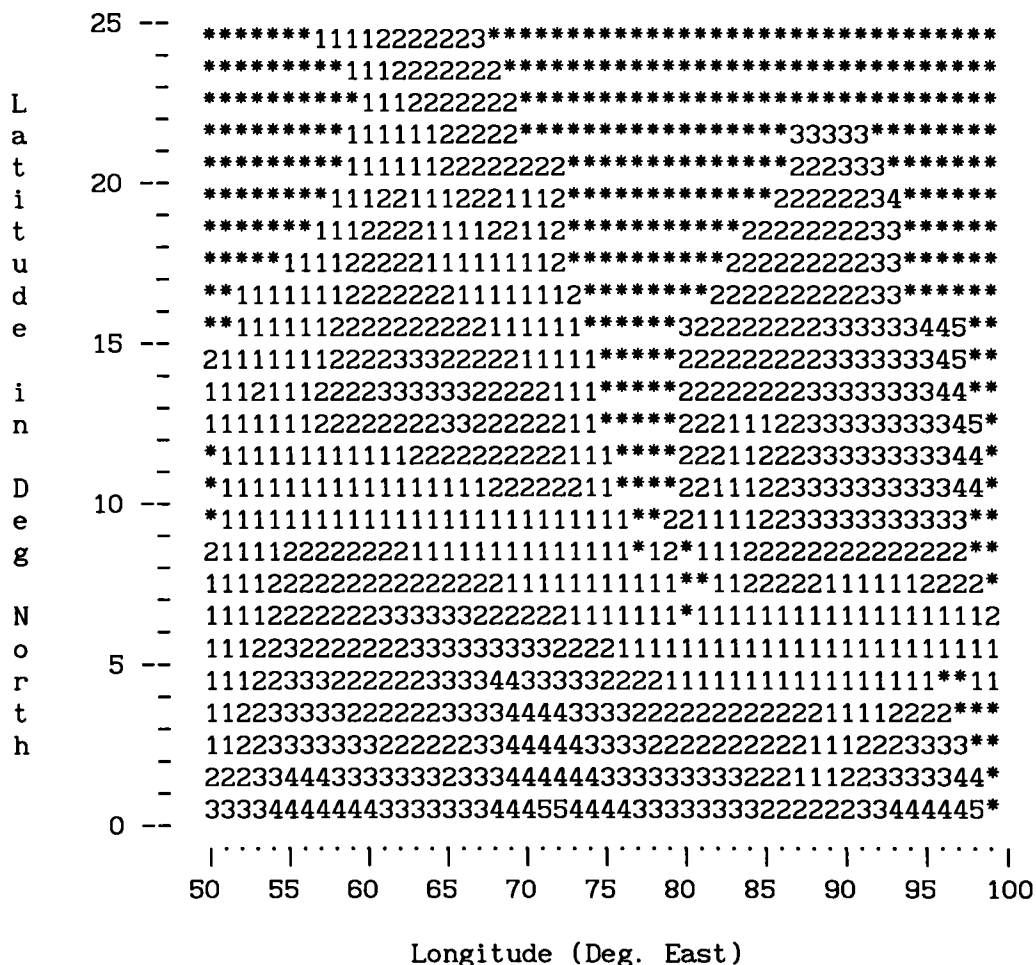
III.6 INPUT DATA SPECIFICATION FOR THE PRESENT STUDY

Ideally, the input data specification to a wave model must allow for the important physical processes of wave generation, growth, and dissipation to be appropriately represented in the wave model. Keeping this in view, a mean climatic year of wind is derived for wave climate simulation using statistical and probabilistic approaches as described below.

It was mentioned in Chapter-I that a mean climatic year of wind can be established by averaging historical data for the corresponding hours of wind observation or at least for each day of the year. However, this is not possible in the present study since the available data strength is insufficient. Therefore, based on the data obtained from IMD, monthly joint probability distributions (Jenkins and Watts, 1968) for u and v components of the wind are computed to establish wind variations for all the required grids. It is considered that each grid should have a minimum of 600 data

points for computing the monthly probability distribution as the data covers a period of ten years (1961-70) and there should be two observations available in a day (i.e. 10x30x2). However, the number of observations could reach close to 600 only for a few grids during some months. Hence the data from neighboring grids were considered to attain the required number of observations. The schematic diagram below shows the search radius for

JANUARY



The above schematic diagram shows the search radius (in degrees) for Indian Seas where each digit represents one particular sea grid (1x1 degree) and star represent land grids.

the grids which do not satisfy the above condition for the month of January. As an example, if the search radius is 1, equal number of observations from each of the adjacent grids distributed over ten years period (by selecting a suitable time window) are used to cater for the observations in short of 600. The total number of grids considered in this

case is nine (3x3). For a search radius of 2, data from 25 grids including the representative grid are considered and so on. Search radii for the other months were also estimated.

Fig.6 shows the observed joint probability distribution for two representative grids, one in the Arabian Sea (67.5°E , 12.5°N) and the other in the Bay of Bengal (87.5°E , 12.5°N) during the month of July. The figure indicates that the winds are slightly west of southwesterly in the Arabian Sea grid and exactly southwesterly in the Bay of Bengal grid. It also reveals that the winds are relatively steady in the latter case. Such distributions also give an idea about the period of occurrence for a given u and v component of wind in a month which will be utilized to derive probable wind variations.

In a given month, for any particular region in the Arabian Sea or the Bay of Bengal, wind variations can take place in a variety of ways and it is very difficult to determine the winds during extreme weather conditions such as cyclones and hurricanes. However, if one excludes extreme weather conditions, there are few simple rules which may apply for the weather variations in a given area. It is very likely that strong winds blow southwesterly over long distances in the open Arabian Sea during the month of July. Irrespective of the month and region, winds of low magnitudes vary more in direction compared with winds of high magnitudes. It means that steadiness increases with increase in wind speed. Variations in wind speed can be associated with changes in direction, which can be either clockwise or anticlockwise. If the wind speed goes on increasing, it should start decreasing after it reaches a maximum. Likewise there are a number of thumb rules which can be easily adopted. The present study adopts the most simple pattern of wind variation discussed below. This should fairly represent the mean climatic year of wind for the respective grid areas.

The observed joint probability distributions of wind anywhere in the Indian Seas reveal that the winds more or less vary in speed as well as direction throughout the year although the magnitude may be different from month to month. A simple schematic representation for estimation of winds based on the observed joint probability distribution of u and v components is shown in Fig.7. In this study, the observed wind variations during a month are divided into four phases to take care of the growth and decay of waves. In PHASE-I, it is assumed that wind speed gradually increases from its minimum to the maximum value following the observed probability

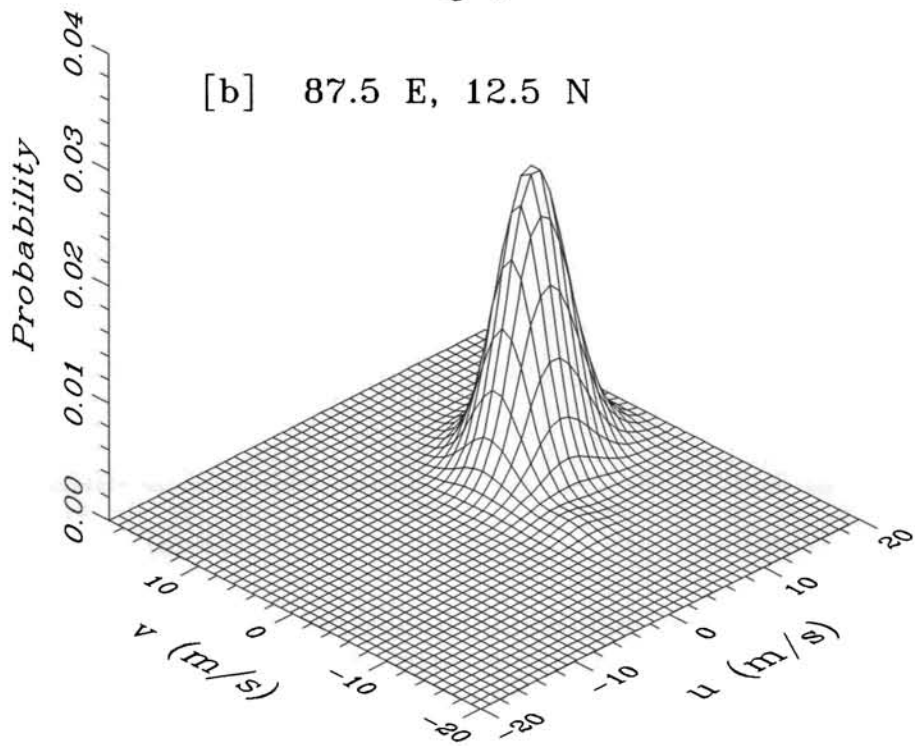
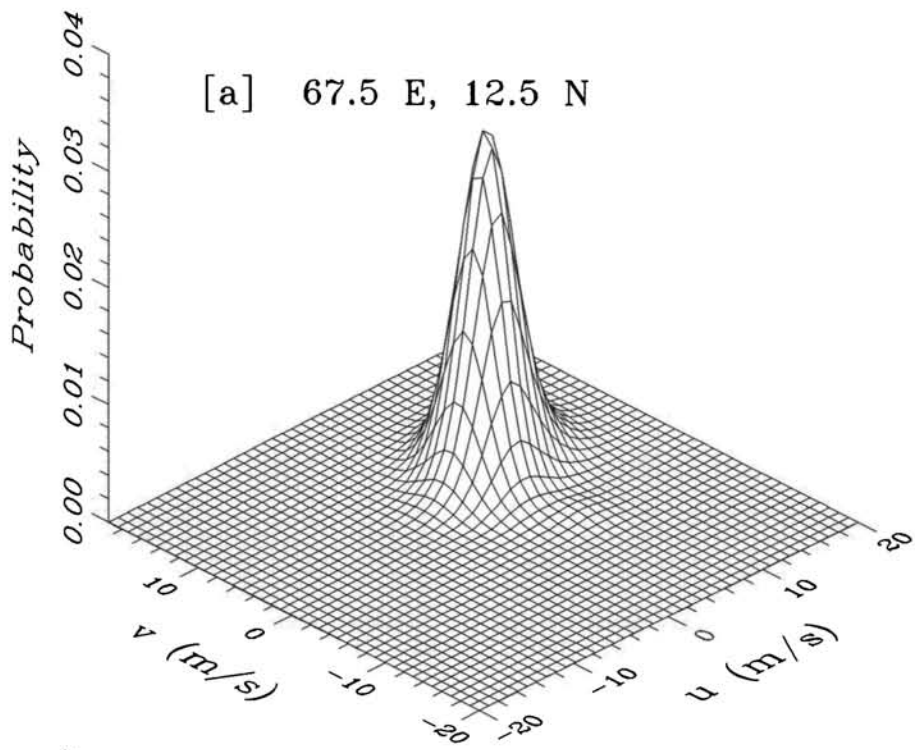


Fig.6 Observed joint probability density for u and v components of wind during July.

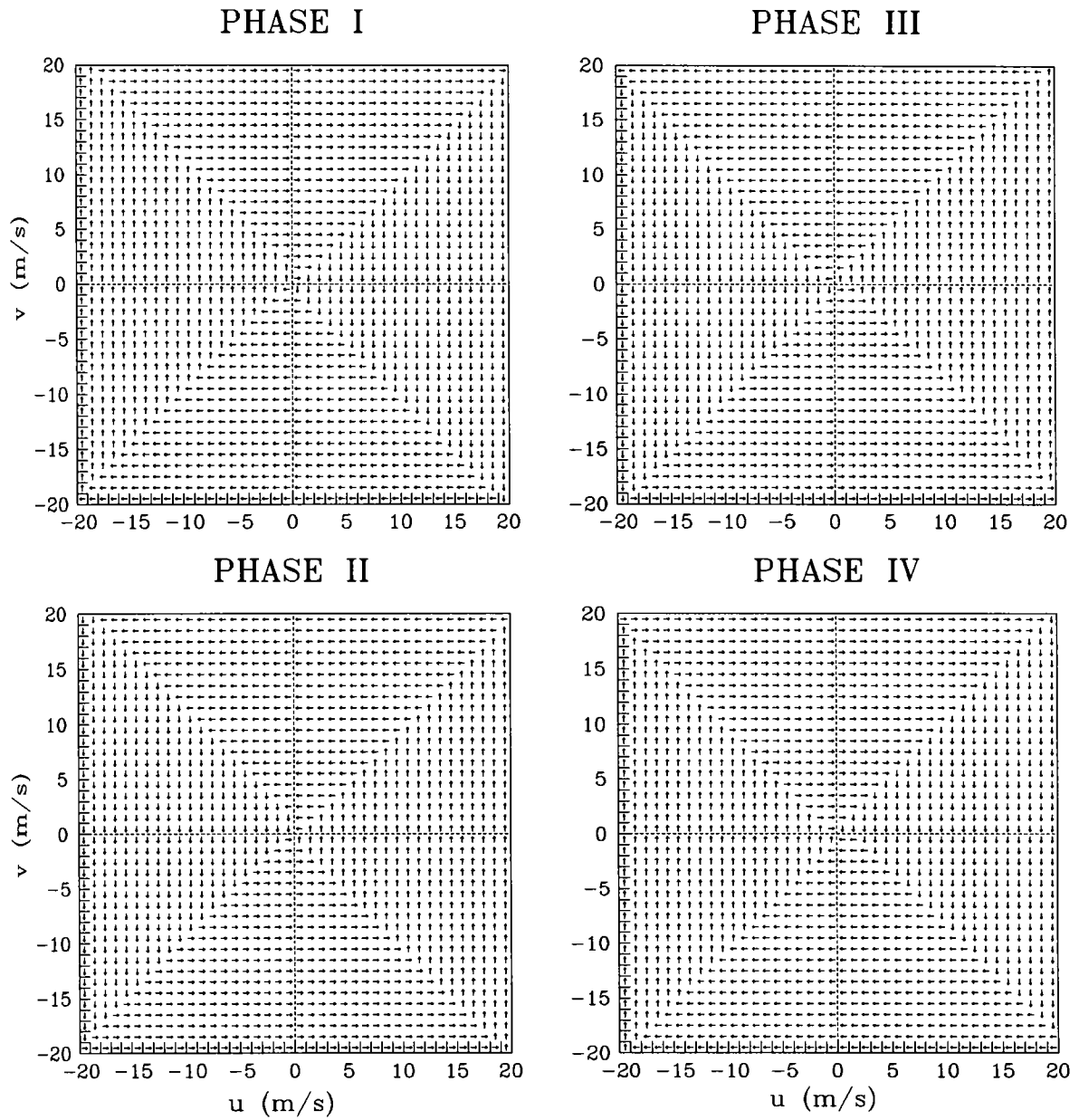


Fig.7 Schematic representation for wind estimation from observed joint probability distribution of u and v components (Arrows indicate the mode of wind shift).

distribution and the change in wind direction is clockwise. The arrows indicates the mode of wind shift which starts with $u=0.5$ m/s and $v=0.5$ m/s. Once the wind reaches its maximum, its magnitude starts decreasing in the opposite direction as shown by the arrows in PHASE-II. PHASE-III and PHASE-IV also follow a similar pattern of wind shift as in the cases of PHASE-I and PHASE-II, with the change in wind direction in PHASE-I being anticlockwise.

In a given month, particular u and v components of wind persist for a duration which is directly proportional to the probability density. Hence, following Fig.7 and walking in the direction of the arrows, winds are estimated for all the required grids based on the probability distributions for January through December. As the probability distributions were computed based on the ten years data from IMD, the estimated winds for establishment of mean climatic year are corrected using the sixty-year mean wind fields shown in Fig.3A-D. The correction is made by multiplying the u and v components of wind uniformly by a factor (C.F.) indicated below:

$$C.F. = \frac{\bar{X}_{60}}{\bar{X}_{umcy}} \quad \dots 3.5$$

\bar{X}_{umcy} is the mean of the uncorrected winds. The corrected winds for the mean climatic year is shown in Fig.8A & B for two selected grids. Each of these figures consists of twelve stick plots representing the gross specification of the temporal wind variation from January to December. Plot for each month contains 144 representative wind sticks that are equally spaced in time. Fig.8A & B give an idea on the general wind pattern for all the months in a year for the two selected grids. As the winds are estimated for all the grids, there are 144 representative wind fields available for a given month. These winds are used as input to drive the wave model. Based on the wind input time step, the number of wind fields can vary accordingly. In the present study, the wind input is provided to the model for 72 hours period representing a month at half an hour interval. Further discussion on this is done in Chapter-IV. However, there is no restriction that only 144 wind fields are to be used as input. The present study restricts the surface current input to representative monthly mean values.

67.5 E, 12.5 N

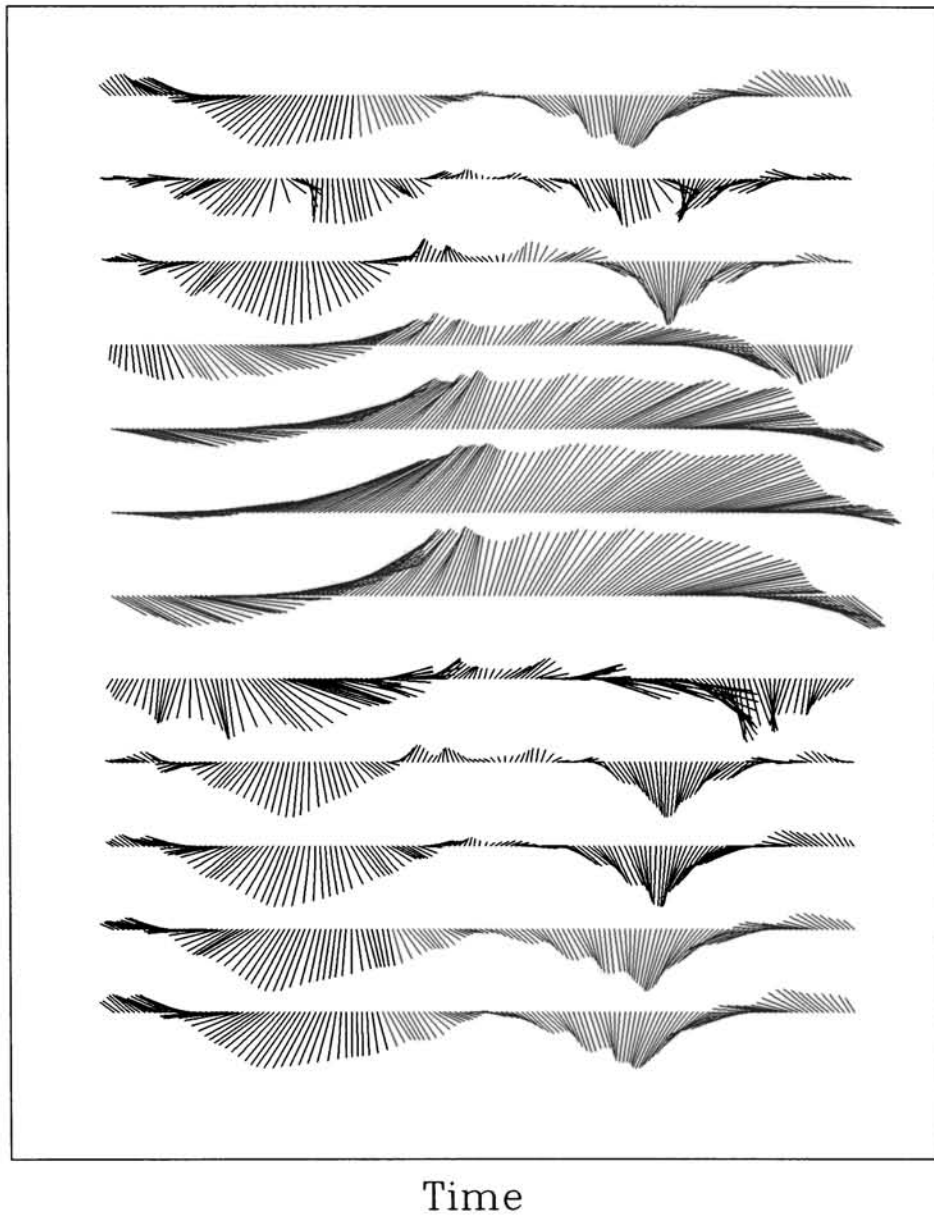


Fig.8A The mean climatic year of winds (January:bottom & December:top).

87.5 E, 12.5 N

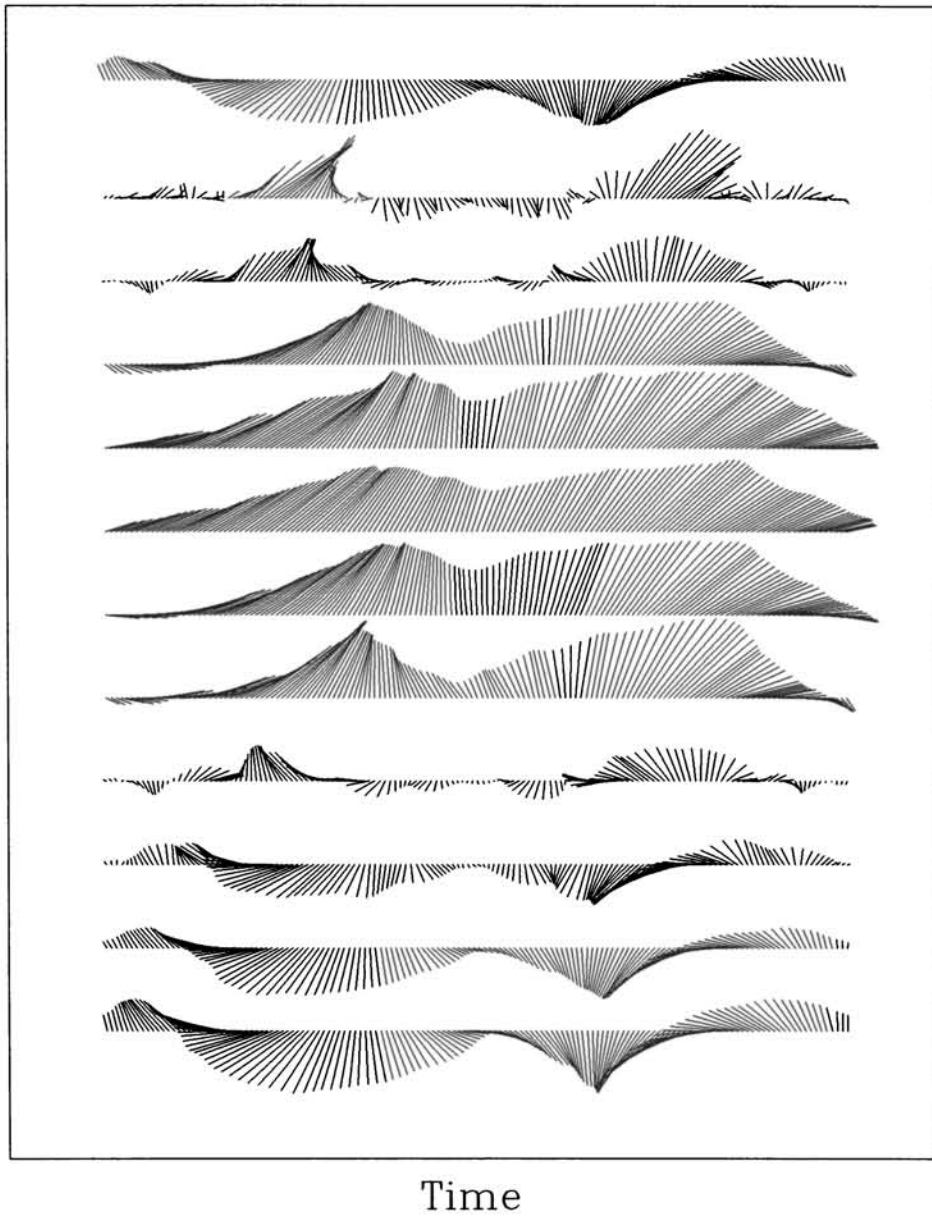


Fig.8B The mean climatic year of winds (January:bottom & December:top).

The input wind specifications to the wave model (e.g., Fig.8A & B) clearly demonstrate the most general pattern of wind variations during different months of the climatic year of winds. They reflect the seasonal reversal of winds between the boreal winter and the boreal summer. Fig.8B show that, the winds are strong and steady during May to September but variable during March. Normally, deep depressions and cyclones occur in the Bay of Bengal during October and November. Thus abnormally strong winds lasting for about a week or more may be noticed during October (Fig.8B). By and large, these winds estimated using the statistical and probabilistic approaches follow the general patterns of wind variation during a year and the same will be utilized for the present simulation experiment.

CHAPTER IV. SIMULATION OF WAVE CLIMATE

IV.1 INTRODUCTION

Simulation is the process of designing a model of the real system, conducting experiments for the purpose of understanding the system behavior, and evaluating various strategies within the boundary conditions that are imposed for executing the modelled system. In fact, real world systems are often complex and composed of several subsystems and their interactive components. The same is the case with the evolution of wind-induced surface gravity waves in the ocean. In this study, a well established wave model has been adopted. Although the model represents the physics of the wave evolution in accordance with our knowledge today, there can be a number of potentially important effects which are not included in this model. Air-sea temperature differences, particularly under highly stable situations modify the energy input from the wind (Cardone, 1969). The effect of rain may be significant in certain circumstances. The most trivial effect is the attenuation produced in a heavy downpour resulting in the disappearance of short gravity waves. The attenuation coefficient is the product of rain fall rate and the wave number (Phillips, 1987). In addition, rain may also modify the effective mean wind profile. These are some of the examples which are to be considered in the wave prediction models used for operational wave forecasting purposes. In the present study the above mentioned effects seem to be less important as we are dealing with the problem of wave climate simulation based on the mean climatic year of winds derived using long-term historical data. Here the main interest is to estimate monthly and seasonal variability of the sea-state for the region of interest.

The following sections will summarize: i) the details of wave model implementation, ii) the various strategies that are adopted in specifying inputs to the model and evaluation of simulated results within the specified boundary conditions, and iii) compilation of simulated outputs.

IV.2 WAVE MODEL IMPLEMENTATION

The presently used wave model 3g-WAM was originally developed at Max-Plank-Institut fur Meteorologie in Humburg, Germany by S. Hasselmann with the help of P. Janssen, G. Komen, L. Zambreski and H. Gunther (Gunther et al., 1992). The model has been installed at about 35 institutions world

wide. Naval Physical and Oceanographic Laboratory (NPOL) is one of the users of this model. The model code designed for the CRAY supercomputer with UNICOS operating system is suitably modified by the author at NPOL for DOS & WINDOWS platforms. Incidentally, this is the first attempt to implement 3g-WAM for the Indian Seas (Swain et al., 1995).

IV.2.1 Regional grid system

In the present study, 3g-WAM has been implemented for wave climate simulation for the Indian Seas (0° - 25° N, 50° - 100° E). The regional grid system for this region is shown in Fig.9. The land grids are indicated with solid squares. It may be noted that the regional grid system as shown in Fig.9 has only one open sea boundary to its south (0° Latitude) and there are a few sea grids to its west. Most of the wave energy that may propagate out or into the area under study is only across the southern boundary. However, both the southern and western boundaries of the grid system are extended up to 10° S and 40° E respectively to take care of advection. The sea grids and the open sea boundary grids are indicated with plus (+) and cross (x) symbols respectively. The grids which are indicated with symbols other than "+" and "x" (plus with circle around, hollow plus, and stars) also represent open sea grids. There are 915 open sea grids out of which 570 grids belong to the Arabian Sea and the rest 345 belong to the Bay of Bengal. The total number of grids between 40° and 100° E, and 10° S and 25° N is 1540 as there are 625 additional open sea boundary grids considered outside the regional grid system.

IV.2.2 Input and output specifications

The input data which are supplied to the wave model are the estimated mean climatic year of winds and the mean monthly surface currents as discussed in Chapter-III. Fig.3A-C and 5A-C show the mean monthly wind and surface current fields only for the region between 0° and 25° N latitudes and 50° and 100° E longitudes, data are also available for the open sea boundary grids shown in Fig.9. The mean monthly surface current data are supplied to the wave model at each grid point for all the model grids only once for a representative month. However, the estimated mean climatic year of winds are provided at each input time step for all the grid points of the regional grid system but the open sea boundary grids are provided with only the sixty-year mean monthly values (H&L, 1911-70).

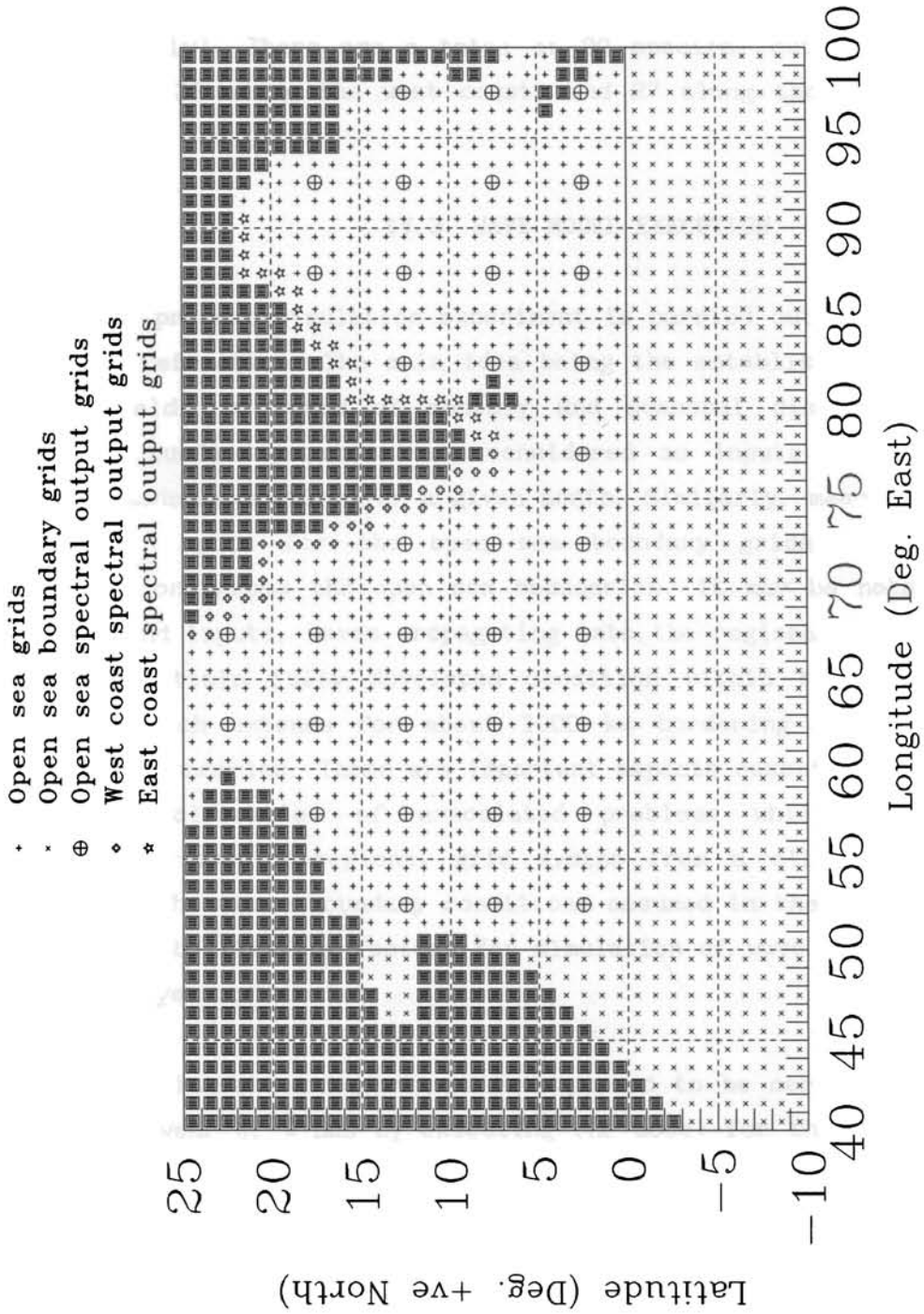


Fig.9 Model grid system for Indian Seas.

All the gridded outputs of the model as given in Chapter-II are stored at the end of each input time step while the spectral outputs are stored only for selected grids. The central grids of each $5^0 \times 5^0$ square boxes in the regional grid system are indicated in Fig.9 with the plus symbols (+) enclosed in a circle. These grids are the open sea spectral output grids. Spectral outputs are also stored for all the sea grids along the west and east coasts of India (shown with hollow plus symbols and stars respectively). There are a total of 90 spectral output grids, 35 in the open sea, 28 along the west coast, and 27 along the east coast of India (Fig.9).

IV.3 WAVE MODEL EXECUTION

The present simulation experiment is carried out for deep waters with current refraction. The main idea being the establishment of the climatic wave fields in terms of monthly and seasonal distributions, the mean monthly surface currents are considered as inputs which do not change during model execution for a given month. Similarly, mean monthly winds are used as inputs for the open sea boundary grids to cater for wave propagation across the open sea boundaries. It may be noted that for the above wind inputs, waves propagating into the regional grid system will be able to attain fully developed condition within the open sea boundary region which extends for about 1000 km bordering the southern and the western boundaries. These are important aspects essentially required in the gross specification of associated problems while dealing with the simulation over a regional grid system from a climatic point of view. However, the above boundary conditions assumed in the present study do not appear to be limiting factors for simulation of wave climate based on mean climatic year of winds.

The simulation experiment is supposed to be carried out for the full climatic year of winds by executing the model for the inputs covering the twelve calendar months of the year or 365 days. However, computer time can be saved significantly by reducing the duration of wind input appropriately. In doing so, care has been taken to achieve the desired level of accuracy for the simulated outputs. Instead of a 31 days model run, say, for the month of January, the model is executed only for 72 hours of wind input. This is done by reducing the time axis from 31 days to 72 hours keeping the wind inputs the same. This means that the winds that are shown in Fig.8A for one particular grid in the month of January are

considered as the winds that have varied for 72 hours duration, with each wind stick representing the mean over 30 minutes.

A three-days model run representing a month is found to be very appropriate in this simulation experiment which reduces computation times by a factor of ten. First of all, the estimated mean climatic year of winds which are to be used as inputs to the wave model will allow the waves to grow and decay in four phases so that it can satisfy the most general patterns of wind and wave variabilities often encountered in the field. During the first 18 hours, with the increase of wind speed, waves will grow from either zero sea-state (cold start) or the equivalent of the initial wind field. The waves will start to decay during the second phase as the winds gradually decrease for the next 18 hours. Towards the end of the decay phase, the winds again increase gradually for the next 18 hours (Phase-III) resulting in further growth of waves. During the last 18 hours, waves will again decay gradually with the withdrawal of wind. These are the four stages through which growth and decay of waves have been taken care of in this study. It may be noted that the growth of waves during the simulation continues for the period of 36 hours in two phases. Therefore, even for a wind speed of 20 m/s the waves will be able to attain the fully developed stage within a period of 18 hours since fetch is not a limiting factor. Similarly, the swell waves of 9 to 25s period either in the Arabian Sea or Bay of Bengal can propagate from one end of the of the regional grid system to the other in 72 hours. Moreover, a wave of 5s period can also propagate over 2000 km. Hence, a minimum of 72 hours model run representing a month does also satisfy the propagation of waves from the other generating areas within the Arabian Sea and Bay of Bengal.

Model execution is carried out for 72 hours of wind input at steps of 6 hours (total 12 model runs) for each of the twelve calendar months. The initial wave field was set to the fully developed sea following Phillip's spectrum. Normally, the initial winds are of low magnitudes. Therefore, the parameters of the wave spectrum are chosen accordingly to compute initial wave energy. The wind input, source integration, and propagation (spherical co-ordinates) time steps are set to 1800, 600, and 1800s respectively. The output time step for the integrated wave parameters for total sea and swell are set as 1800s. The spectra of total sea and swell were stored for every 3 hours. All the user inputs are given in Appendix-D (input Files: *.DAT). Since these are self explanatory, further discussions on the same are avoided here.

Fig.10 shows the evolution of the simulated wave spectrum for 72 hour of model run for one particular grid during the month of July. It is just an example and it is quite interesting to note that the spectra gradually grow for the initial 18 hours and decay for the next 18 hours. The same sequence is followed for the subsequent 36 hours. The peak of the spectrum gradually becomes sharper and the energy slowly shifts to the lower frequencies. During the decrease in winds, a secondary peak develops at the high frequency region although it is not very significant for this representative grid. By and large, Fig.10 reveals that the simulation results are in close agreement with the input winds specified to the wave model as discussed in Chapter-III.

IV.4 COMPILATION OF MODEL OUTPUTS

All the integrated wave parameters (Chapter-II) namely the significant wave height, mean wave direction, mean wave frequency, friction wind speed, friction wind direction, peak wave frequency, sea-state dependent drag coefficient, normalized wave stress, swell wave height, mean swell direction, mean sea direction, and mean swell frequency are stored for all the grids of the regional grid system for every 30 minutes interval. Thus there would be 144 output fields in a month. A complete analysis of all these parameters would not be practical in this study. Therefore, out of the twelve output parameters, only six of them namely significant wave height, significant wave period (inverse of peak wave frequency), windsea direction (mean sea direction), swell wave height, swell wave period (inverse of mean swell frequency), and swell direction (mean swell direction) are compiled and the monthly mean fields are estimated. Moreover, seasonal mean fields are obtained only for the significant parameters. The bivariate and cumulative distributions of significant wave height and period are also computed for both the rough weather (May-September) and fair weather (October-April) seasons in the Arabian Sea and Bay of Bengal. Lastly, the average wave spectra for a selected grid in the Arabian Sea are computed for the rough and fair weather seasons. Analysis of the model outputs will be presented in Chapter-VI.

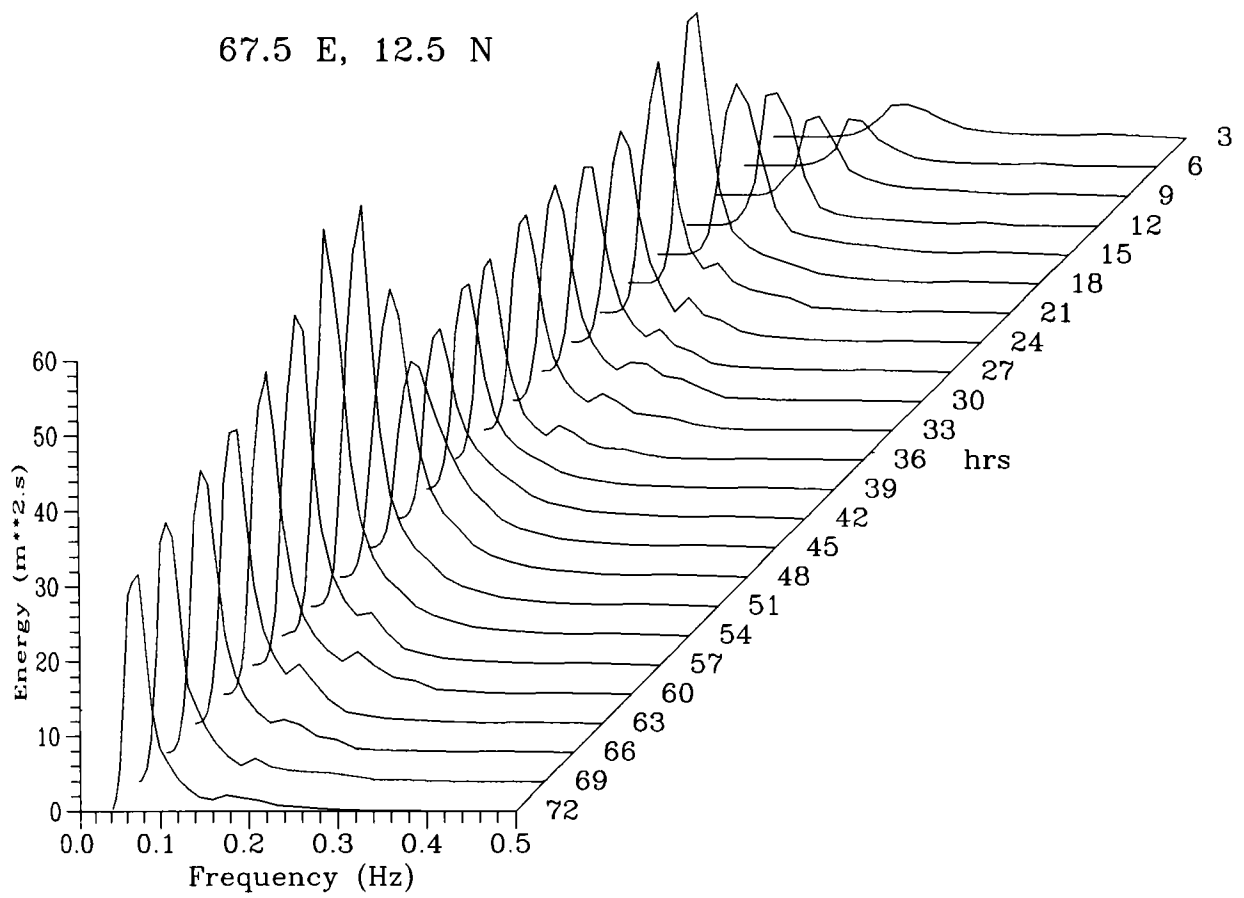


Fig.10 Evolution of wave spectrum for 72 hours of model run using estimated mean climatic wind fields for the month of July.

CHAPTER V. VALIDATION OF SIMULATED WAVE CLIMATE

V.1 INTRODUCTION

The most important requirement for an appropriate validation of the simulated wave climate of a region is the availability of adequate and reliable sea-state measurements. However, the present simulation experiment for the Indian Seas has been carried out in spite of limited deep water wave measurements which are of short durations. Certainly, it is not possible to have a detailed validation of the simulation results with the available wave measurements. Therefore, a qualitative validation of the wave parameters are carried out using available data namely ship-borne wave recorder data in deep waters (> 30m depth), ship-reported visually observed data and the GEOSAT altimeter data. The following sections deal with the validation of the simulated wave climate with these data sets.

V.2 VALIDATION USING VISUALLY OBSERVED WAVE DATA

In the absence of sufficient wave measurements using state-of-the-art equipment, attempt is made to compare the simulation results with visually observed mean monthly wave parameters. The visually observed wave data are available over long durations covering large part of the Indian Seas. Along with the wind data, the wave data used for the comparison were obtained from IMD for the same ten-year period (1961-70). In spite of the limitations as explained in Chapter-I, the ship-reported wave heights and periods are closer to the respective significant wave parameters obtained from instrumental measurements (Draper and Tucker, 1971). The distributions of windsea and swell data for the Indian Seas are shown in Fig.11A and 11B respectively. Fig.11A-B are presented in a way similar to Fig.2A-C. Table 4 shows the number of windsea and swell observations over the whole of the Arabian Sea and Bay of Bengal for different months. If we compare Table 4 with Table 3 of Chapter-III, the total number of windsea and swell observations reported by the ships of opportunity are about 60% and 40% respectively compared with the wind reports. Normally, ships do not report windsea direction. Thus windsea observations consist of wave heights and periods while swell observations include the directions as well. It may be noted that visually observed swell directions are reported to the nearest multiple of 10 degrees while there are only 12 directional bands considered for the wave model. The comparison between visually observed and simulated swell directions is not shown here. However, the model simulated mean

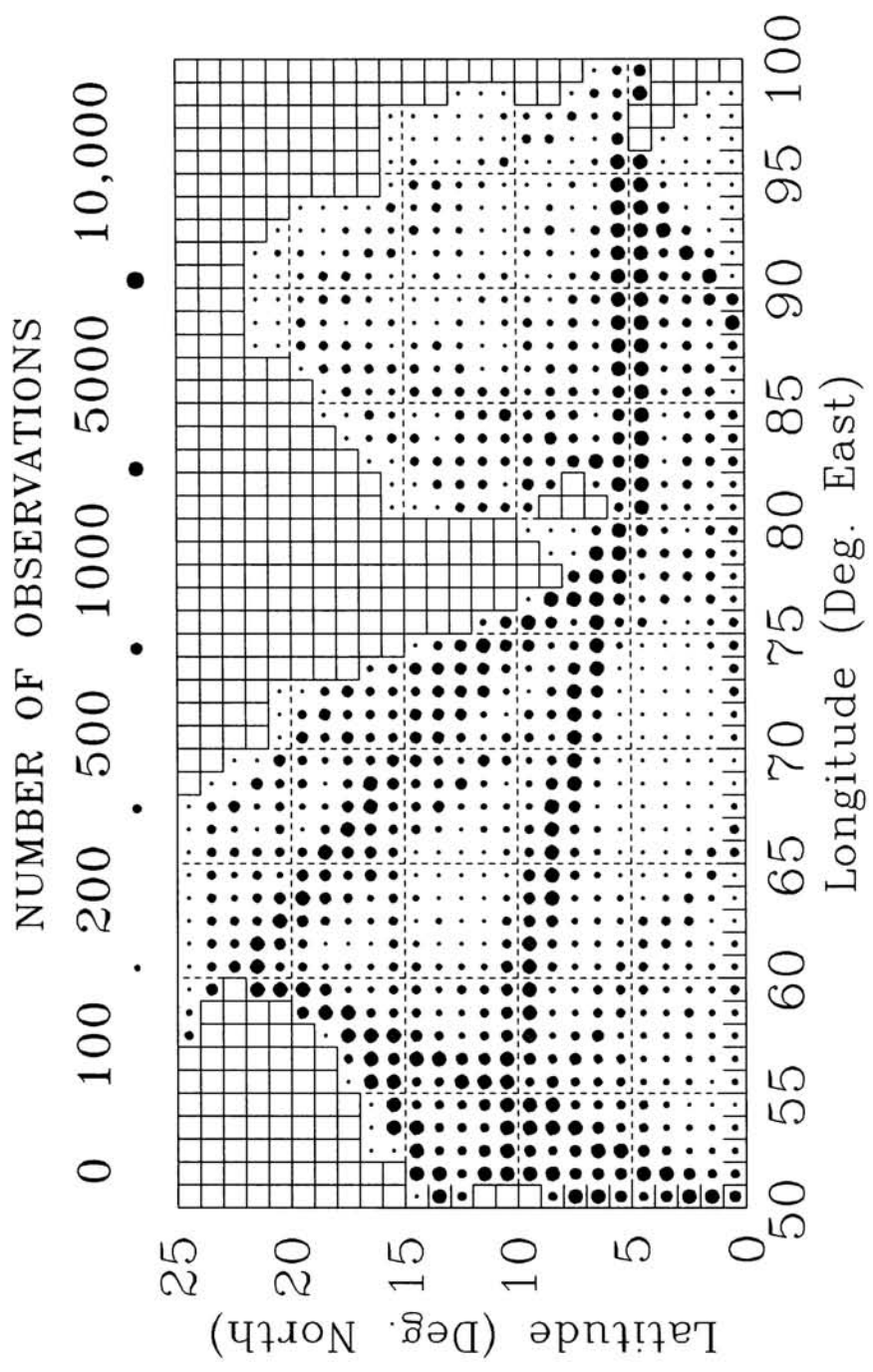


Fig.11A Visually observed windsea data distribution for Indian Seas (1961-70).

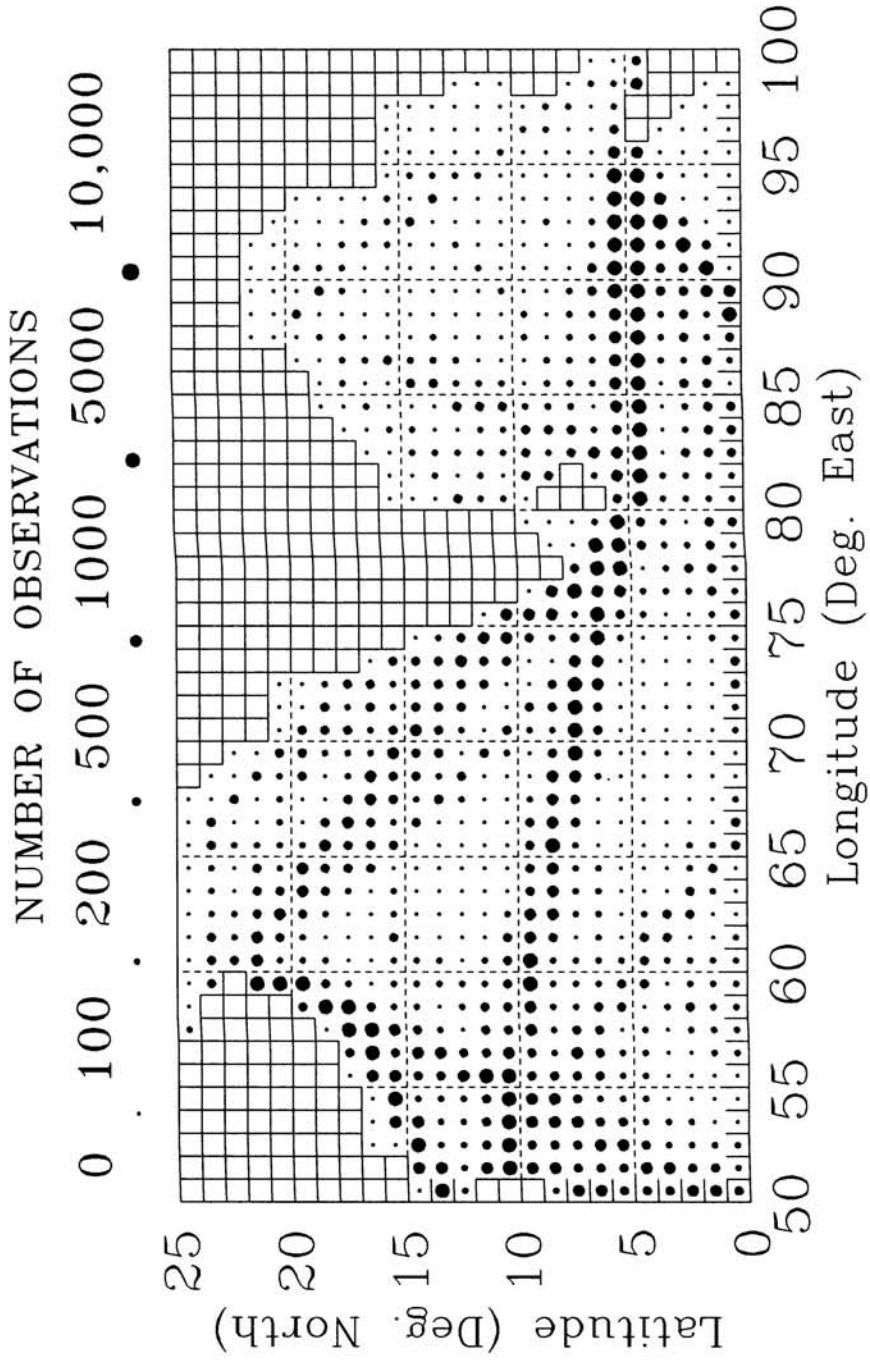


Fig.11B Visually observed swell data distribution for Indian Seas (1961-70).

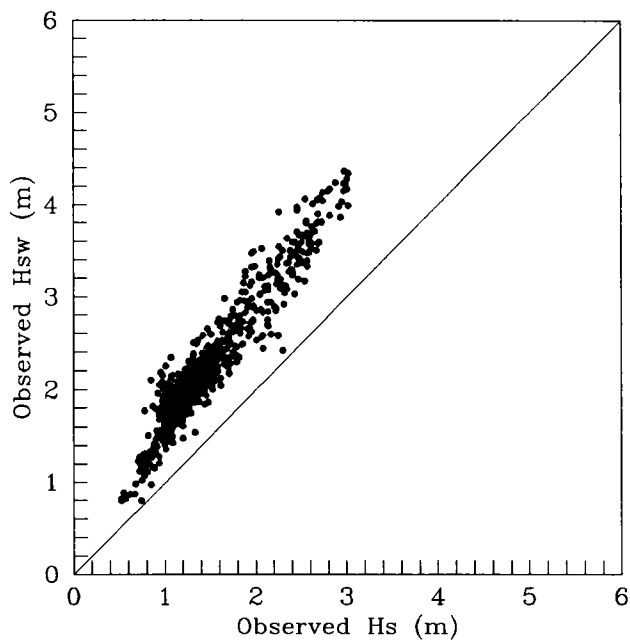
monthly swell directions have general agreement with observed wind distribution, especially in the strong wind zones which generate high waves. For comparisons between the observed and simulated height and periods, the swell observations that do not contain the directions are also considered.

Table 4. Number of visually observed windsea and swell observations obtained from IMD for the period 1961-70

	Month	Windsea	Swell
1	January	30,414	17,525
2	February	29,966	16,609
3	March	29,005	17,245
4	April	24,767	17,829
5	May	33,988	23,086
6	June	36,683	24,894
7	July	37,253	25,617
8	August	37,596	26,163
9	September	31,266	22,243
10	October	26,978	19,574
11	November	27,576	18,258
12	December	30,523	18,139
	Total	3,79,015	2,47,182

For the comparisons between the observed and simulated wave parameters, the mean monthly fields of visually observed windsea and swell heights are estimated over $1^{\circ} \times 1^{\circ}$ square grids. The grids having less than 30 observations are excluded for comparison. These mean monthly fields reveal that swell wave height reported by ships are mostly higher than windsea heights. Hence the mean monthly windsea and swell heights for different months are grouped into rough weather and fair weather seasons and the gridded information is shown in the form of scatter plots in Fig.12. The figure clearly indicates that swell wave heights are always more compared to windsea heights during both the seasons. Swell heights can exceed windsea height under certain circumstances especially during the fair weather season. Field measurements indicate the presence of swells during southwest monsoon period, but their magnitudes remain less unless the prevailing winds are relatively weak (Swain and Ananth, 1992). Baba and

[a] Rough weather season



[b] Fair weather season

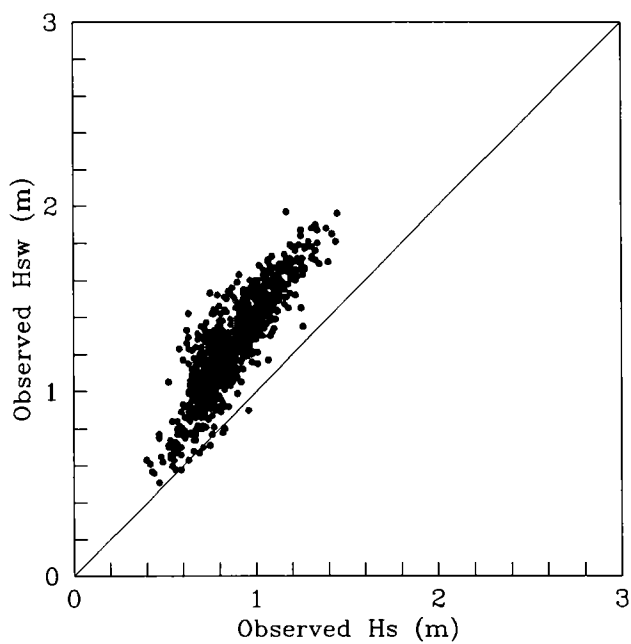


Fig.12 Visually observed significant wave height vs swell wave height for Indian Seas.

Harish (1986) have analyzed the wave spectra collected from some locations along the southwest coast of India which also reveals the presence of secondary peaks in the low frequency region. It is most likely that the mean swell heights during the rough weather season are lower than the mean windsea height for both the Arabian Sea and Bay of Bengal. But the reverse is the case in Fig.12. Probably, it becomes difficult for a visual observer to estimate the actual swell wave height as the windseas always ride on top of the longer period swells. Hence, there can be a bias during the estimation of swell heights onboard ship. It may also be noted that visually observed wave heights are reported to the nearest 0.5m. Hence, the error in the estimation can be less for higher wave heights.

Fig.13A and 13B show the observed versus simulated H_s and T_s for the Arabian Sea and Bay of Bengal during rough and fair weather seasons respectively. All the four plots in Fig.13A show that the visually observed H_s are generally low compared with the simulated H_s which exceeds 1.0m. One of the reasons for this may be that ships normally avoid rough weather conditions. During the fair weather season, visually observed H_s remain higher for both the Arabian Sea and Bay of Bengal compared to simulated $H_s < 1.0m$. The comparison between observed and simulated T_s reveals that the former is higher during rough as well as fair weather seasons in both the Arabian Sea and Bay of Bengal. In general, the visually observed T_s varies between 4 and 11s while the simulated T_s varies from as small as 1.5 to 13s. Moreover, the visually observed T_s is supposed to be always higher than 4s as this is the minimum period reported by ships. Lower periods obtained from the simulation experiment are acceptable for windseas. This is evident from field measurements using wave-rider and wave directional buoys in the Indian Seas (Swain et al., 1993; Swain and Ananth, 1994, Sanil Kumar et al., 1996).

Although visually observed swell heights (H_{sw}) are usually overestimates, the observed and simulated H_{sw} and swell periods (T_{sw}) for the Arabian Sea and Bay of Bengal during rough as well as fair weather seasons (Fig.14A and 14B) are compared to assess the extent of agreement between them. Observations are widely scattered during the rough weather season but there are a few observations for the Arabian Sea which compare well with one another. However, the mean deviations for all the data points considered for both the Arabian Sea and Bay of Bengal are relatively higher during the fair weather season compared to the rough weather season. The comparison of observed and simulated T_s and T_{sw} show considerable

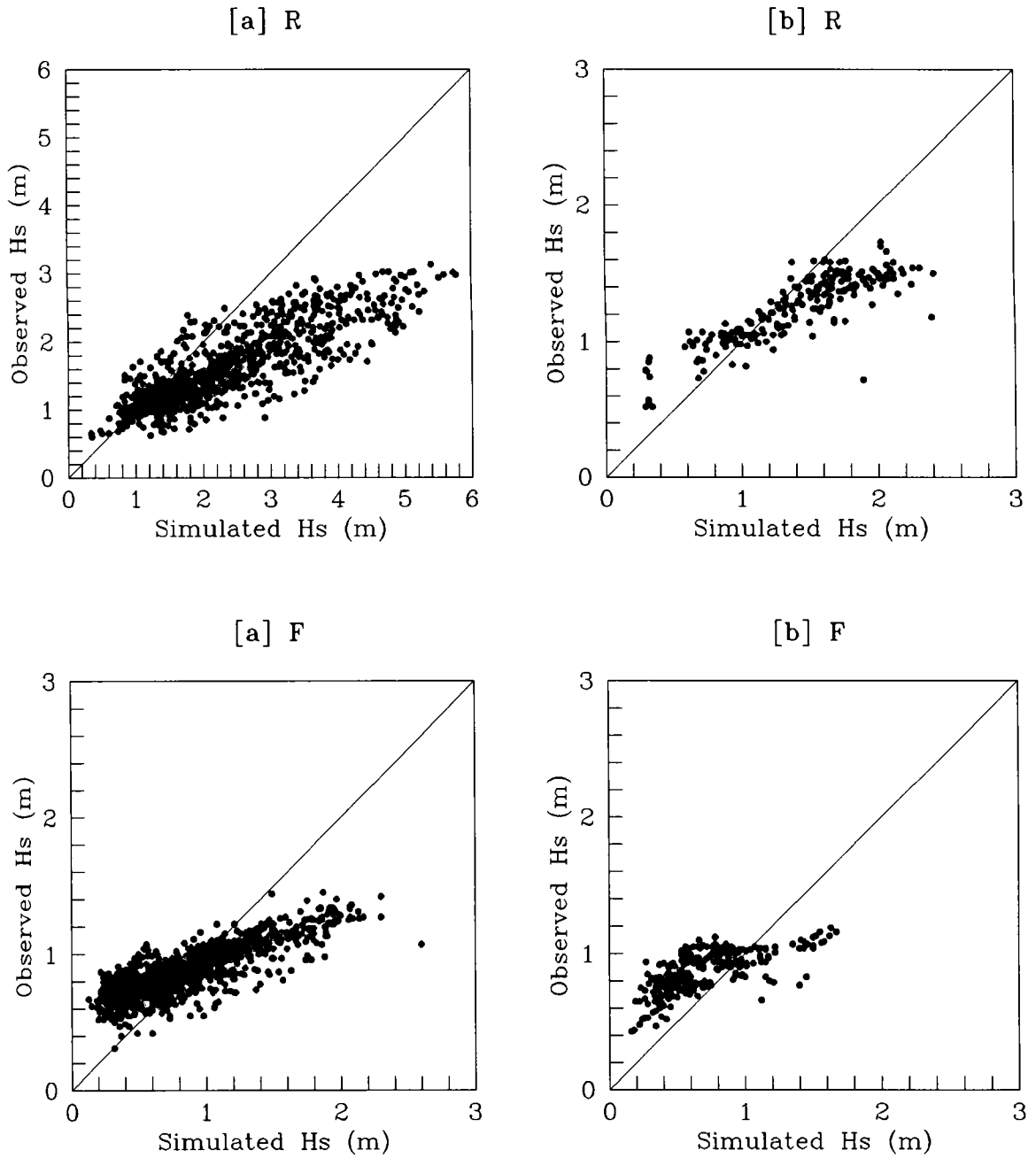


Fig.13A Comparison between simulated and visually observed Hs.
 [a] - Arabian Sea, [b] - Bay of Bengal, R - Rough
 weather and F - Fair weather.

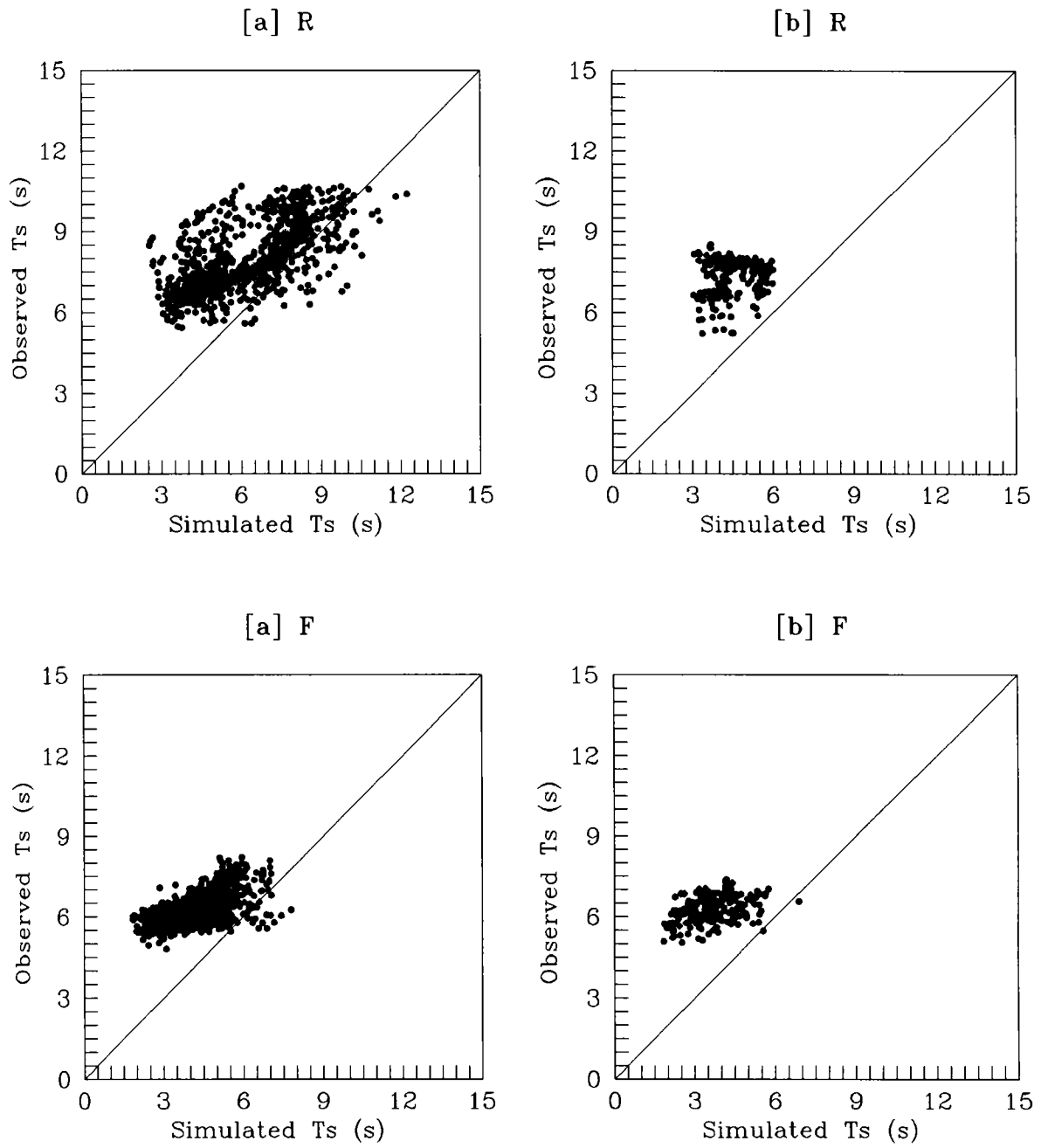


Fig.13B Comparison between simulated and visually observed Ts.
 [a] - Arabian Sea, [b] - Bay of Bengal, R - Rough weather and F - Fair weather.

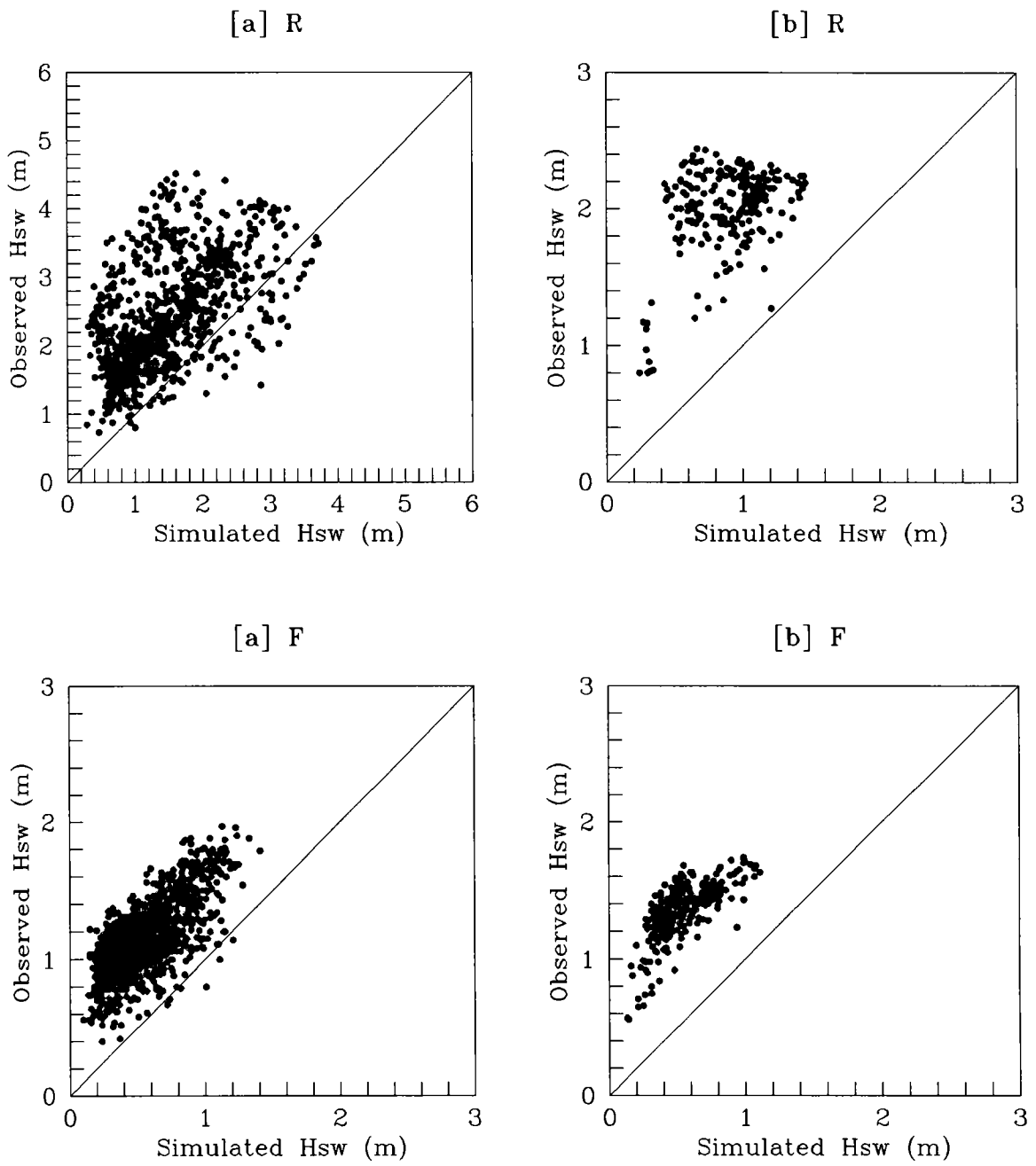


Fig.14A Comparison between simulated and visually observed Hsw. [a] - Arabian Sea, [b] - Bay of Bengal, R - Rough weather and F - Fair weather.

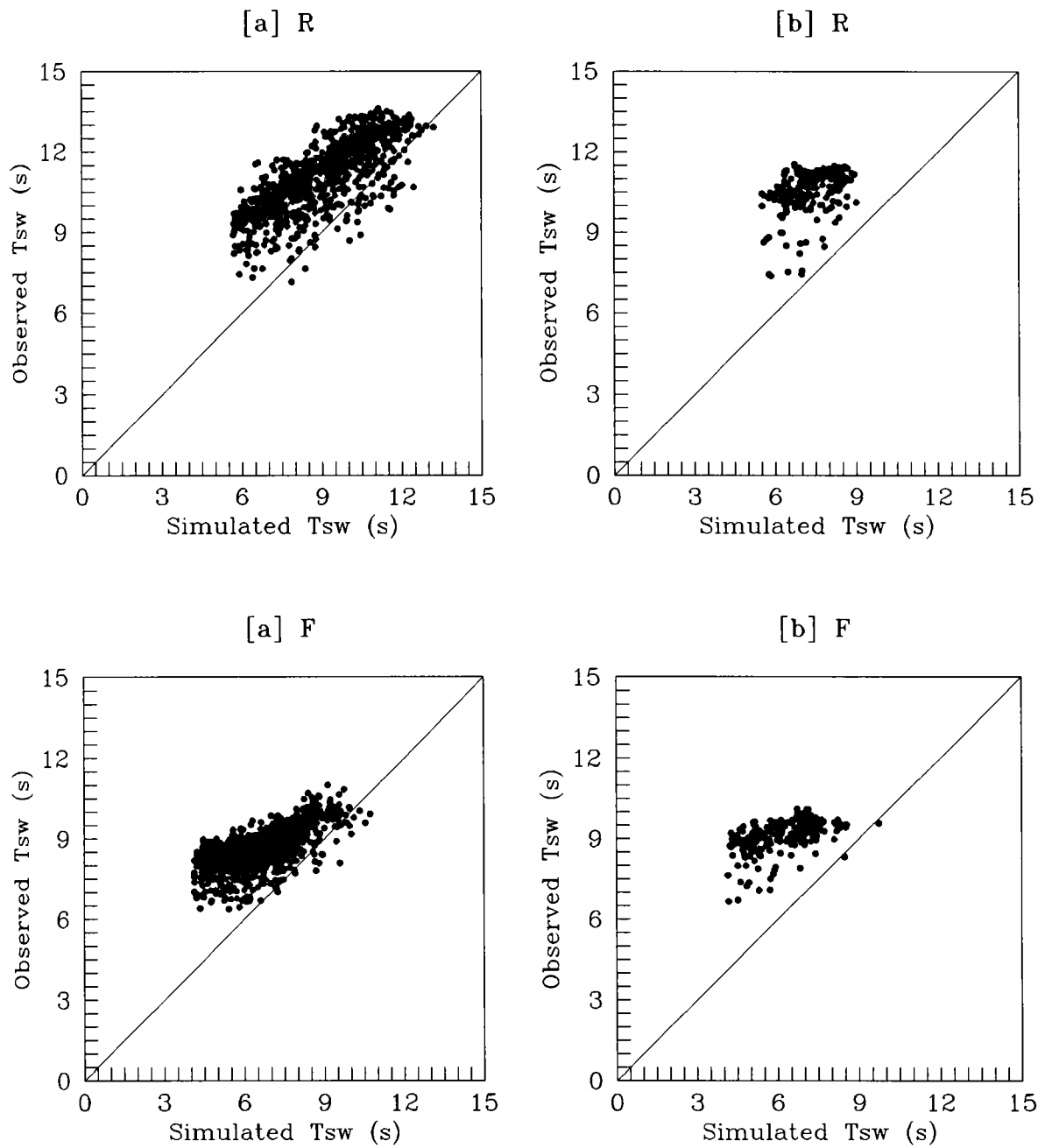


Fig.14B Comparison between simulated and visually observed Tsw. [a] - Arabian Sea, [b] - Bay of Bengal, R - Rough weather and F - Fair weather.

similarity (Fig.13B and 14B). This gives an indication that observed Tsw do not have significant deviations compared with Hsw as discussed earlier.

V.3 VALIDATION USING MEASURED WAVE DATA

The ship-borne wave recorder (SBWR, Model 5254, Institute of Oceanographic Sciences, UK) data for the Indian Seas covering the period 1978-93 was obtained from the Indian National Oceanographic Data Centre (INODC) of NIO, Goa, and used for validation of the simulated wave climate. These data were collected during various oceanographic programmes. Data records of 15 minutes duration were analyzed following Tucker (1961) and Draper (1970). Further details of this data are available in the data report issued by NIO (Sarupria et al., 1995). Data distributions for the rough weather and fair weather seasons are shown in Fig.15A and 15B respectively. There are 785 observations during the rough weather season and 984 observations during the fair weather season for the whole of the Arabian Sea and Bay of Bengal. The digits shown are the number of observations for the respective $1^{\circ} \times 1^{\circ}$ square grid. About 50 percent of the grids do not have any data. In the case of visually observed wave data, monthly means are obtained for all the grids of the regional grid system with minimum 30 observations and compared with the respective mean values by grouping them into seasons. However, the same could not be done in this case due to insufficient data. Therefore the mean monthly Hs and Ts are computed based on the available observations for rough weather and fair weather seasons. The seasonal mean parameters are then compared with the seasonal means of simulated parameters.

The scatter between observed (SBWR) and simulated Hs and Ts for both the Arabian Sea and Bay of Bengal during rough weather and fair weather seasons are shown in Fig.16A and 16B respectively. The observed Hs is underestimated compared with the simulated results during the rough weather season. The comparison for the Arabian Sea during fair weather season appears to be better. Observed Hs in the Bay of Bengal during fair weather season varies over a wider range compared to the simulation output. Both the observed and simulated Hs during fair weather season indicate higher wave activity in the Bay of Bengal compared to the Arabian Sea. This is probably due to the frequent occurrences of deep depressions and cyclones in the Bay of Bengal during October-December. Fig.16B reveals that the simulated Ts is underestimated for the Arabian Sea during the rough weather season. In general, the observed Ts shows more variability compared to the

Rough weather season

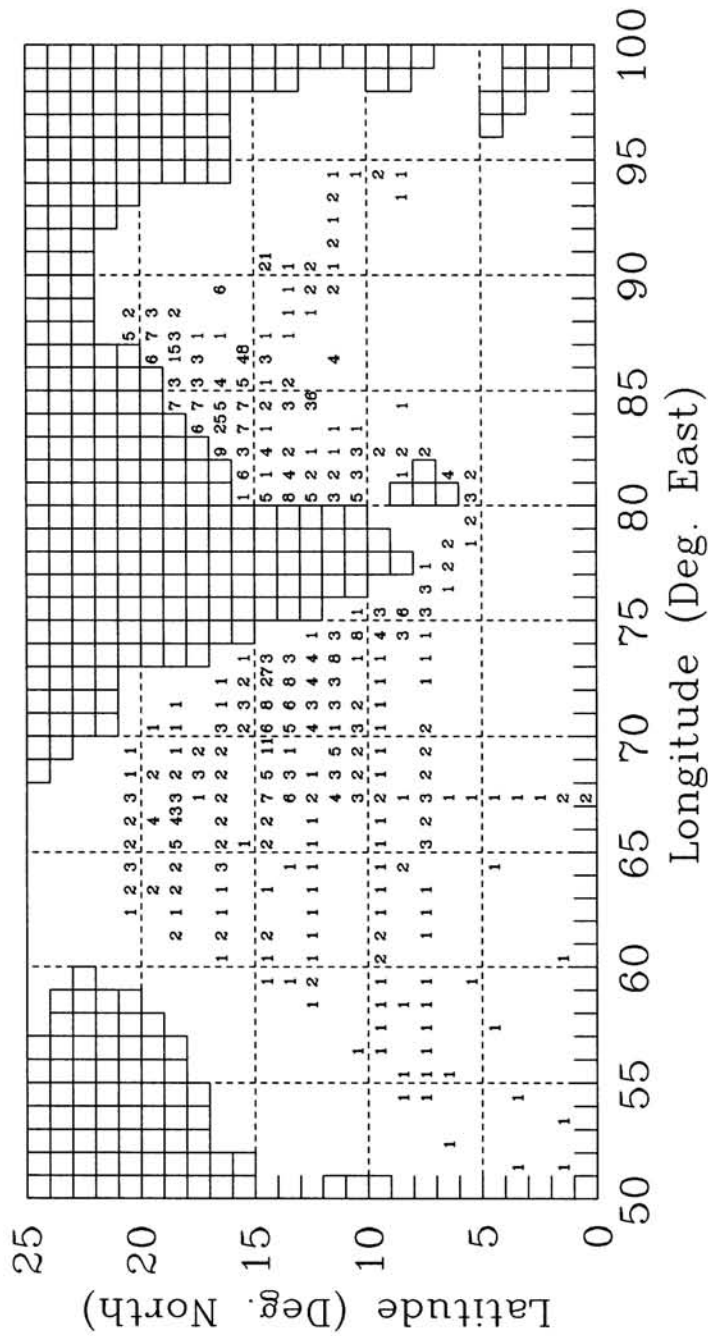


Fig.15A Measured wave data distribution for Indian Seas using shipborne wave recorder (1976-93).

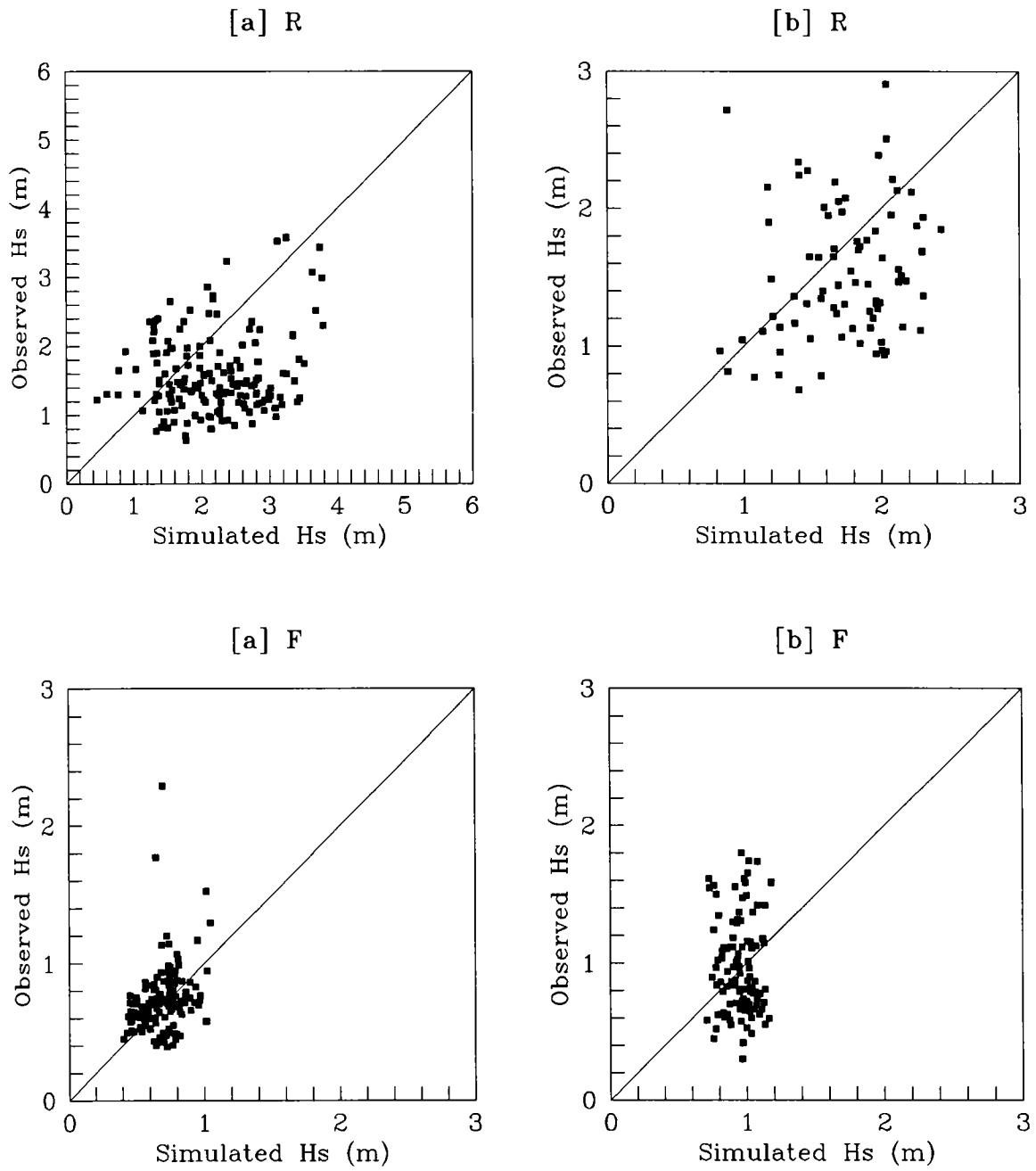


Fig.16A Comparison between simulated and measured (SBWR) Hs.
 [a] - Arabian Sea, [b] - Bay of Bengal, R - Rough weather and F - Fair weather.

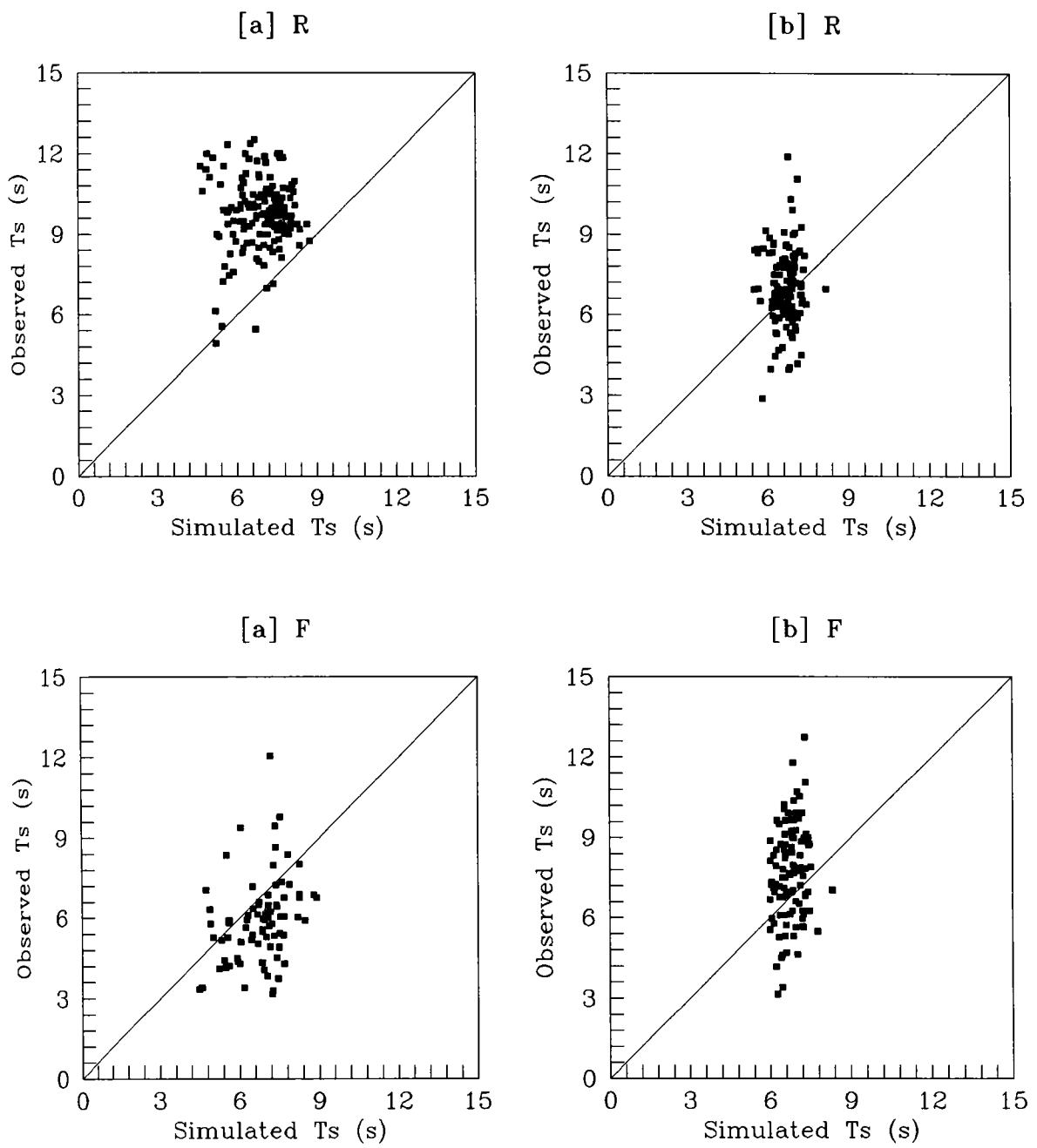


Fig.16B Comparison between simulated and measured (SBWR) Ts.
 [a] - Arabian Sea, [b] - Bay of Bengal, R - Rough weather and F - Fair weather.

simulated Ts. In general, the SBWR and simulated data do not show considerable agreement. One of the important reasons may be the insufficiency of the data although it covers a period of sixteen years.

It was earlier mentioned in Chapter-I that Young and Holland (1996) have published the "Atlas of the oceans: wind and wave climate" based on data from the GEOSAT satellite mission. The atlas contains global and regional estimates of mean monthly wind speed, wind direction, and wave height as well as exceedence probabilities for wave heights and wind speeds. Although the mean monthly fields of Hs are presented over a coarser grid resolution, they agree reasonably well with the simulated fields. The comparison between the GEOSAT and the simulated mean monthly Hs for two selected sites are shown in Fig.17. The comparison is quite encouraging in the case of GEOSAT data. The reason for a good comparison may be the availability of satellite data over a uniform temporal (17 day repeat cycle) and spatial resolution.

The above comparison between the measured and simulated wave parameters gives a qualitative picture of the simulated database. It also gives an idea regarding the range of wave heights and periods that are observed at different times and regions within the study area and they are well within the range of simulated results. Moreover, the comparison is quite useful in resolving the advantages/disadvantages of different kinds of data sets and the extent of their reliability.

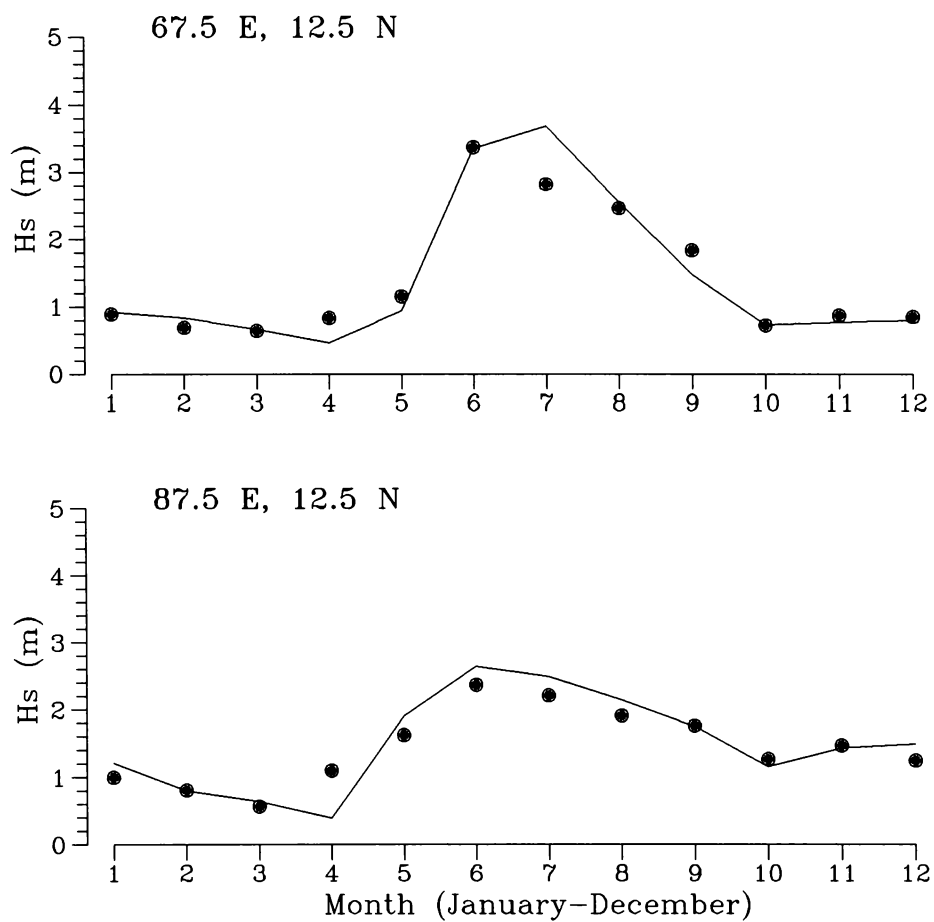


Fig.17 Comparison of results obtained from wave climate simulation (solid line) and GEOSAT satellite mission (solid circles) for two selected sites.

CHAPTER VI. SIMULATED WAVE CLIMATE FOR THE INDIAN SEAS

VI.1 INTRODUCTION

The general description of wave climate of a region can be expressed in several ways. Some typical presentations are: i) monthly, seasonal and annual fields/distributions of significant wave parameters such as significant wave height (H_s) and significant wave period (T_s) or average period with or without standard deviations; ii) graphical representation of H_s and T_s in the form of histograms in several ranks and various directions similar to wind roses and iii) bivariate distribution of H_s and T_s or average period with or without classification in wave direction (Goda, 1990). From the bivariate distribution of H_s and T_s , their marginal distributions can be easily obtained. It is generally expressed in the form of percentage exceedence diagrams or cumulative probability distributions. The wave model outputs of the present simulation experiment is also compiled in the similar lines (explained in Chapter-IV). As it is not practicable here to carry out a detailed study on the spectral characteristics based on the simulated results, two sample wave spectra for a selected site in the Arabian Sea during rough and fair weather seasons are presented. This chapter also includes comparative studies of wave climates between the Arabian Sea and Bay of Bengal and between the east and west coasts of India. The last two sections present limitations of the simulated wave climate and the future outlook.

VI.2 SPATIAL DISTRIBUTION OF WAVE PARAMETERS

The monthly, seasonal, and annual distributions of the simulated H_s and T_s in the form of contour diagrams are shown in Fig.18 to 32. In addition to H_s and T_s , the monthly fields include swell wave height (H_{sw}), swell wave period (T_{sw}), windsea direction, and swell directions shown with arrows (Fig.18 to 29). Appropriate contour intervals are used for height (0.2, 0.3 & 0.5m) and period (0.5 & 1.0s) depending on the magnitude of the wave field variation in space.

VI.2.1 Monthly distribution

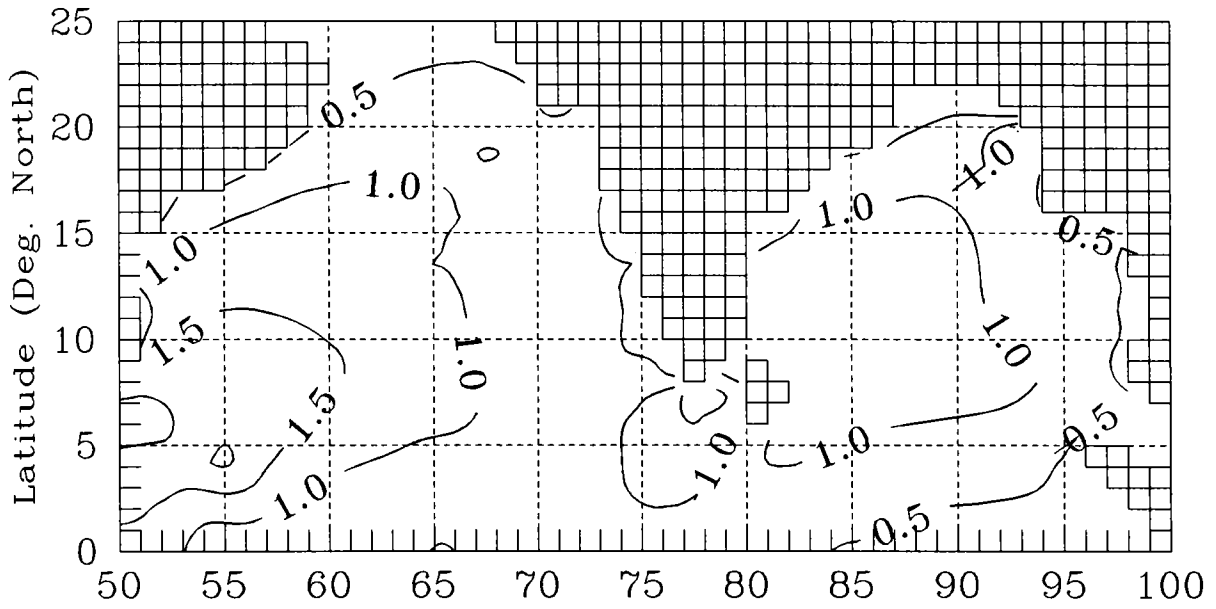
Mean monthly wave heights for the Indian Seas were earlier estimated based on empirical relations (Ray, 1990) using mean monthly wind fields (Hastenrath and Lamb, 1979) over 5 degree square grids. The estimated wave

heights for one representative week during June 1979 were also compared by Ray with actual observations using the wind and wave data collected during ISMEX-73 and MONEX-79. The comparisons showed certain variations as the prevailing mean winds over any particular region may not reflect the actual wave condition unless the wave field is composed of local windseas alone. Therefore estimated wave fields which are directly computed using mean wind fields are supposed to follow similar spatial variations as that of wind and can be regarded as the first estimates. In the absence of any other information they can also be used in practical applications, though to a limited extent.

Mean monthly wave fields based on the present simulation study are shown in Fig.18 to 29. The simulated wave fields reveal significant spatial variations resulting from the combined effects of windseas generated by the local winds and swells if they are propagating into the area of wave generation from other sources. In another study, Prasada Rao and Durga Prasad (1992) carried out wave hindcast using SMB method in the Bay of Bengal for the summer monsoon months (June, July and August) based on the IDWR winds from 1976 to 1980. They computed the windsea height, swell height, and the maximum possible significant wave height over 3 degree square grids for these months. It is seen that there is no considerable agreement between those hindcast results using SMB model and the present simulation results.

The monthly mean variations of H_s , T_s , H_{sw} and T_{sw} for the Arabian Sea and Bay of Bengal based on the present study are given in Table 5. The height and period parameters in this table are rounded off to the nearest 0.1m and 1s respectively. Salient features for all the twelve calendar months are presented in the following sections. It may be noted that unless specified otherwise, all discussions in this chapter on wave parameters refer to mean monthly values. Another important point to note is that the deep water wave measurements considered beyond 30m of water depth (Michael Clancy and Johnson, 1997) reported in the literature are very few in number and mostly not available to substantiate some of the features associated with the simulated mean monthly wave fields. Hence the deep water time-series measurements using ship-borne wave recorder, Datawell wave rider buoy, and wave directional buoy (WAVEC) during the different field experiments of NPOL and other research establishments which have appeared in the literature will be cited in the discussion. However the time-series measurements carried out till recently are of short durations (about 2 to

January [a]



[b]

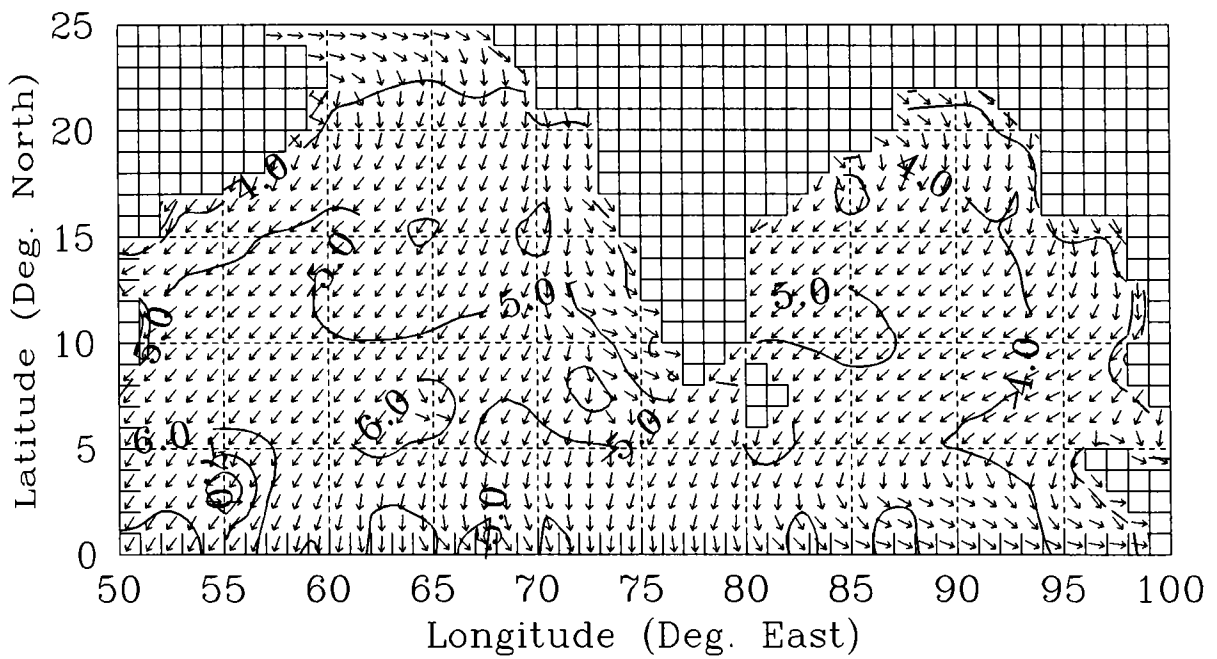
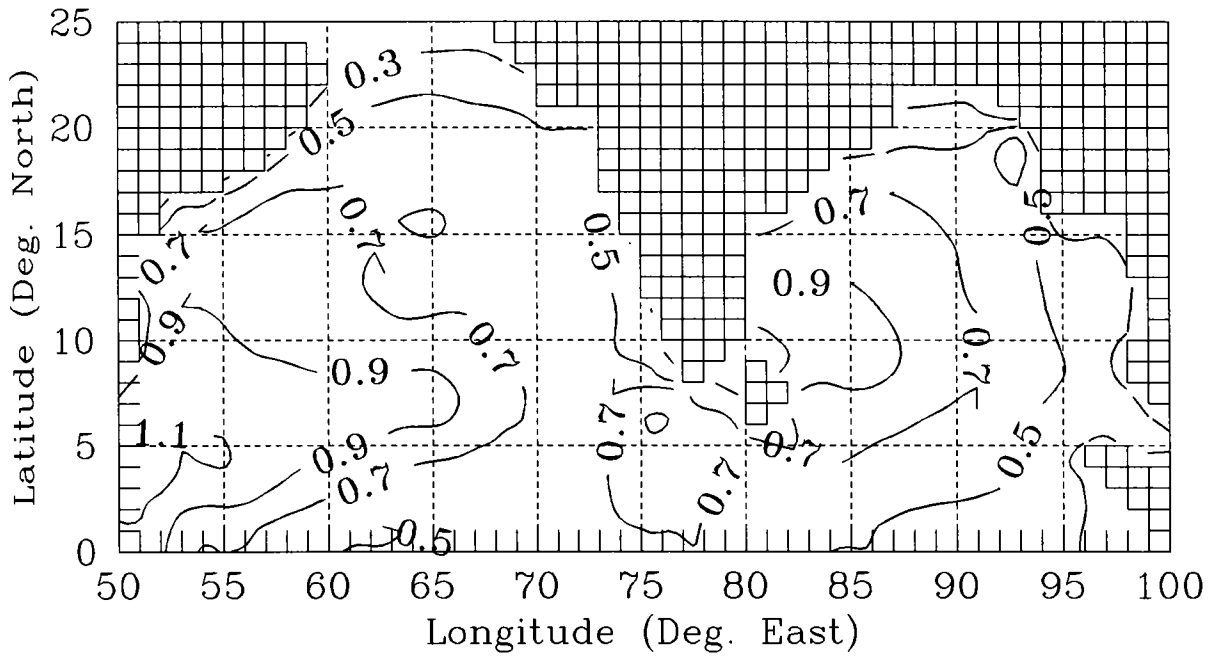


Fig.18A [a] The significant wave height (m), [b] Significant wave period (s) and windsea direction.

January [a]



[b]

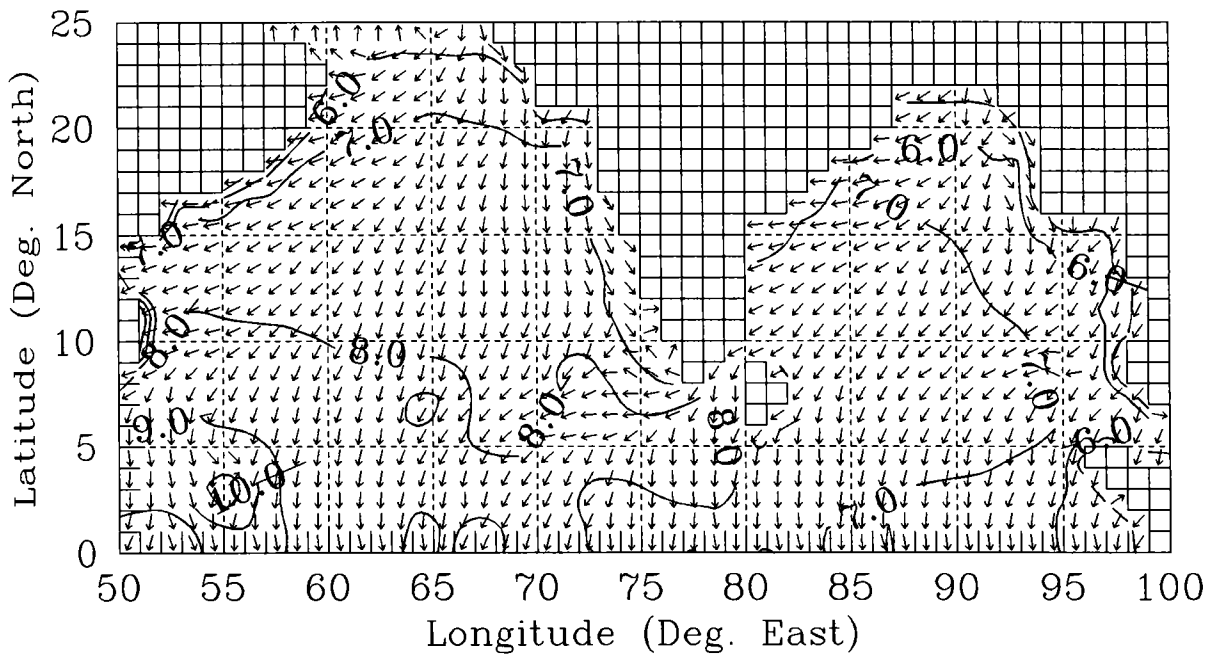
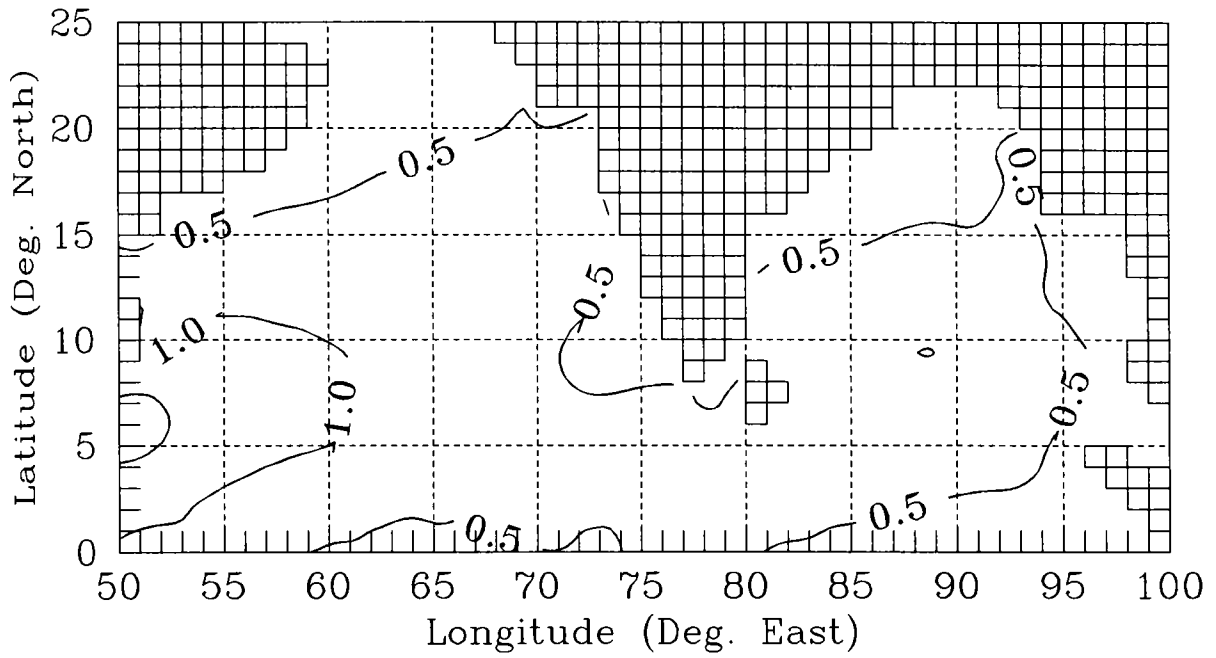


Fig.18B [a] The swell wave height (m), [b] Swell wave period (s) and direction.

February [a]



[b]

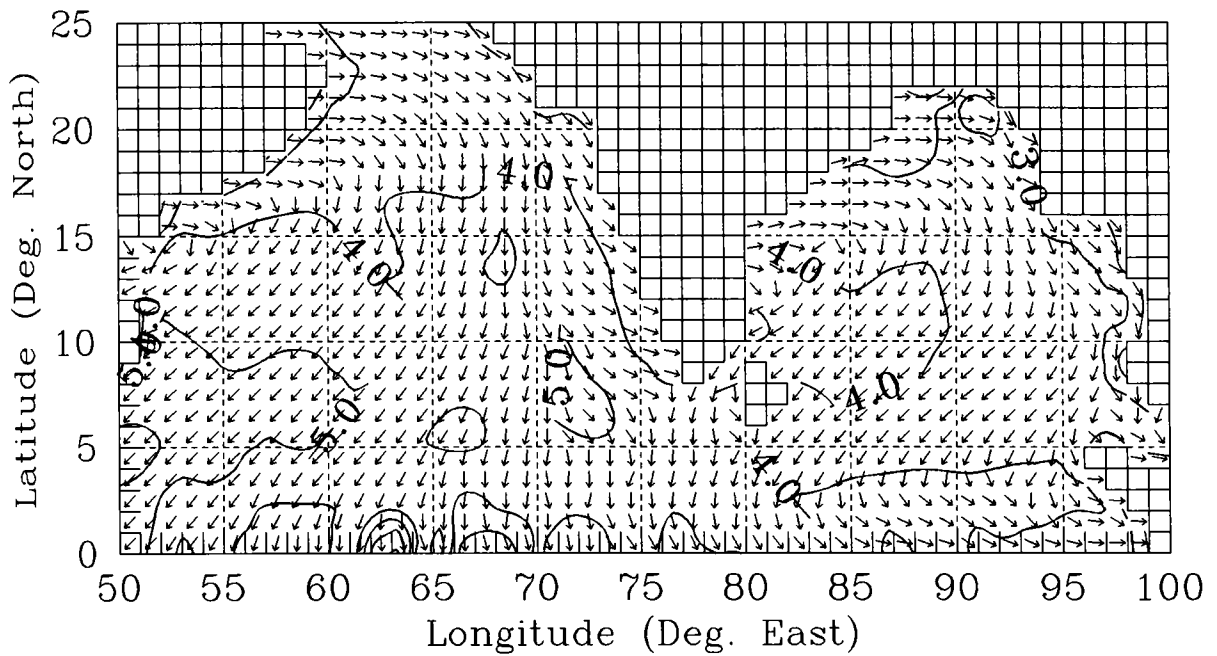
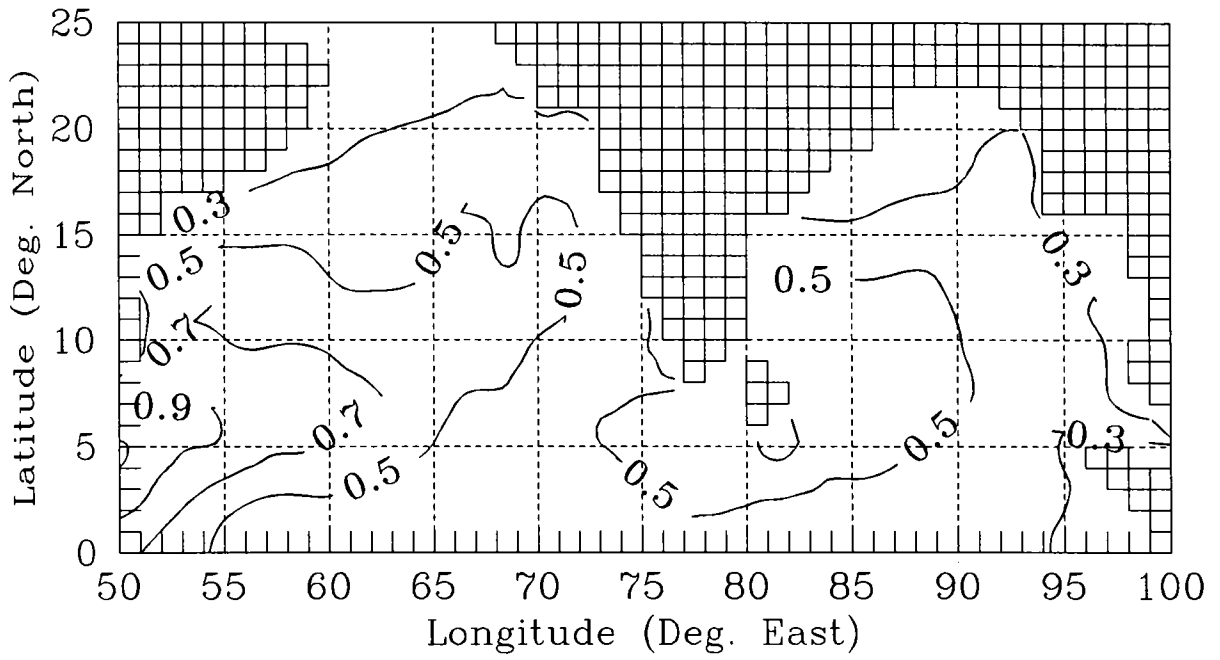


Fig.19A [a] The significant wave height (m), [b] Significant wave period (s) and windsea direction.

February [a]



[b]

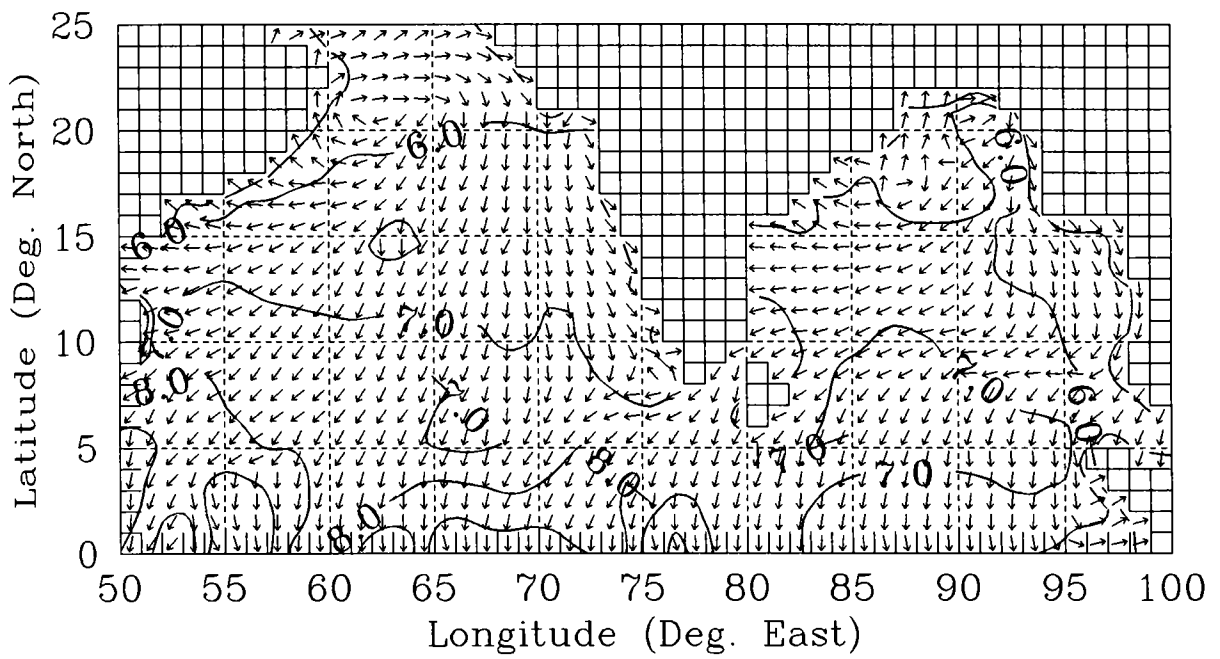
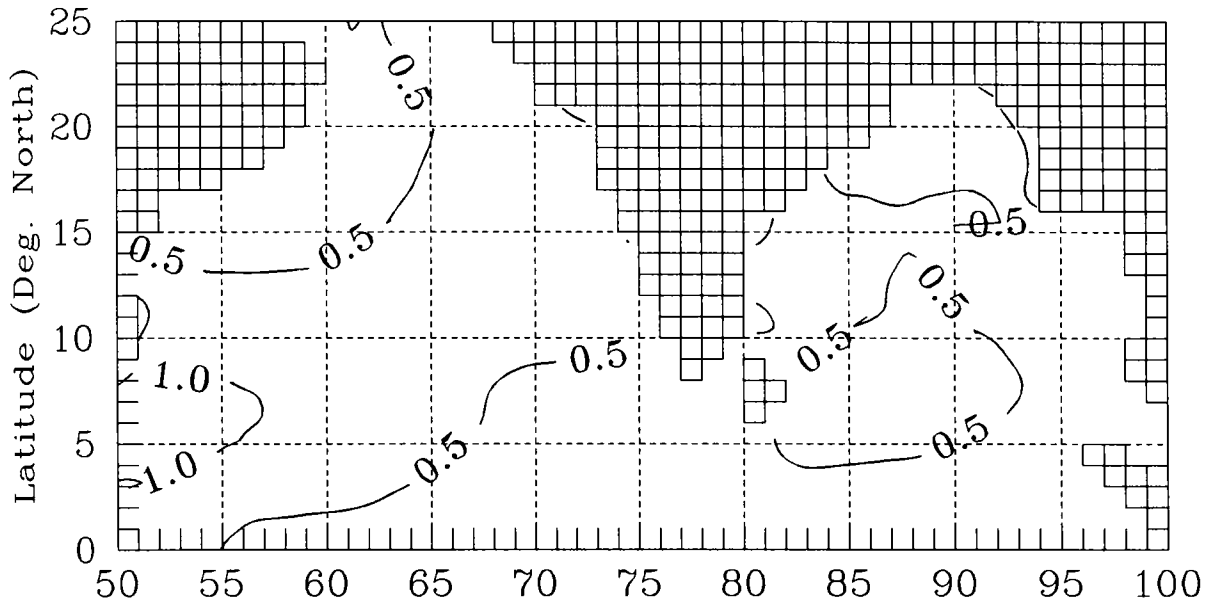


Fig.19B [a] The swell wave height (m), [b] Swell wave period (s) and direction.

March [a]



[b]

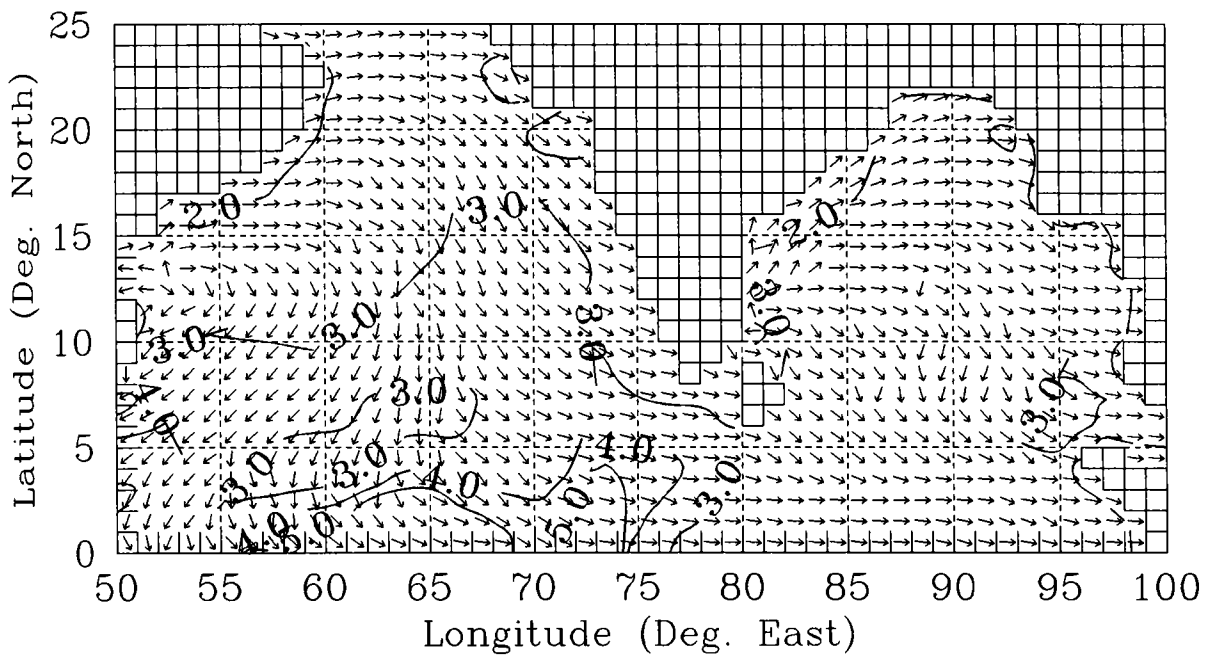
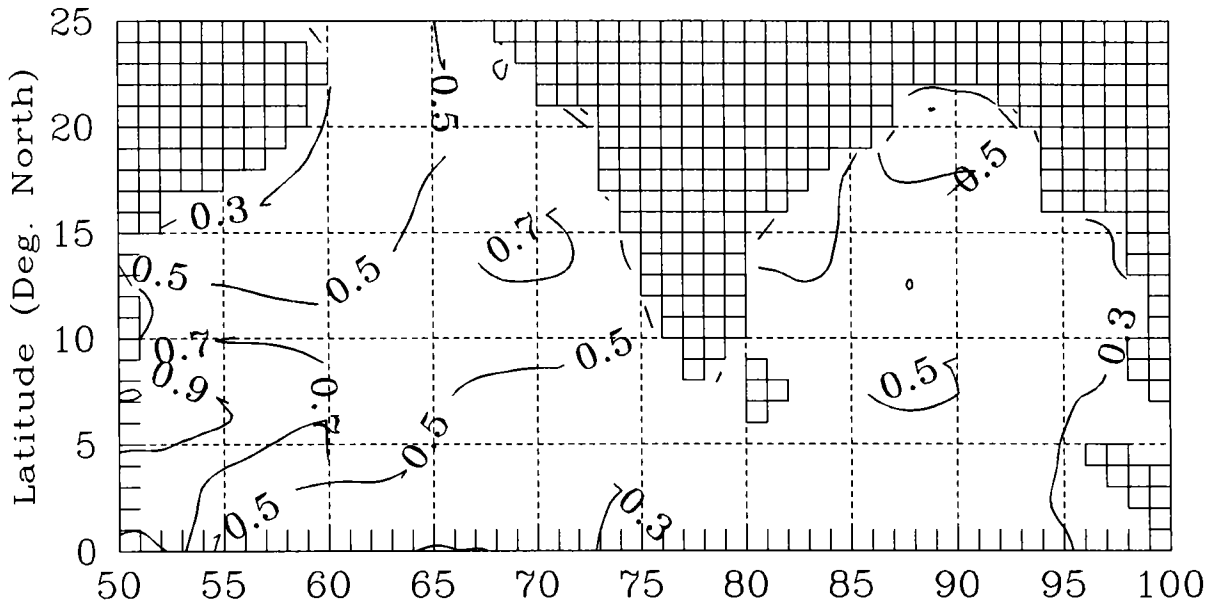


Fig.20A [a] The significant wave height (m), [b] Significant wave period (s) and windsea direction.

March [a]



[b]

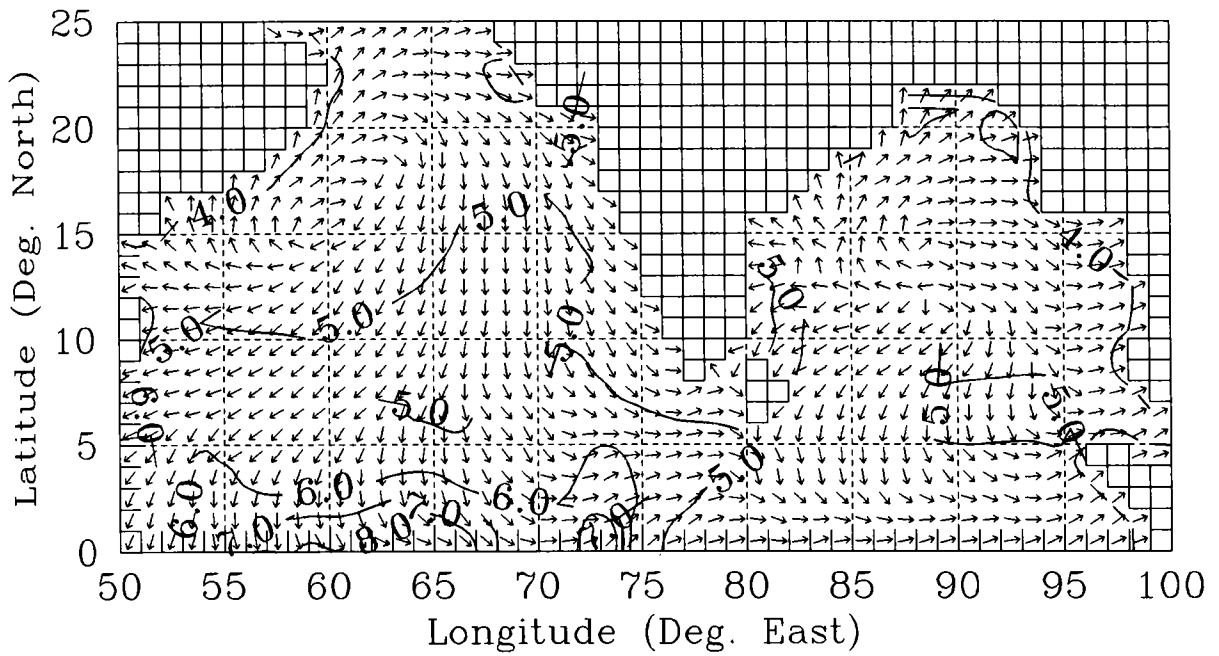
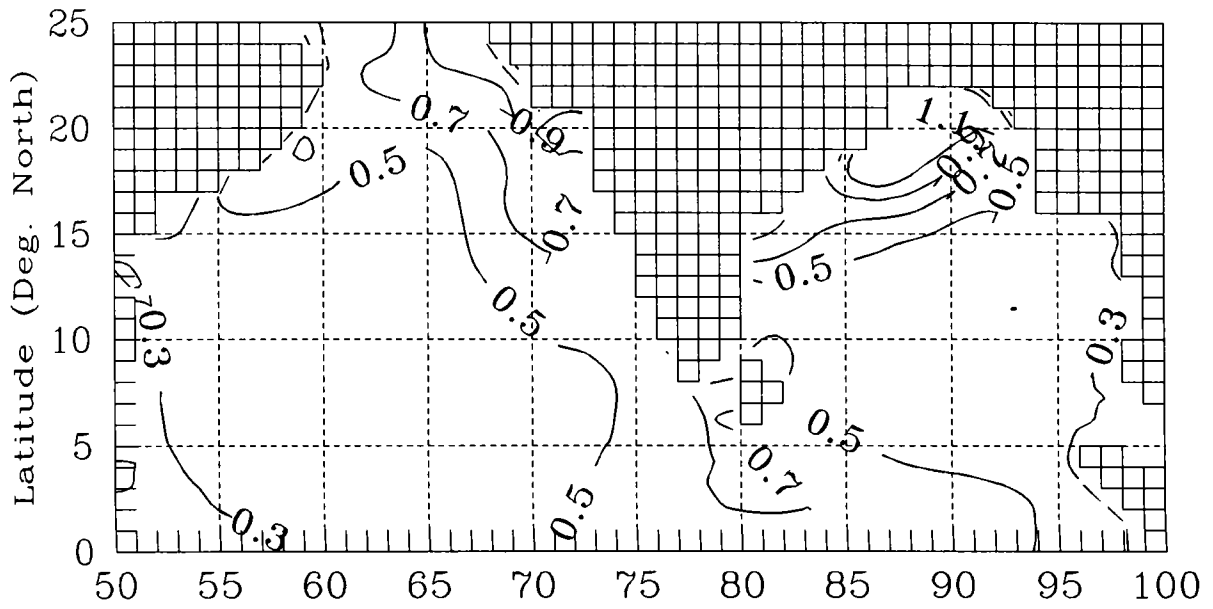


Fig.20B [a] The swell wave height (m), [b] Swell wave period (s) and direction.

April [a]



[b]

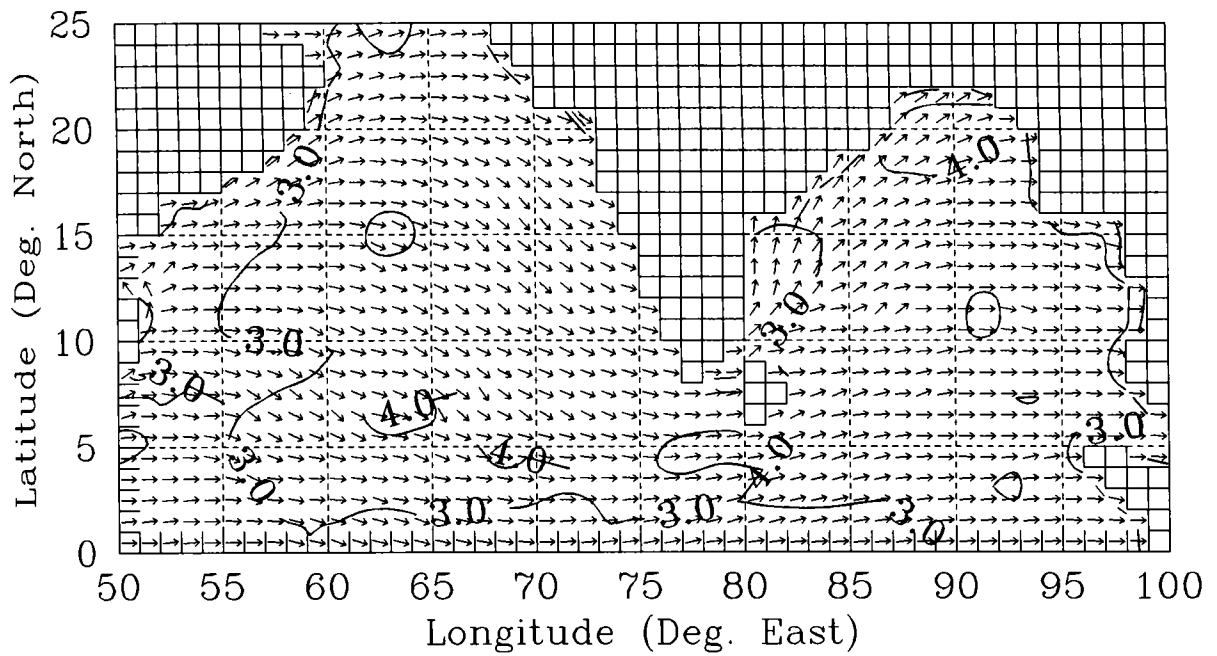
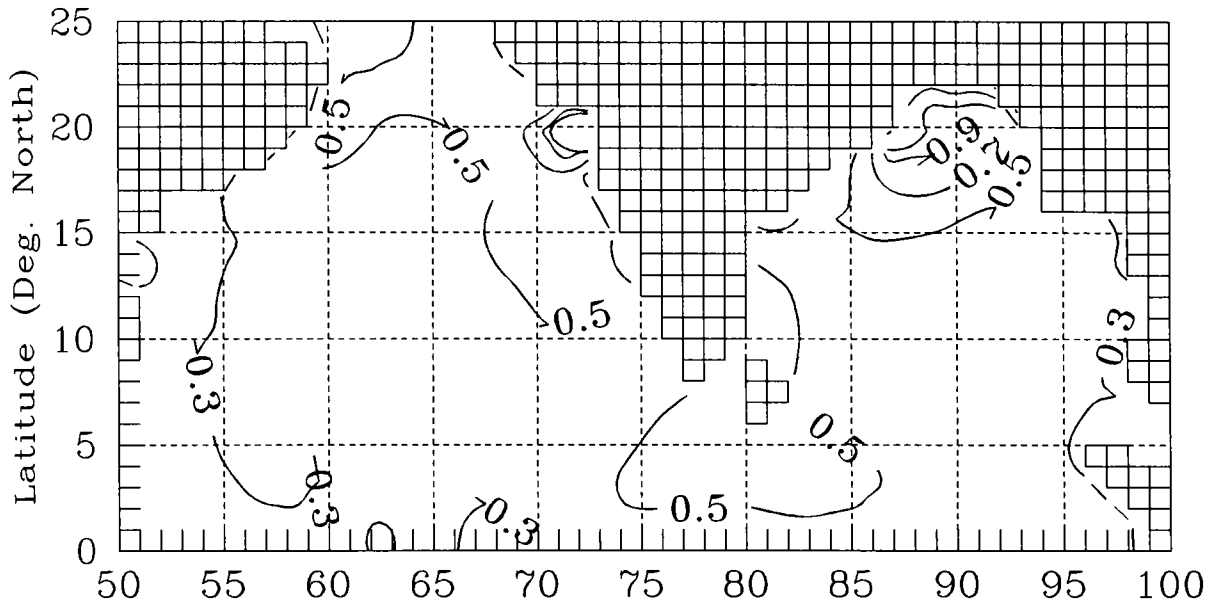


Fig.21A [a] The significant wave height (m), [b] Significant wave period (s) and windsea direction.

April [a]



[b]

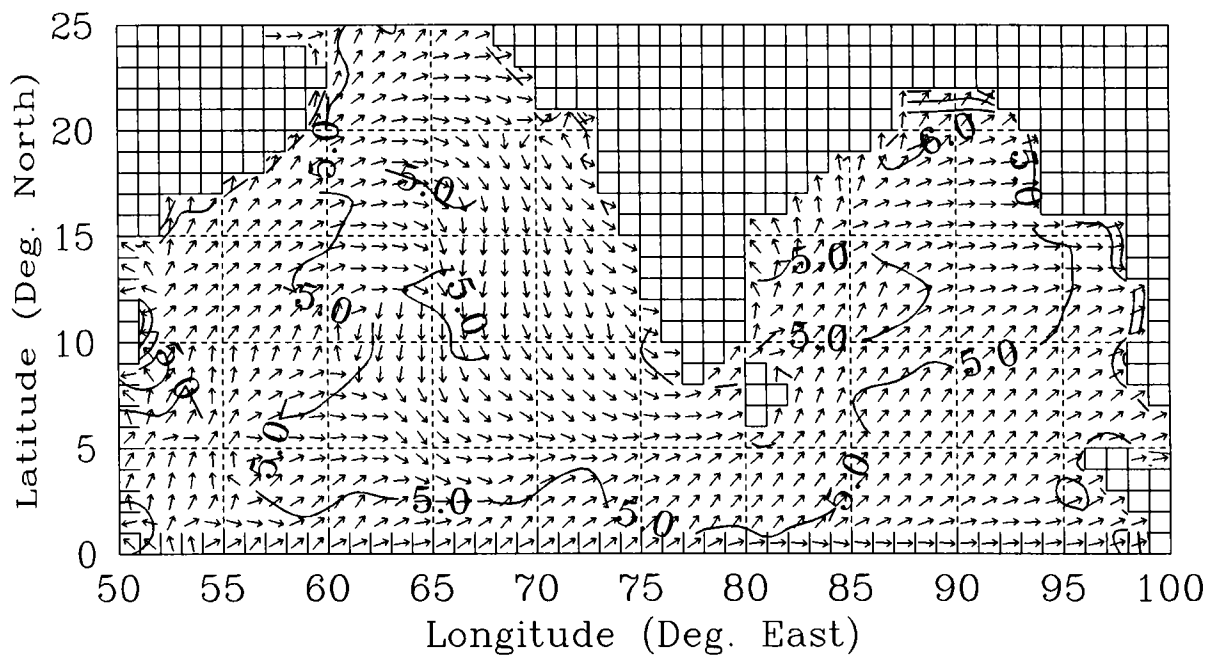
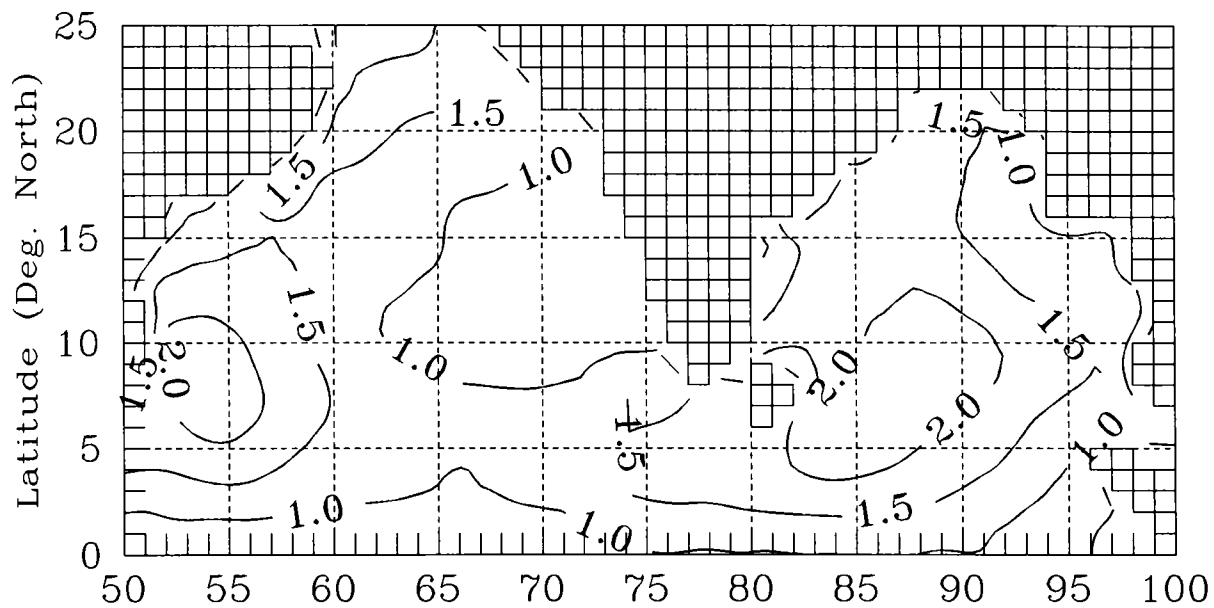


Fig.21B [a] The swell wave height (m), [b] Swell wave period (s) and direction.

May [a]



[b]

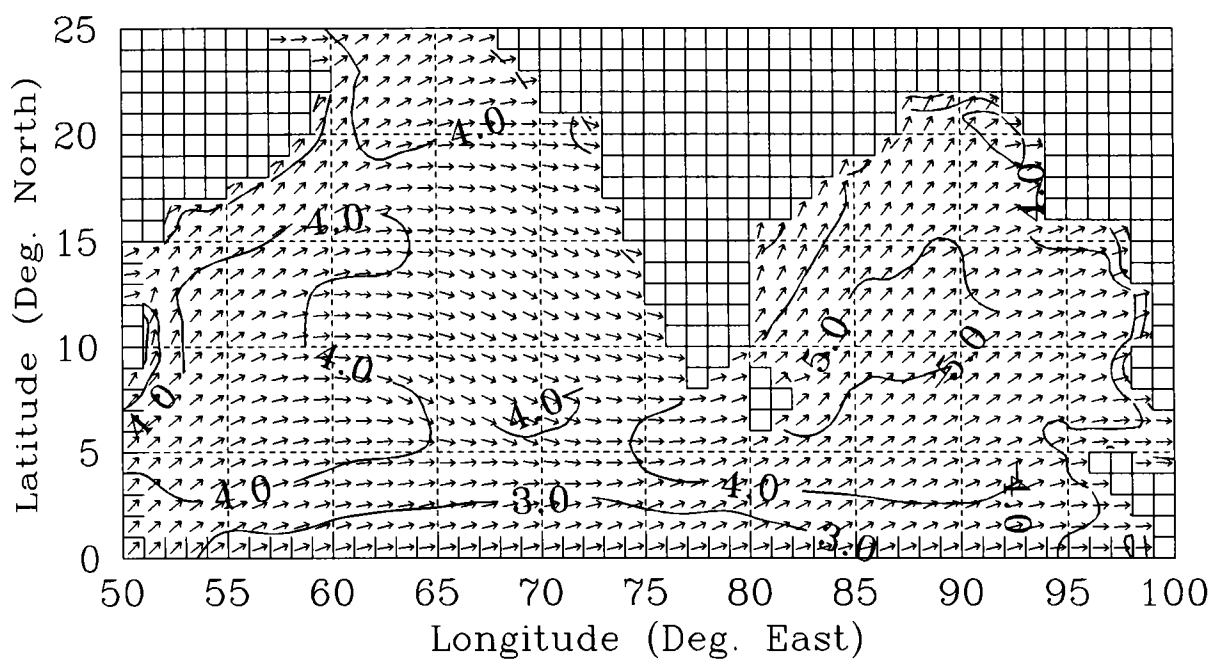
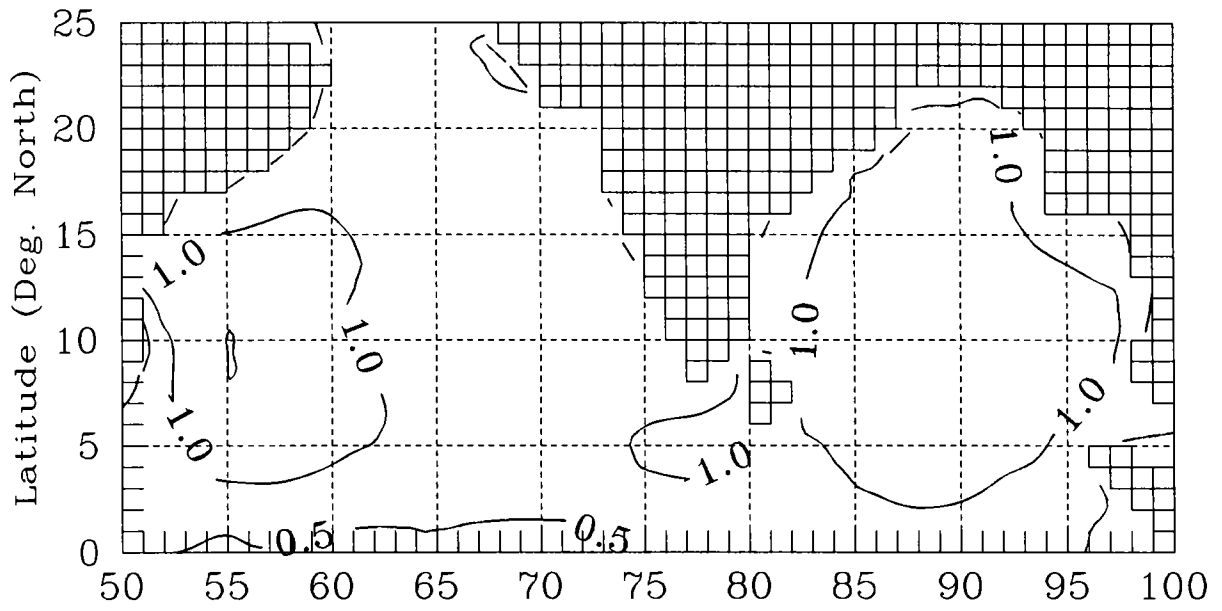


Fig.22A [a] The significant wave height (m), [b] Significant wave period (s) and windsea direction.

May [a]



[b]

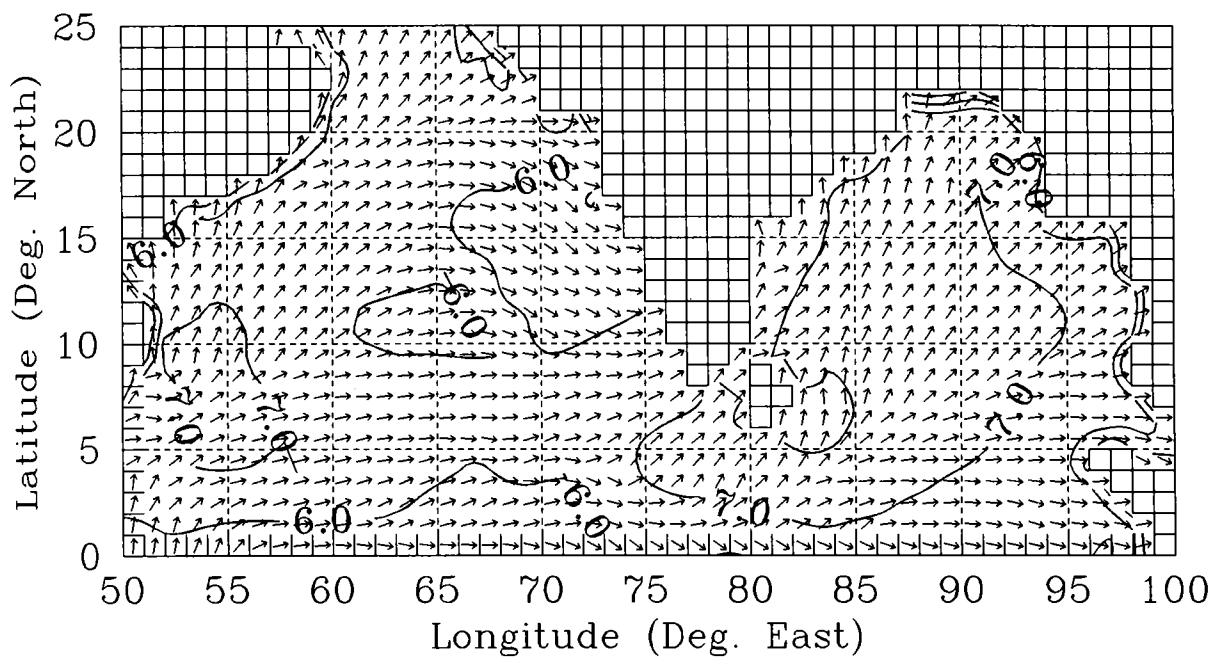
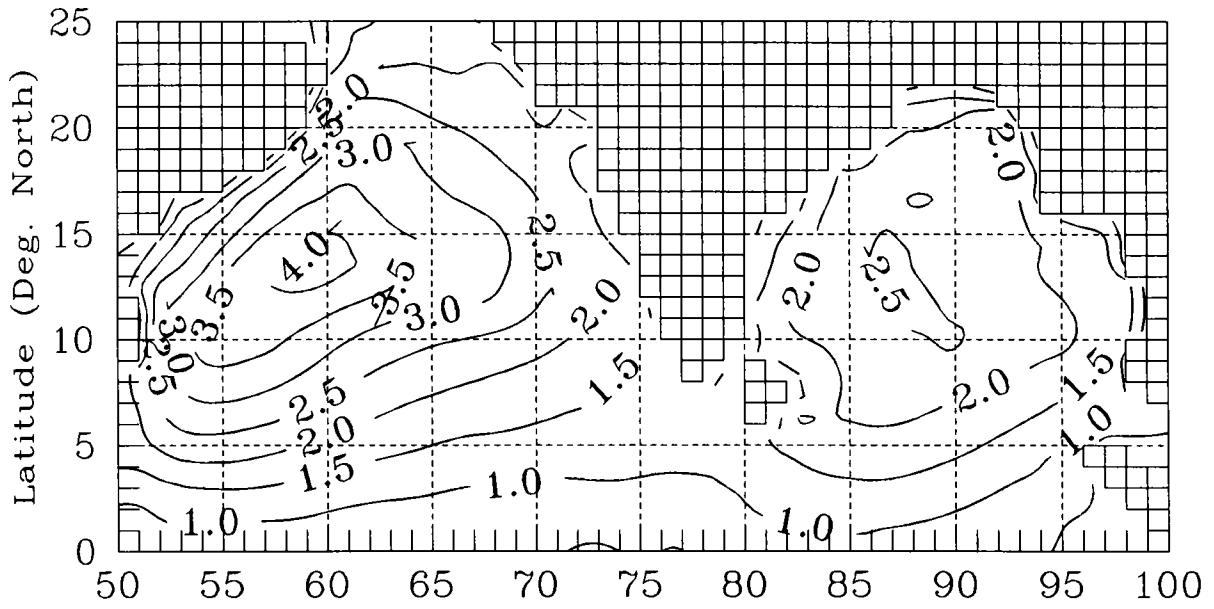


Fig.22B [a] The swell wave height (m), [b] Swell wave period (s) and direction.

June [a]



[b]

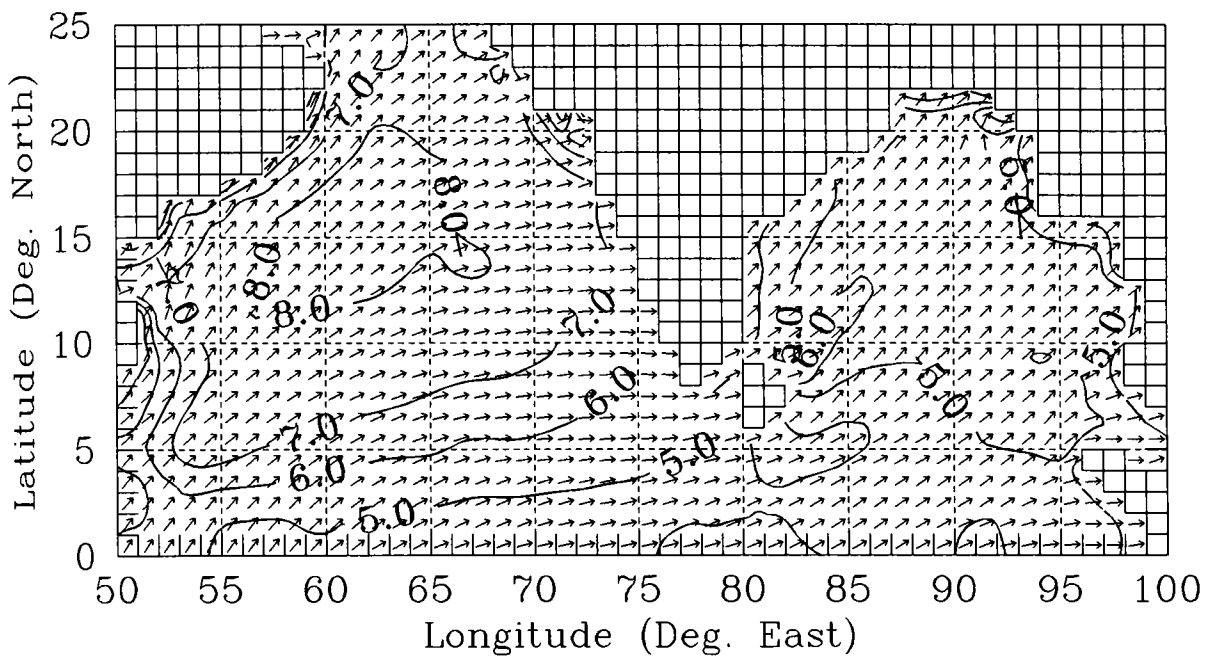
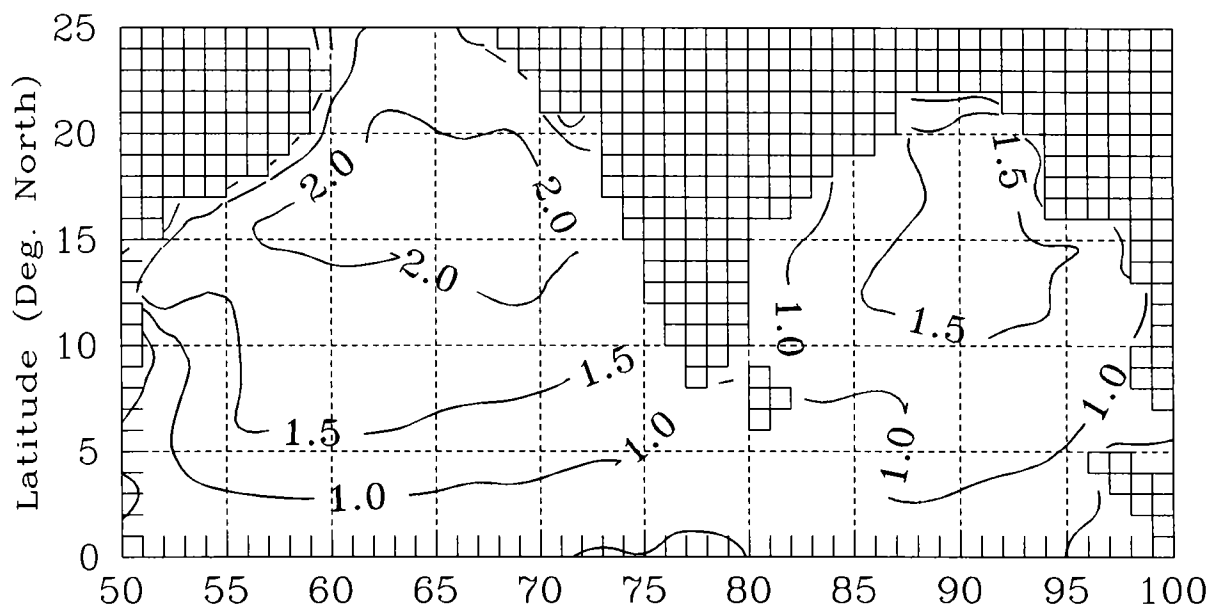


Fig.23A [a] The significant wave height (m), [b] Significant wave period (s) and windsea direction.

June [a]



[b]

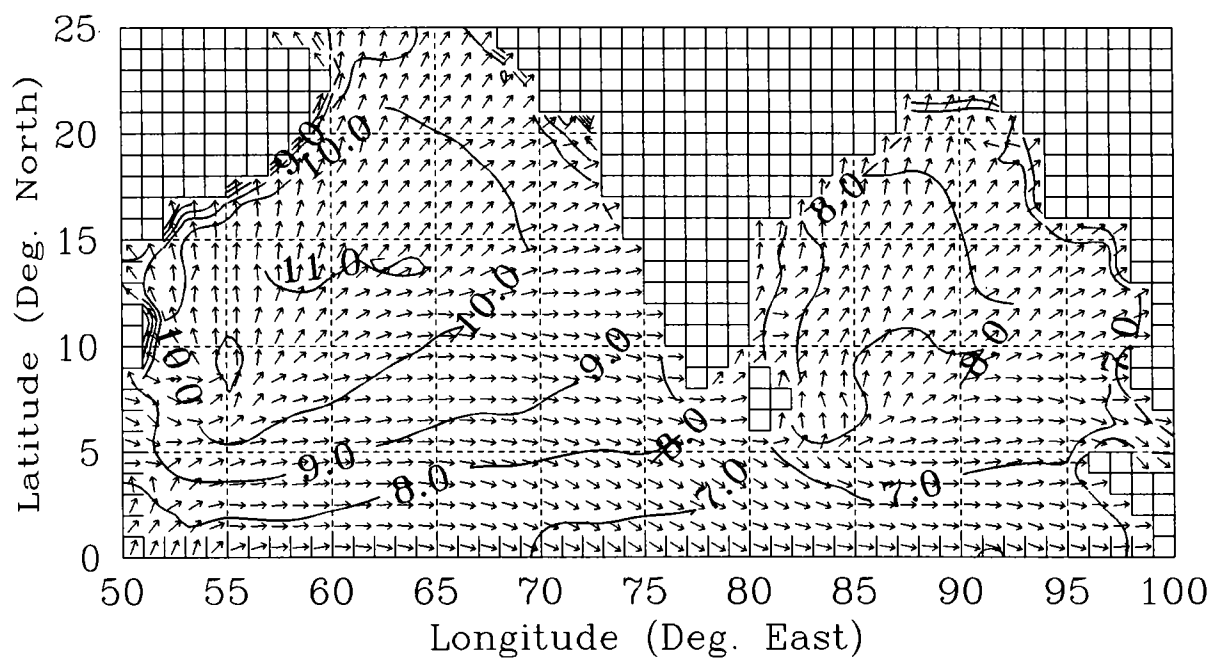
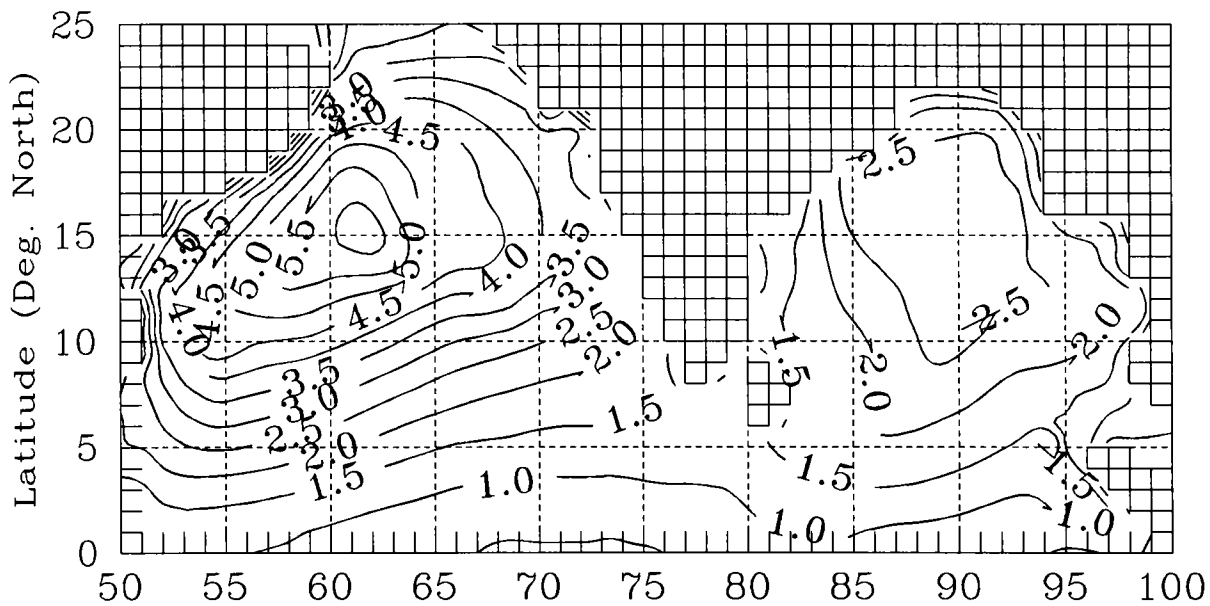


Fig.23B [a] The swell wave height (m), [b] Swell wave period (s) and direction.

July [a]



[b]

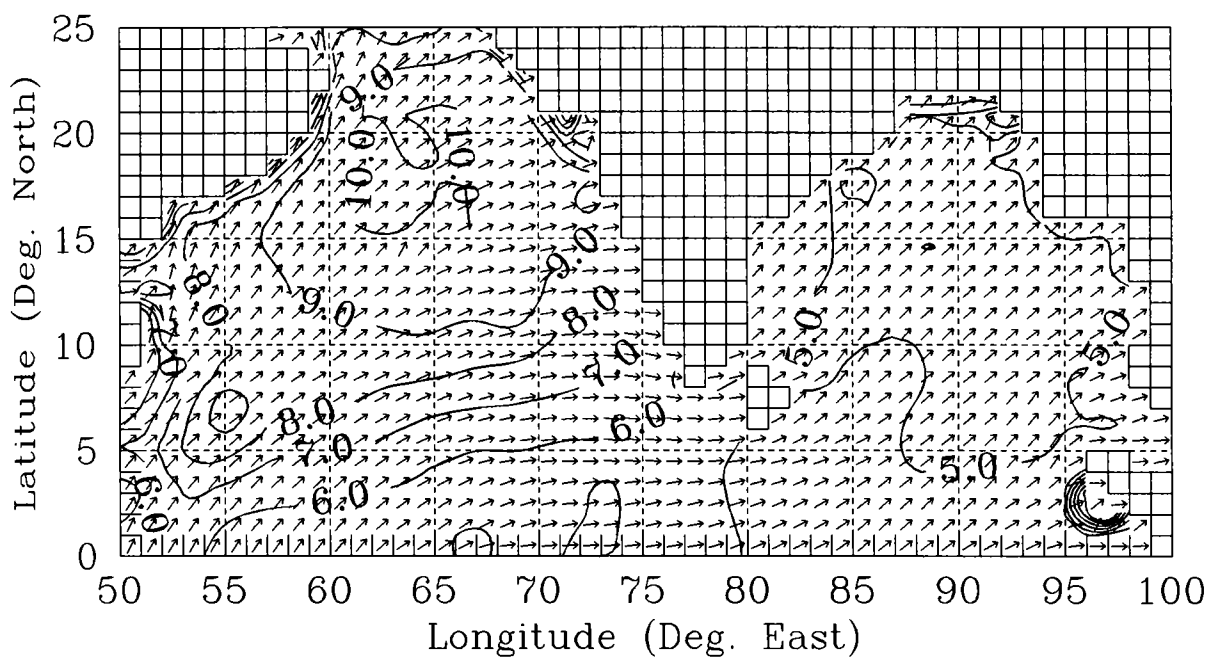
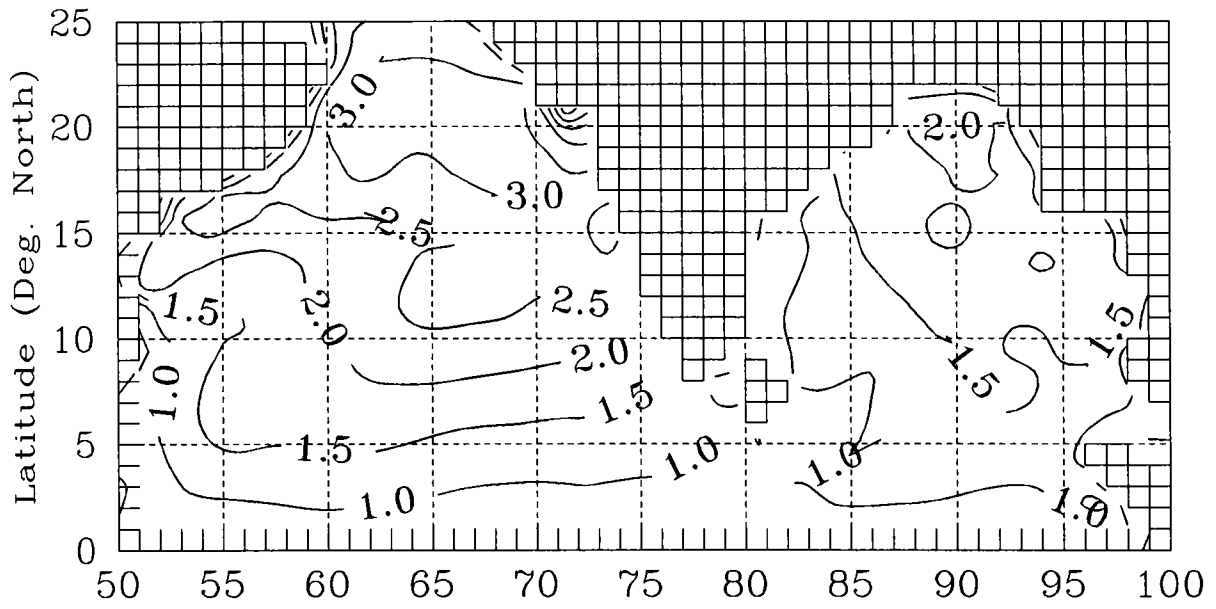


Fig.24A [a] The significant wave height (m), [b] Significant wave period (s) and windsea direction.

July [a]



[b]

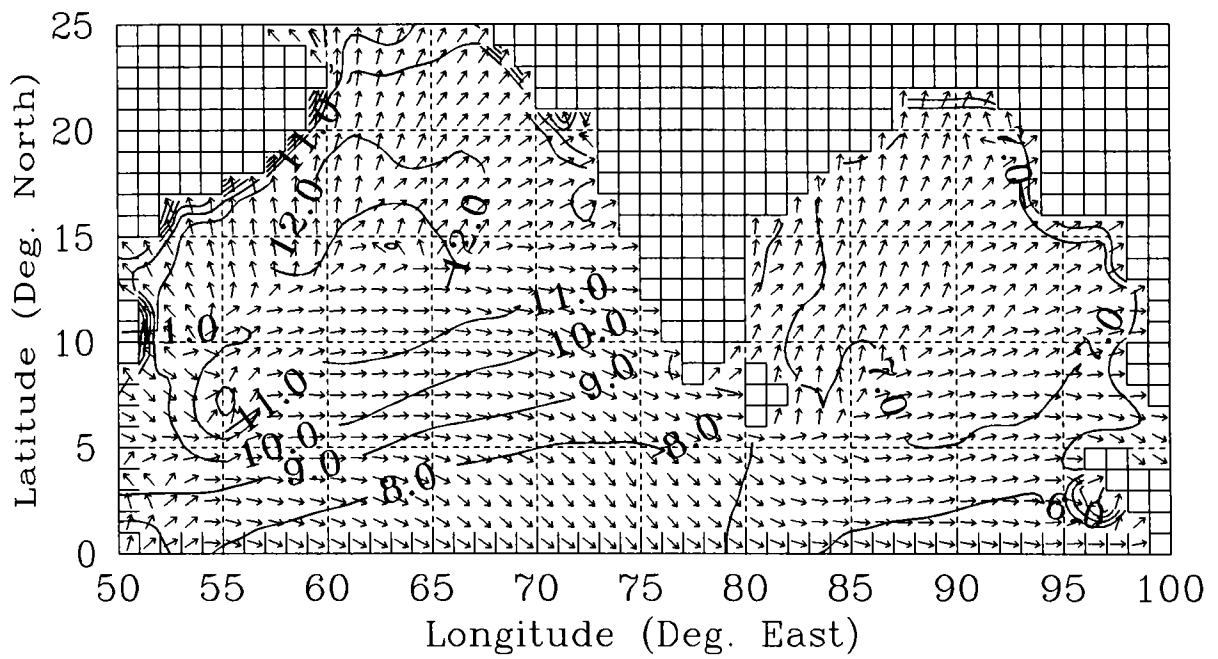
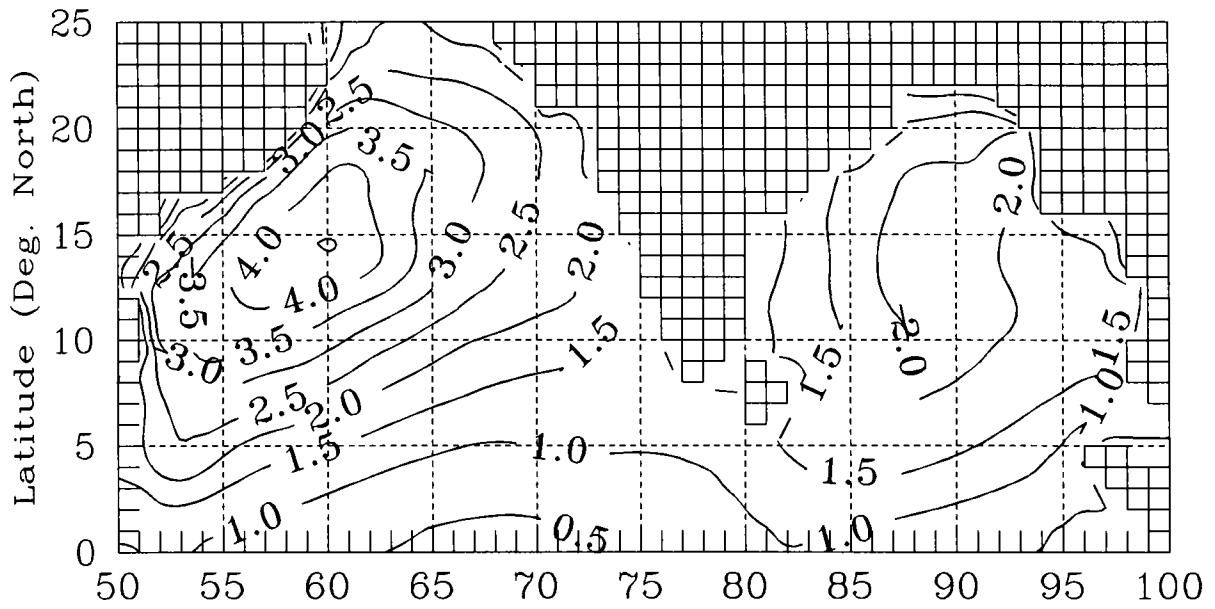


Fig.24B [a] The swell wave height (m), [b] Swell wave period (s) and direction.

August [a]



[b]

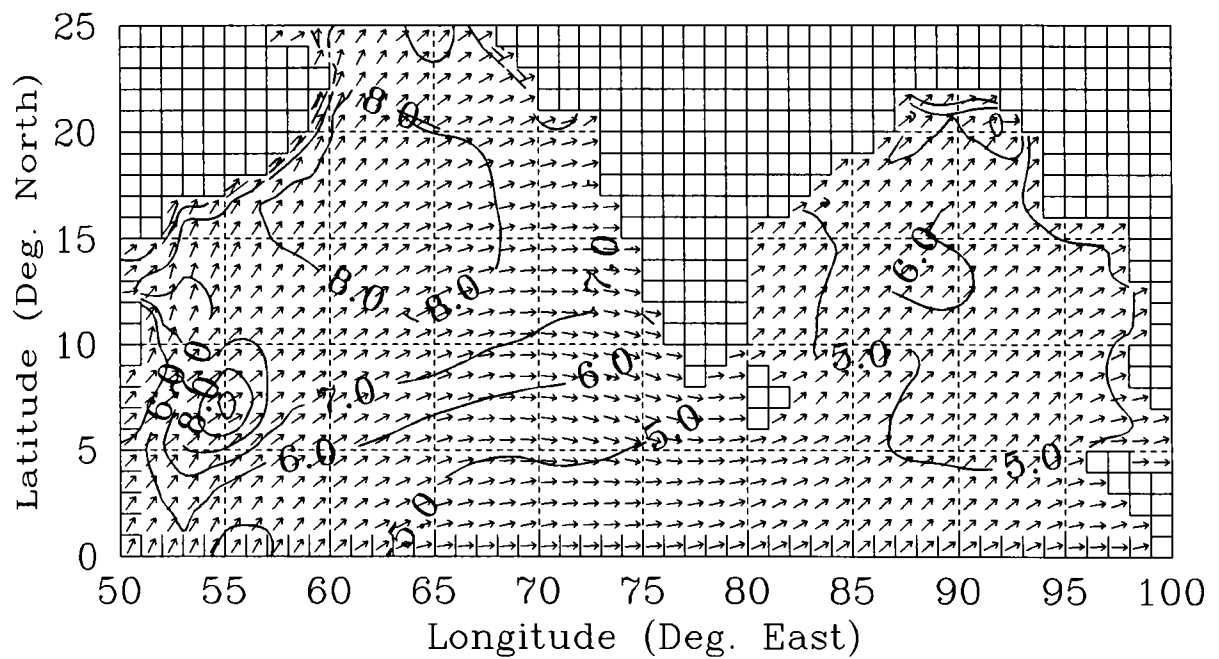
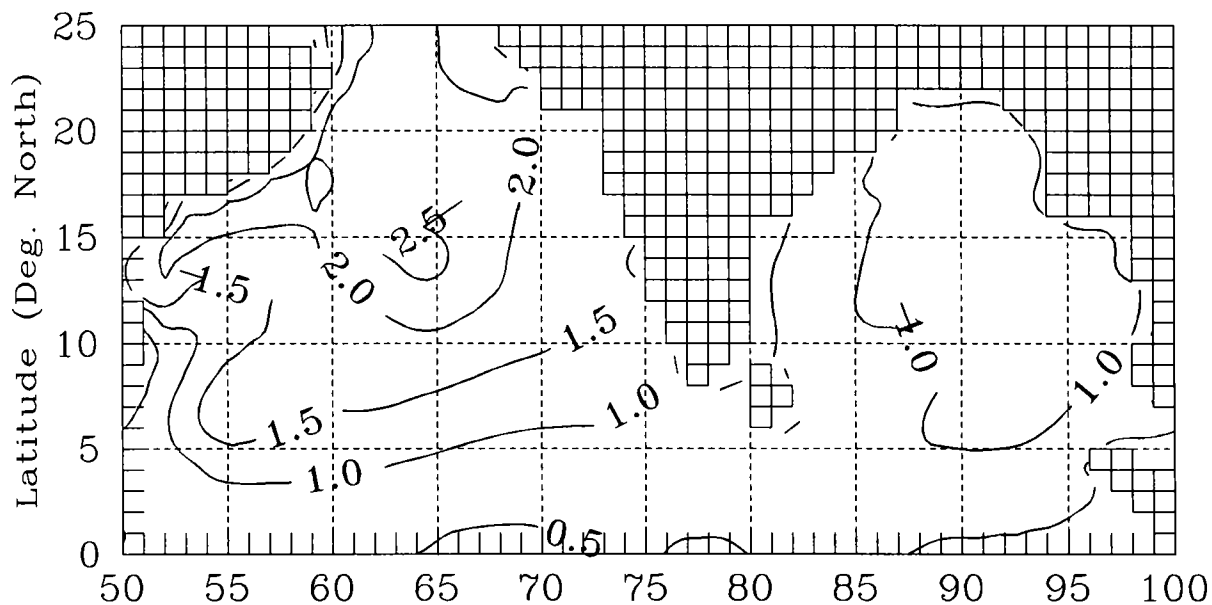


Fig.25A [a] The significant wave height (m), [b] Significant wave period (s) and windsea direction.

August [a]



[b]

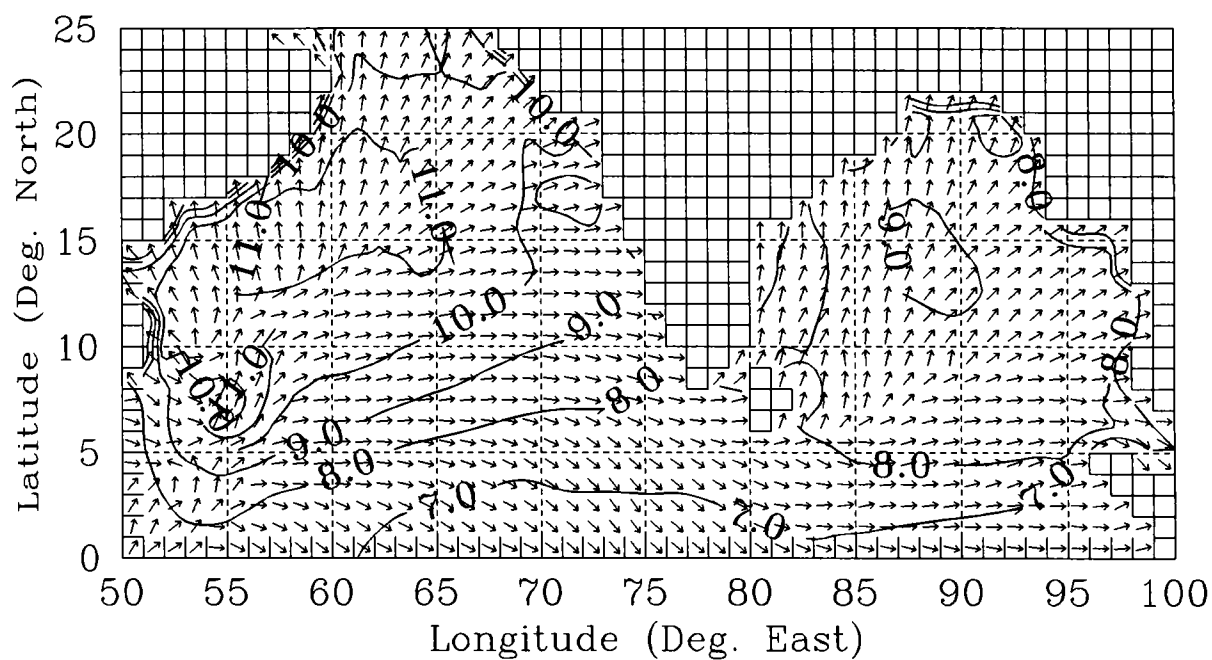
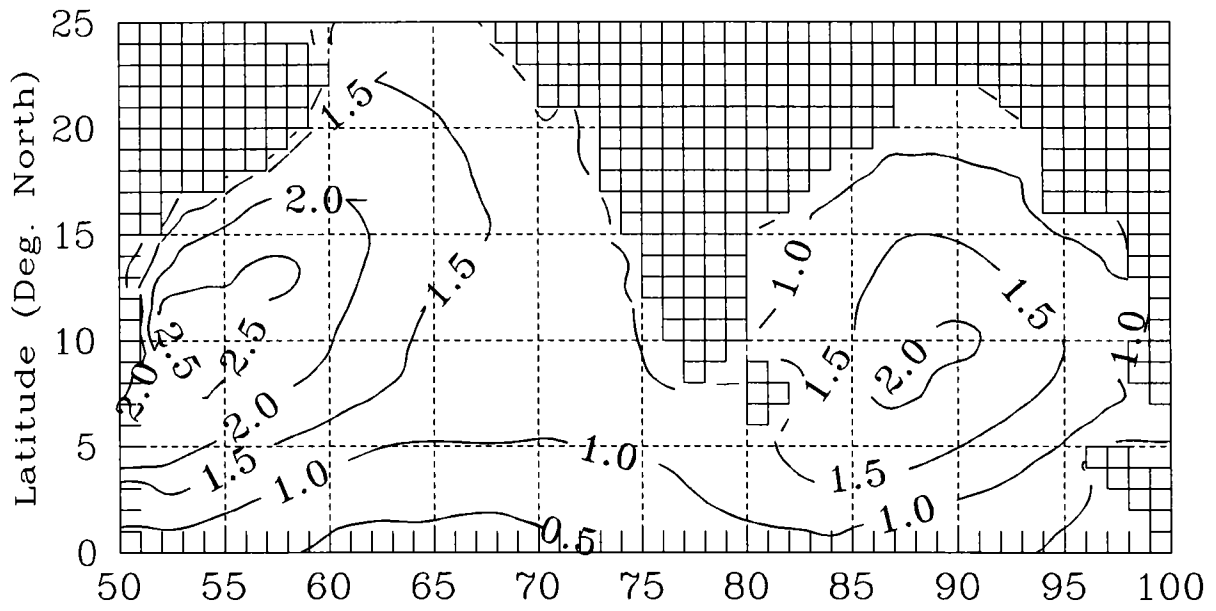


Fig.25B [a] The swell wave height (m), [b] Swell wave period (s) and direction.

September [a]



[b]

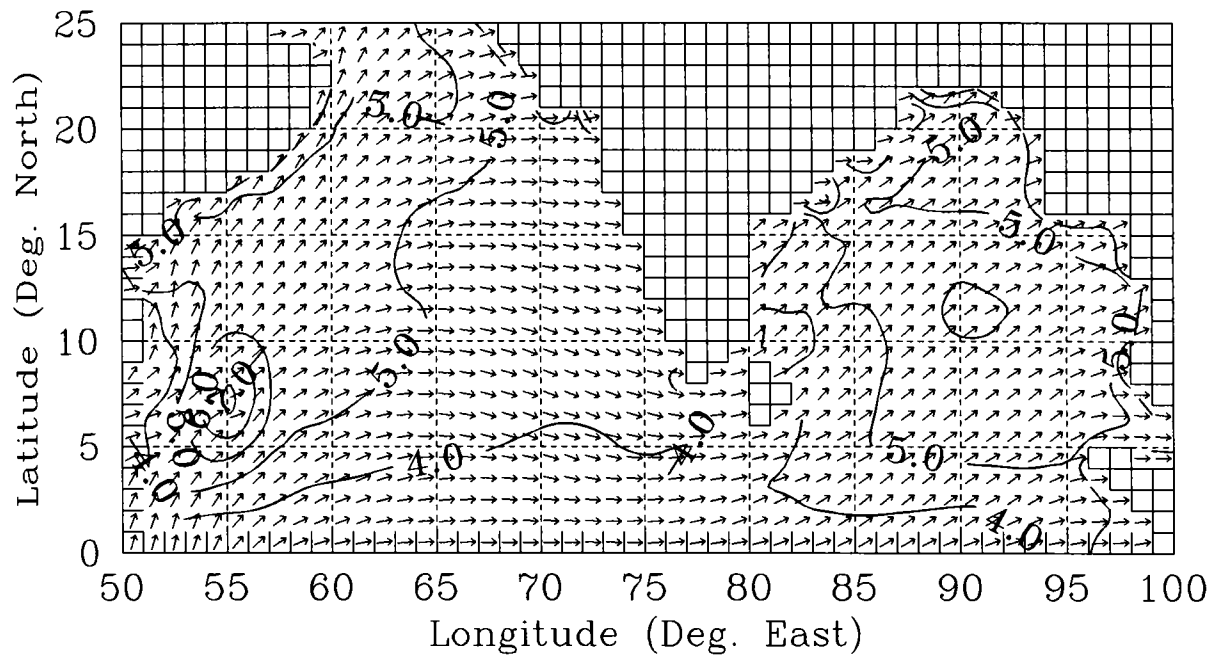
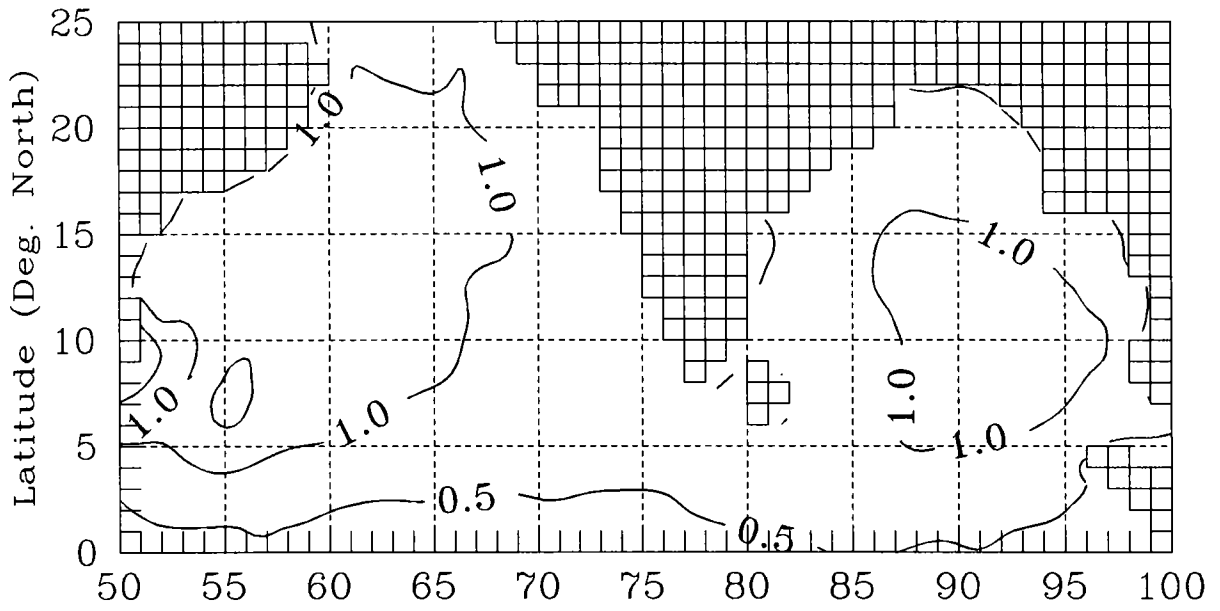


Fig.26A [a] The significant wave height (m), [b] Significant wave period (s) and windsea direction.

September [a]



[b]

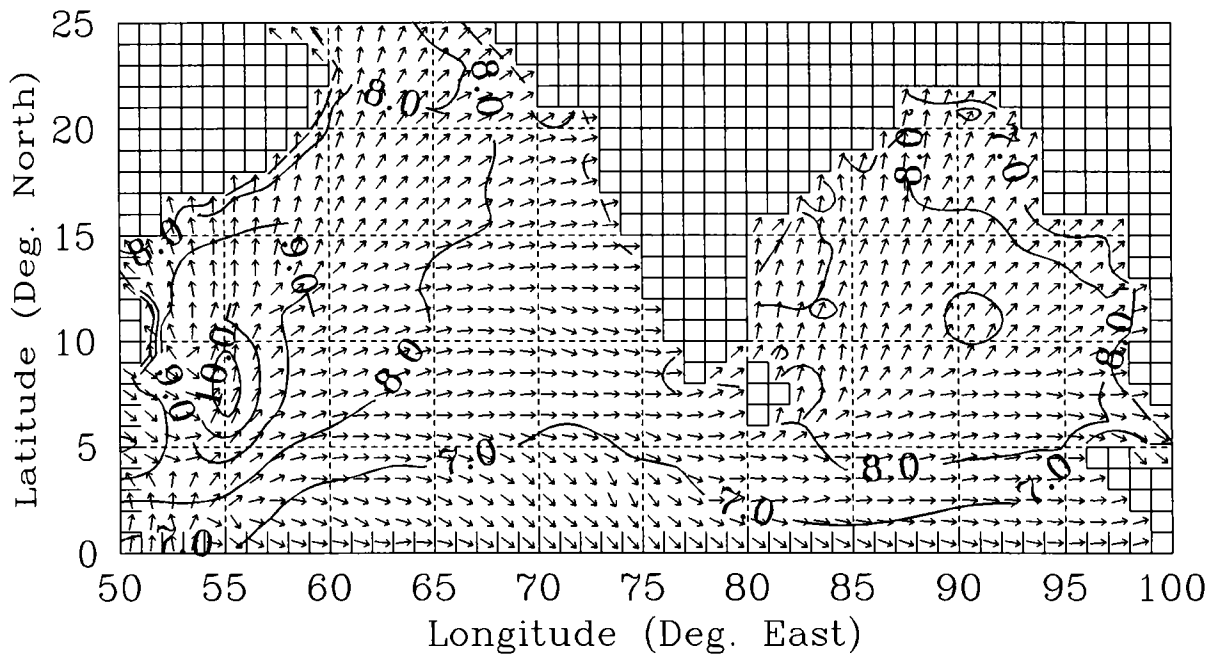
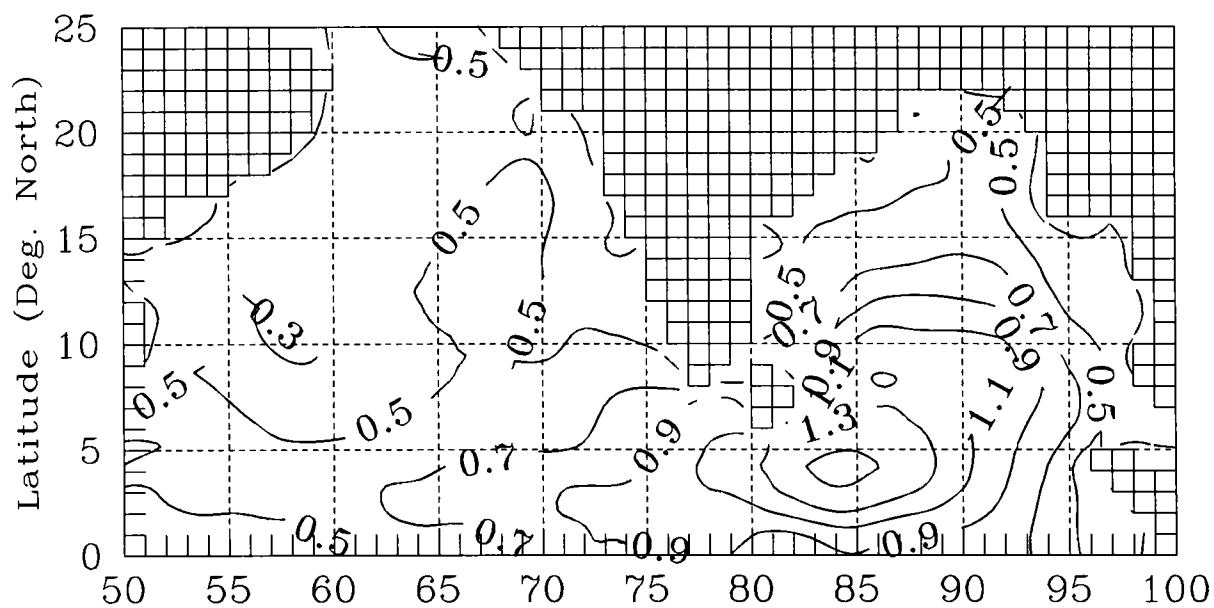


Fig.26B [a] The swell wave height (m), [b] Swell wave period (s) and direction.

October [a]



[b]

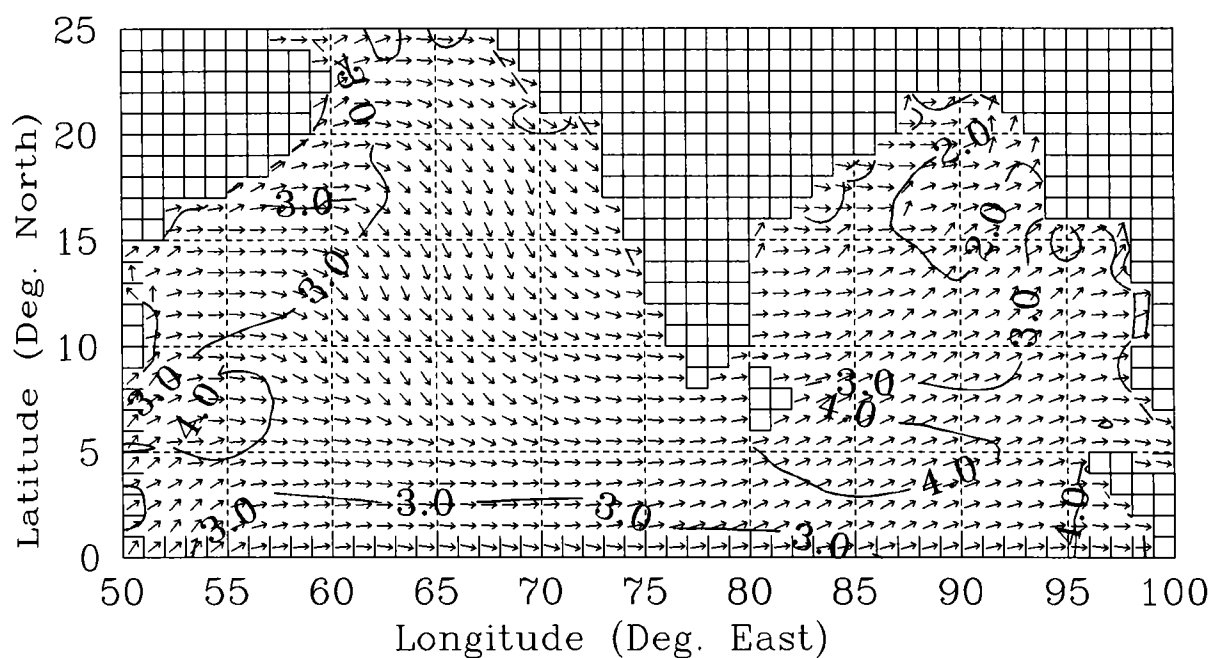
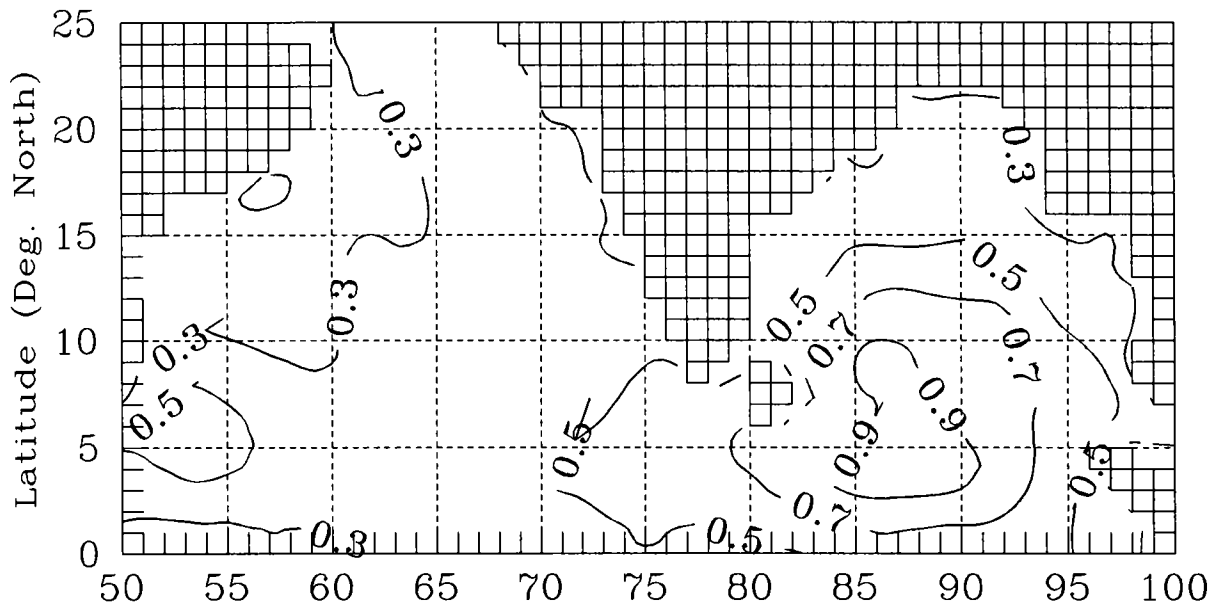


Fig.27A [a] The significant wave height (m), [b] Significant wave period (s) and windsea direction.

October [a]



[b]

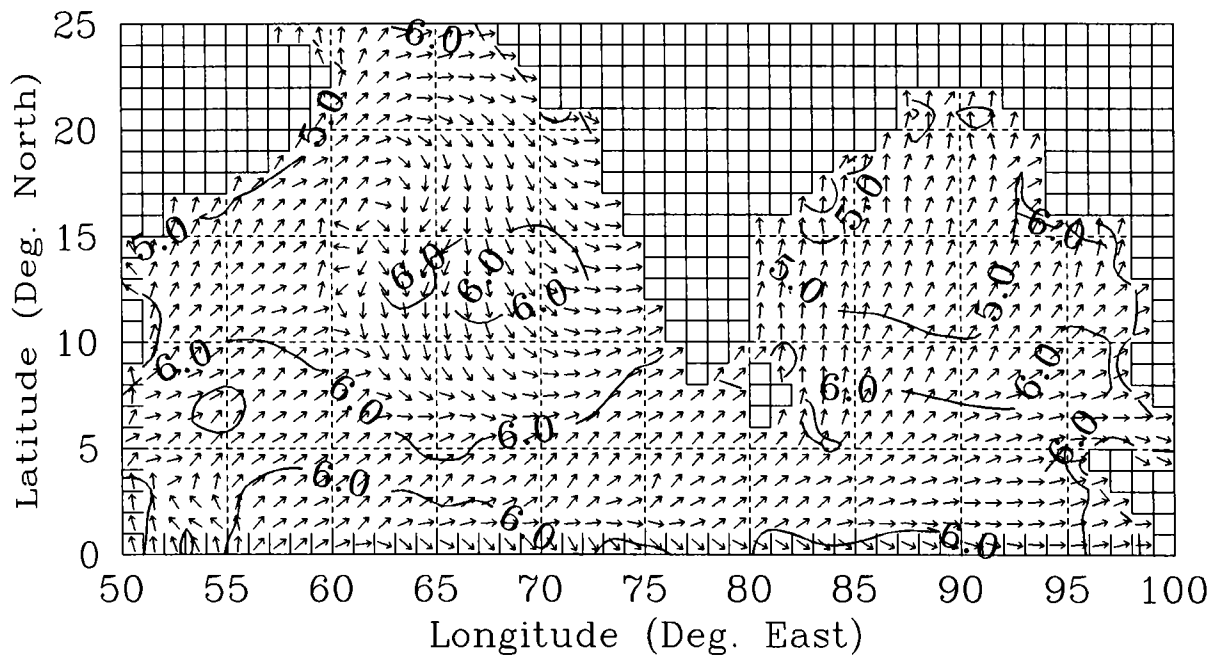
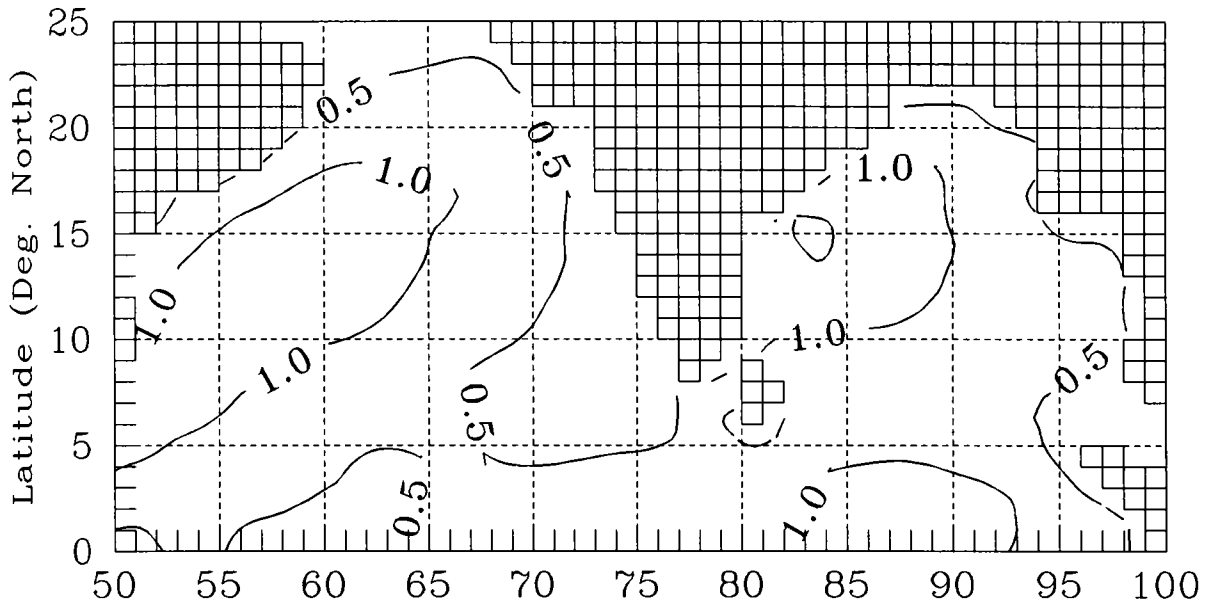


Fig.27B [a] The swell wave height (m), [b] Swell wave period (s) and direction.

November [a]



[b]

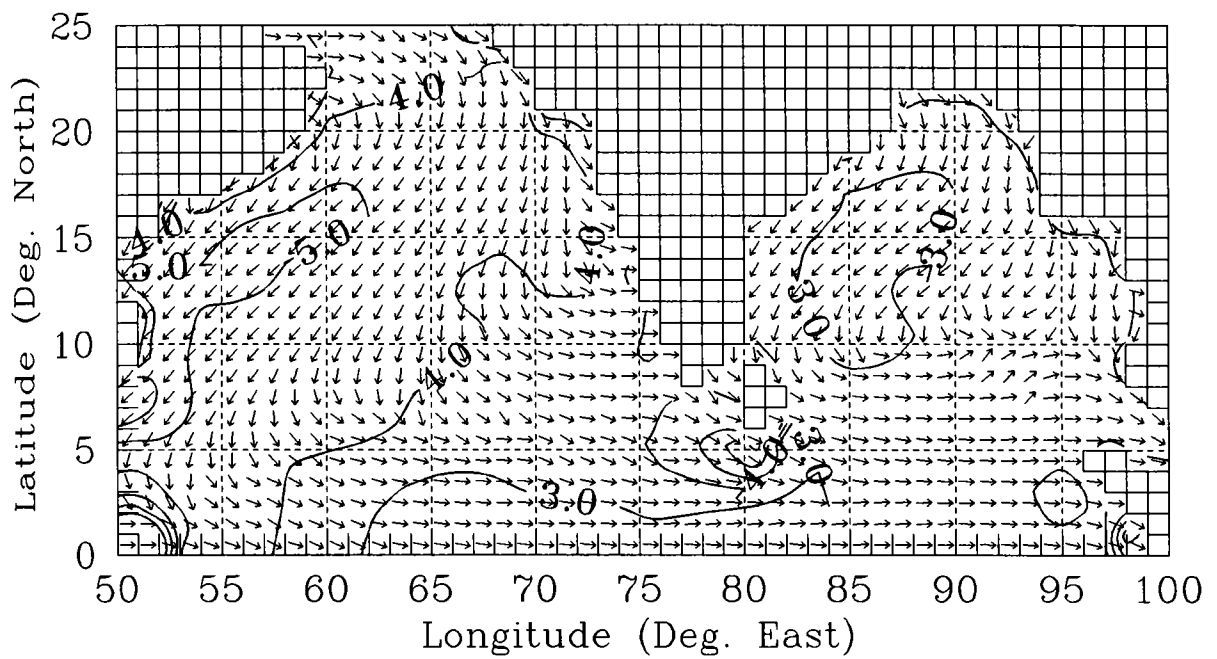
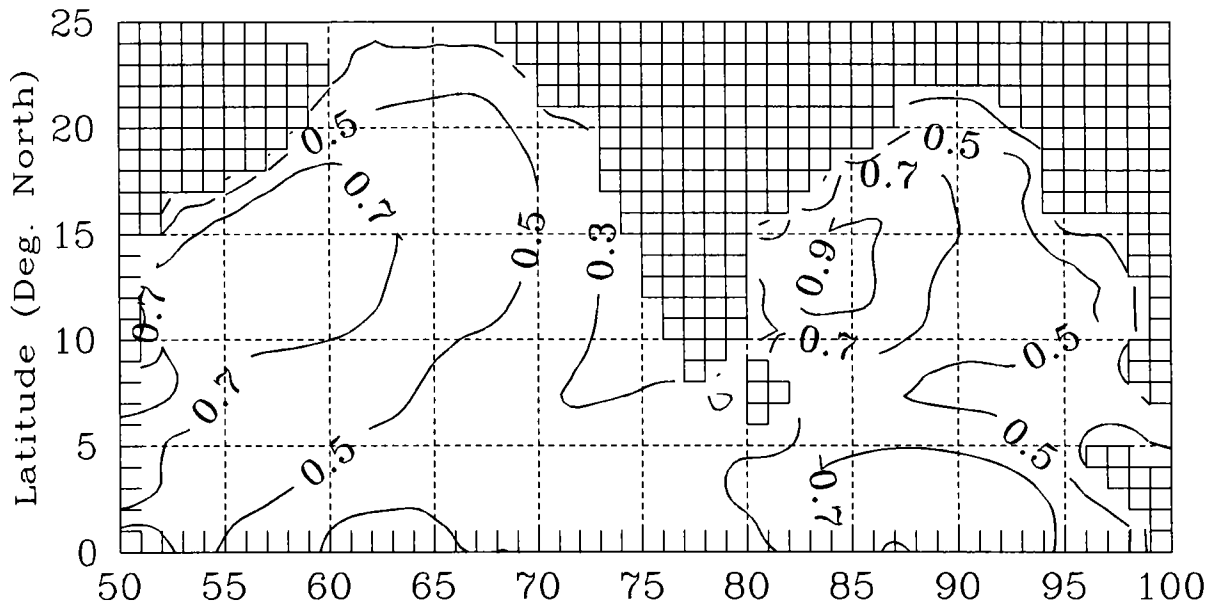


Fig.28A [a] The significant wave height (m), [b] Significant wave period (s) and windsea direction.

November [a]



[b]

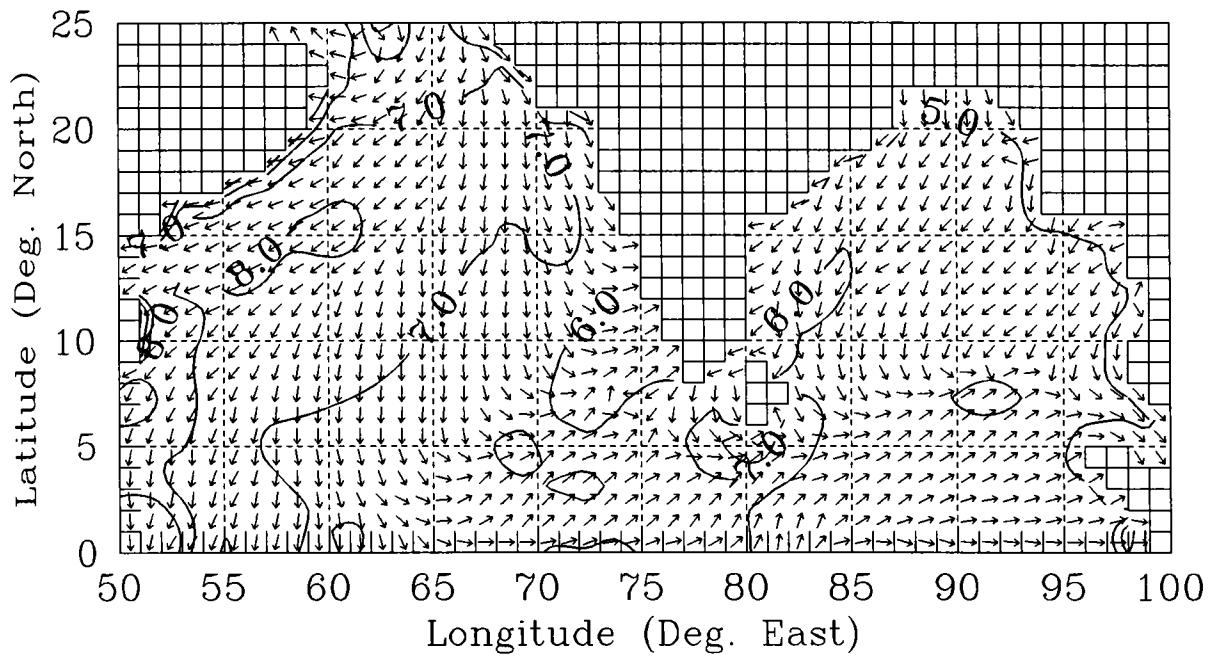
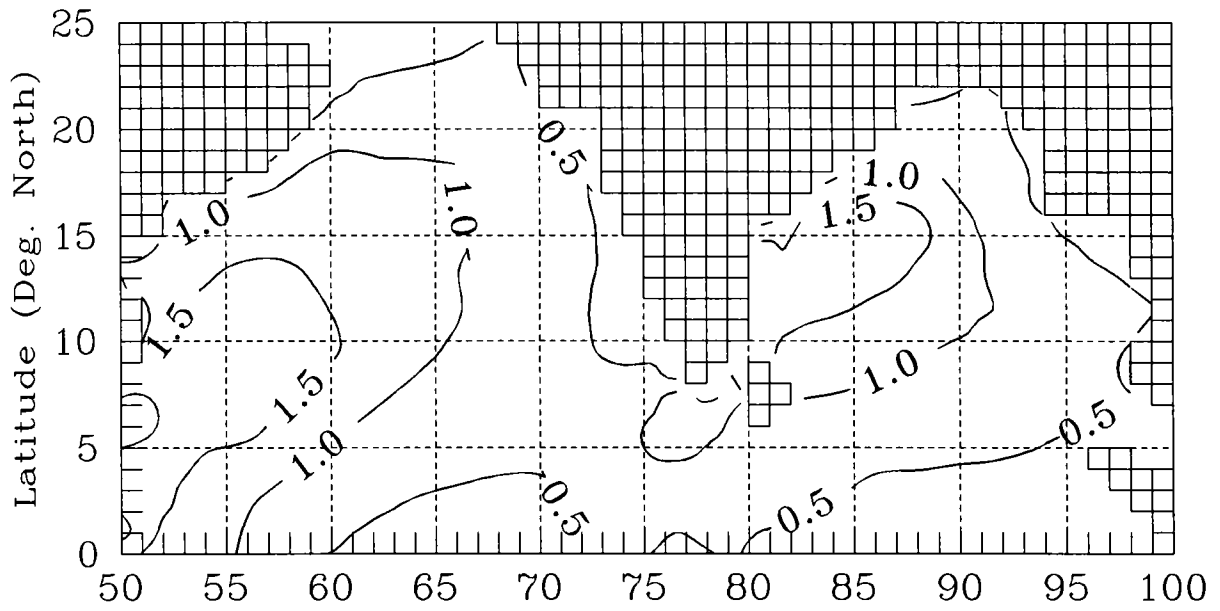


Fig.28B [a] The swell wave height (m), [b] Swell wave period (s) and direction.

December [a]



[b]

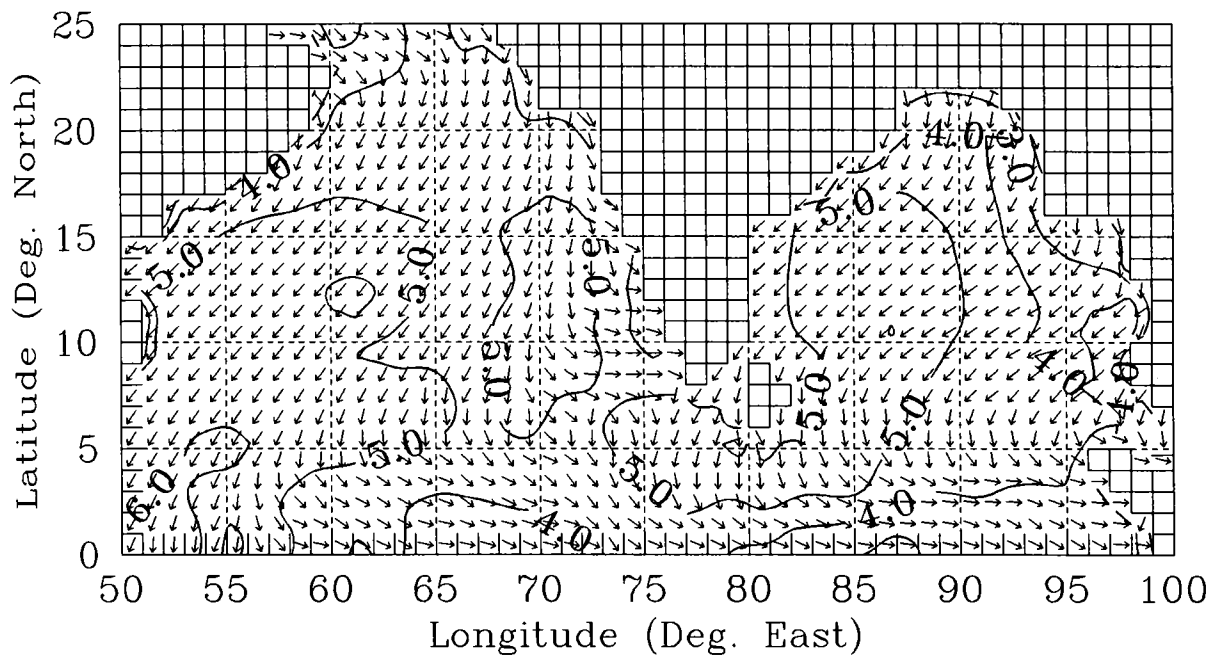
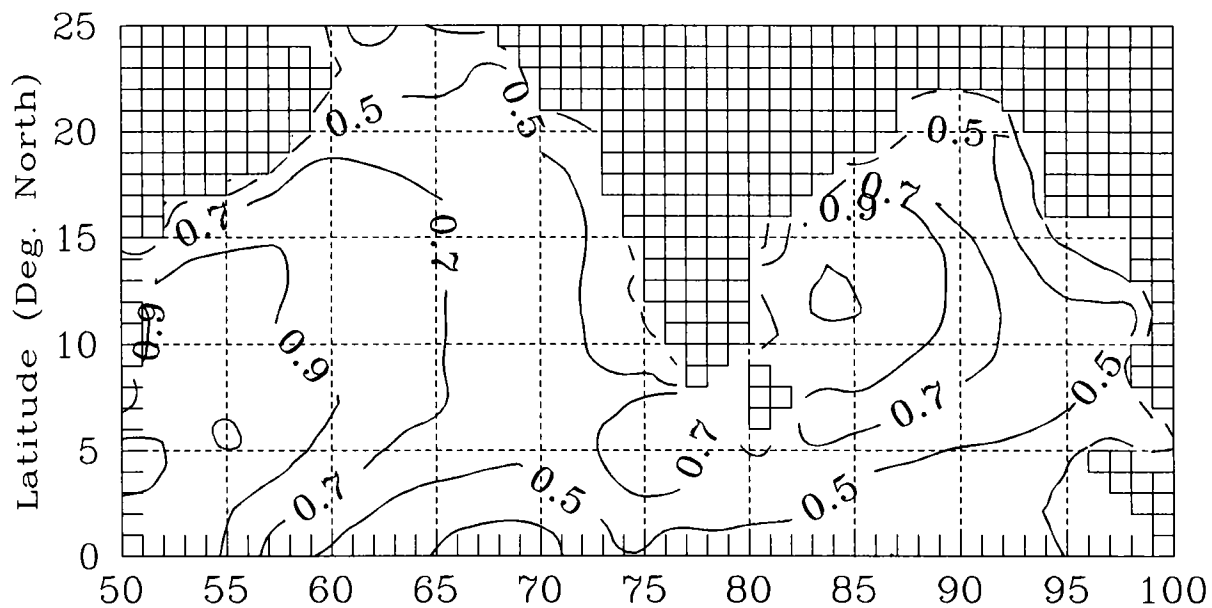


Fig.29A [a] The significant wave height (m), [b] Significant wave period (s) and windsea direction.

December [a]



[b]

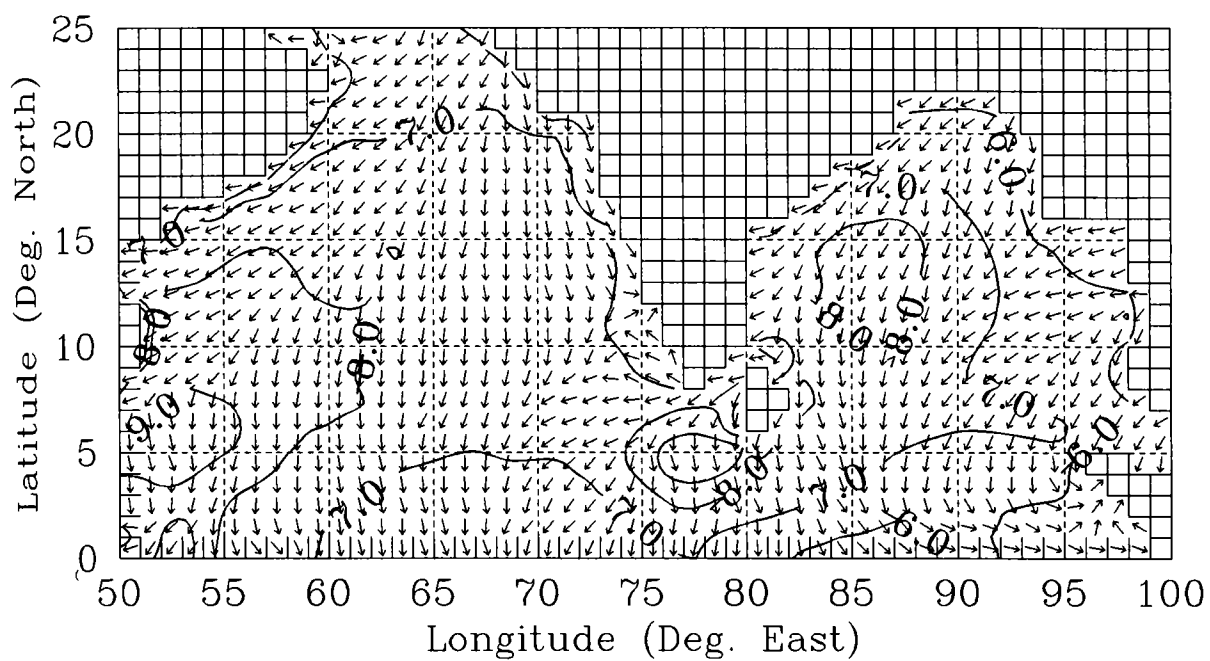


Fig.29B [a] The swell wave height (m), [b] Swell wave period (s) and direction.

15 days) and cover a few selected locations in the Arabian Sea and Bay of Bengal. All these data sets were collected for some specific requirements and they provide only some general idea about the prevailing wave conditions at that point of time. They are just cited as some of the examples of observed wave variability and to convey some relevant information supporting the important findings in the present study.

Table 5. Monthly wave height and period ranges for windsea and swell

Month	Arabian Sea				Bay of Bengal			
	Hs (m)	Ts (s)	Hsw (m)	Tsw (s)	Hs (m)	Ts (s)	Hsw (m)	Tsw (s)
1 January	0.3-2.1	3-8	0.2-1.3	6-10	0.4-1.5	3-6	0.3-1.2	5-8
2 February	0.2-1.6	3-7	0.2-1.1	5-9	0.2-1.0	3-5	0.2-1.0	6-8
3 March	0.3-1.2	2-5	0.3-0.9	4-8	0.2-0.8	2-4	0.2-0.7	4-6
4 April	0.2-0.9	2-5	0.2-0.8	3-6	0.3-1.1	2-5	0.3-0.9	4-7
5 May	0.6-2.4	3-5	0.5-1.5	5-8	0.5-2.1	3-6	0.5-1.4	5-8
6 June	0.7-4.1	4-9	0.6-2.3	6-11	0.5-2.7	4-7	0.5-1.9	6-9
7 July	0.6-6.1	5-11	0.5-3.2	7-13	0.7-3.0	4-6	0.7-2.2	6-8
8 August	0.5-5.2	4-9	0.4-2.6	6-12	0.4-2.4	4-6	0.5-1.3	6-9
9 September	0.4-2.7	3-7	0.4-1.6	6-11	0.3-2.1	3-6	0.3-1.3	7-9
10 October	0.5-1.2	2-5	0.2-0.7	5-7	0.4-1.5	3-5	0.4-1.1	4-7
11 November	0.4-1.4	3-6	0.4-0.9	5-8	0.4-1.6	2-5	0.3-1.0	5-7
12 December	0.4-1.9	4-6	0.3-1.1	6-9	0.3-1.7	3-6	0.4-1.1	6-9

VI.2.1.1 January: Time-series measurements using ship-borne wave recorder in deep waters off Cochin during January 1984 and off Bombay during January 1986 show variation of Hs from 0.6 to 1.0m and 0.3 to 1.2m respectively (Prasada Rao and Swain, 1985a; Swain, 1989a). The measured wave parameters cited here are well within the range of wave heights obtained from the simulation experiment for the month of January. However, it is not possible to establish the mean wave parameters for the measurement sites during January based on one or a few similar measurements of short durations. The simulated mean wave field as shown in Fig.18A shows the variation of mean wave parameters from one region to another. It reveals that, during the month of January wave activity remains higher in the southwestern Arabian Sea ($H_s \approx 1.5m$) while the north eastern region experiences low wave activity ($H_s \approx 0.5m$). The East coast of India, the central Bay of Bengal,

and the region adjacent to the southern extreme of the Indian subcontinent (Off Kanyakumari) experience nearly 1m waves with 4 to 5s period. The general wave direction is northeasterly in January but the waves approach the west coast of India from a north to northwesterly direction (Fig.18A & B). The distribution of Hsw is more or less similar to that of Hs although the magnitude is relatively less. The Hsw remains nearly the same along the west coast but along the east coast it shows gradual increase from north to south. Swell approach the east coast from a direction around east of northeast. Ts and Tsw are higher in the southwestern Arabian Sea. In general, wave conditions remain more or less the same during December and January. During these two months wind and wave activities are higher compared with the rest of the fair weather period.

VI.2.1.2 February: Wave activity reduces by 30 to 50 percent over the different parts of Indian Seas during February compared with January (Fig.19A & B). Hs is around 0.5m in the Bay of Bengal and most parts of the Arabian Sea except the southwestern region which experiences relatively higher waves ($\approx 1.0\text{m}$). Ts and Tsw show gradual increase from north to south. Measured Hs off Cochin using ship-borne wave recorder during February 1985 varied from 0.2 to 0.6m (Prasada Rao and Swain, 1985a). Similarly, during another field measurement using WAVEC buoy off Cochin during February 1990, Hs and Ts varied from 0.2 to 0.8m and 4.4 to 6.7s respectively and windsea direction ranged between 280 and 360 degrees (Swain and Ananth, 1994). It may be noted that the observed windsea direction off Cochin during February 1990 is in agreement with the simulated mean wave direction (Fig.19A). The general mean windsea direction for the Indian Seas as shown in Fig.19A is more or less similar to that for January except for the northwestern Bay of Bengal. Along the northeast coast of India, the windsea direction is almost west which gradually changes to northeasterly while approaching towards the central Bay of Bengal. Similarly, the swell directions start showing spiral patterns in the northwestern Arabian Sea and the Bay of Bengal. Except for these regions, swell directions are more or less the same as in January for the rest of the Indian Seas.

VI.2.1.3 March: It may be seen from Fig.20A & B that the sea-state further reduces by March compared to February. Hs is around 0.5m along the east as well as west coast of India. Off the central west coast, the windsea magnitude is almost equal to swell wave magnitude. Surprisingly, the wave measurements Off Goa using wave-rider buoy reveals unusually higher wind

and wave activity (Prasada Rao and Swain, 1989) in the month of March. During the data collection period (18 to 24 March 1986), Hs and Ts varied from 0.5 to 2.0m and 2.5 to 6.5s respectively (Swain et al., 1996). Another remarkable feature was the variation of wind and wave parameters over a diurnal cycle. Such situations may occur at some point of time even during the fair weather season. However, wave activity during March remains low as it may be seen from Fig.20A. Along with the changes in the wind pattern from February to March (Chapter-III), wave direction also shows noticeable changes. In the south eastern Arabian sea, the windsea direction changes from around northwest to westerly and moves towards the Bay of Bengal. Similarly, the windseas in the Bay of Bengal between 5° and 10° N latitudes also move towards east as they approach the eastern boundary whereas the swells move in different directions. The gyral pattern in the wave propagations shifts further towards south-west.

VI.2.1.4 April: Being the pre-monsoon period, the winds are low and highly variable during April (Chapter-III). The central Bay of Bengal as well as the west of central Arabian sea region show minimum resultant wind speed around 1 m/s. Hence, the mean monthly wave fields in these areas also indicate very low waves (Hs around 0.4m). Higher Hs and Hsw are noticed in the north eastern extreme of the Arabian Sea (around Gulf of Cambay) and the northern extreme of the Bay of Bengal (Fig.21A & B). Although the winds during this month are variable, the mean windsea direction shows a stream-lined pattern. The windseas which are northeasterly in the southwestern Arabian Sea during March move towards east during April. In the Bay of Bengal, the windsea direction varies from southwest in the northwestern region to west towards the equator. Except in the central and southwestern regions of the Arabian Sea, the arrows showing the swell direction are uniformly aligned in the rest of the Indian Seas and indicate that the swells move along the Arabian coast, west coast of India and finally to the Bay of Bengal. The swell directions in the whole of the Bay of Bengal are uniformly aligned although the prevailing winds remain variable in most part of it.

VI.2.1.5 May: The southwest monsoon winds begin to blow in the month of May and consequently wave activity increases considerably compared to April. Hs varies from around 1 to over 2m in the Arabian Sea (Fig.22A). The area to the south of the central Bay of Bengal also experiences higher waves ($H_s \geq 2m$). Since the sea-state during this period is mainly dominated by windseas, Ts varies from 3 to 5s for the whole of the Arabian Sea and

Bay of Bengal. The time-series wave measurements (wave-rider buoy) off Andamans during May 1987 showed variation of Hs and Ts from 0.5 to 1m and 4.5 to 9.8s respectively (Swain and Ananth, 1992). Similarly, measurements off Cochin in May 1988 with the same equipment showed Hs and Ts variations from 0.8 to 1.4m and 5.0 to 7.9s respectively (Swain and Ananth, 1992). During 22 May to 3 June 1992, WAVEC buoy was moored off Cochin and time-series wave data were collected. During this period of WAVEC deployment Hs, Ts and windsea direction varied from 0.9 to 2.4m, 5.0 to 8.4s and 225 to 045 degrees respectively. The predominant wave parameters such as Hs, Ts and the windsea direction during these observation programs more or less agree with the simulated parameters. It may be seen from Fig.22A that, all along the west coast of India, the windsea direction is around west of northwest whereas the general direction of windseas remains southwesterly in the Bay of Bengal. Similarly, the region adjacent to the southern boundary of the regional grid system also experiences southwesterly waves (Fig.22A & B) which gradually become westerly and north of northwesterly as they move from west to east in the Arabian Sea. Along the west coast, windsea direction remains west of northwest while swells approach the south west coast from a direction around west to southwest. Hsw is around 1.0m for most of regions of the Bay of Bengal and the western Arabian Sea. It may be noted that the Bay of Bengal is relatively rough compared to the Arabian Sea during May. In general, Hs, Ts, Hsw and Tsw are relatively higher in the southern Bay of Bengal compared to the Arabian Sea as the southwest monsoon sets in early in this region.

VI.2.1.6 June: Since the southwest monsoon becomes fully active all over the Arabian Sea and Bay of Bengal by the month of June, the sea becomes further rough (Fig.23A & B) compared to May. The mean monthly fields in Fig.23 show Hs and Ts around 2m and 7s respectively. The simulated mean Hs during June reaches up to 4m towards the west of the central Arabian Sea and 2.5m in the central Bay of Bengal. Windsea direction is almost southwesterly for most of the Arabian Sea and Bay of Bengal. Starting with the central Arabian sea the windseas gradually turn their direction to west as they approach the west coast of India. The maximum Ts is about 9s in the central Arabian sea and 6s in the Bay of Bengal. It may be noted that, the wave-rider measurements off Cochin during June 1987 showed Hs and Ts variations from 2.0 to 2.7m and 6.0 to 7.5s respectively (Swain and Ananth, 1992). During another experiment for a period of two years off Karwar (shallow water, 16m water depth) during the month of June 1989, Hs and Ts

varied from 2.6 to 2.9m and 6.5 to 6.8s respectively (Mandal et al., 1991). The magnitudes of observed Hs and Ts off Cochin (June 1987) are within the range of simulated parameters obtained for June. Although the observations off Karwar is in shallow waters and Hs is slightly higher compared to that of off Cochin, it is difficult to arrive at any conclusion regarding relative magnitudes for both these stations based on just two data sets of this kind. However, the simulated results could clearly indicate that Hs increases considerably from south to north along the west coast but it is more or less the same throughout the east coast. Hsw also follow the same trend for west coast but it is higher ($\approx 1.5\text{m}$) off Calcutta and lower towards the south along the east coast. Swell wave directions show a diverging pattern from south west Arabian Sea towards the north and along the east. The pattern is more or less same in the Bay of Bengal. The swell waves approach the west coast of India almost in the same direction as windseas, southwesterly in north west coast and westerly in south west coast. Their direction remains southerly along the east coast.

VI.2.1.7 July: The southwest monsoon reaches its peak during July. The Indian Seas remain very rough during this month (Fig.24A & B) compared to the rest of the rough weather months. Hs varies from about 1.0 to 6.0m in the Arabian Sea and 1 to 3m in the Bay of Bengal. Wave directions (windsea and swell) are more or less the same during June and July except that the swells in the southeastern regions of Arabian Sea turn further towards the equator. The Hsw show a gradual increase from the southwest to northeast in the Arabian Sea. The distribution of Hsw over the Bay of Bengal is almost similar to that of Hs. It increases from south to north whereas along the southeast coast, it is nearly 1m. The mean swell periods reaches up to 12s and 7s respectively in the Arabian Sea and Bay of Bengal. In general, mean monthly wave parameters Hs, Ts, Hsw and Tsw reach their maxima during July.

VI.2.1.8 August: The wave activity decreases in August compared to July (Fig.25A & B). During August, Hs distributions are similar to those in July. The maximum Hs are about 5.0 and 2.5m in the Arabian Sea and Bay of Bengal. Higher waves are noticed around the northwest regions of the central Arabian Sea while Ts is higher in the southwest Arabian Sea. In general, the wave height maxima (Hs & Hsw) start shifting towards southwest both in the Arabian Sea and Bay of Bengal. Wave directions remain more or less the same from June to September. During July, the northeastern Arabian Sea region experiences higher swells which shift towards the central Arabian Sea during August. The maximum Hsw in the Bay of Bengal during this

month is around 1m.

VI.2.1.9 September: The southwest monsoon starts to withdraw towards end September. Hence, from wave climate point of view, September is the end of the rough weather season. Wave activity considerably reduces in September (Fig.26A & B) compared to August. Since the monsoon gradually starts withdrawing during this period, wave height (Hs & Hsw) maxima also shift further towards southwest of the Arabian Sea and Bay of Bengal. The maximum Hs which is about 5m during August decreases to 2.5m in the Arabian Sea. However, the maximum Hs in the Bay of Bengal remains more or less the same during August and September. The average sea-state for the whole of the Arabian Sea and Bay of Bengal is lower during September compared to August. The Hsw also shows a similar decrease compared to August.

VI.2.1.10 October: This is the post monsoon period. From wave climate point of view, it is considered as the beginning of the fair weather season and wave field weakens further compared to September. The southwestern Bay of Bengal remains relatively rough ($H_s \geq 1.5m$). However, in the Arabian Sea, the maximum Hs is towards the southeastern extreme (adjacent to Hs maxima in the Bay). Along the east coast, wave height increases from north to south. Windsea directions in the Arabian Sea show significant changes compared with September. The directions vary from northwesterly to westerly while approaching the west coast. Distribution of Hsw is similar to that of Hs. Hsw maxima occur to the south of the Bay of Bengal and are close to the Hs maxima. Swells approach the southwest coast of India from the west of southwest. Swell direction is south of southwest along the northwest coast. The difference in swell direction is over 90 degrees in contrast to eastern and western parts of central Arabian Sea. The central Bay of Bengal experience southwesterly swells. For both the Arabian Sea and Bay of Bengal, Tsw varies from about 4 to 7s.

VI.2.1.11 November: The northeasterly winds become stronger during November. The most important feature is the change in wind as well as wave direction compared with the previous month. The general wave activity increases from October to November. Hs exceeds 1m towards the central and western parts of the Arabian Sea. The east coast and the southern extreme of the Bay of Bengal experience higher wave activity ($H_s \geq 1m$). Windsea direction is mostly northeasterly to the north of 10° latitude. The windseas in the southeastern Arabian Sea (south of 10° latitude) move towards east which extend up to the eastern limit of the Bay of Bengal (80°

longitude). The windseas approach the east coast from northeast direction. Higher Hsw is noticed off the southeast coast and the maxima appear off Madras. In general, the pattern of Hsw distribution over the Arabian Sea and Bay of Bengal remains the same as that for Hs. The swell direction is northerly off the west coast between 65° and 70° E longitudes and some adjacent regions to the west except the southern extreme. However, the southwest coast experiences lower swells ($H_{sw} \approx 0.3$ m) and the mean swell direction off the southwest coast is around southwest. In the northern Bay of Bengal, the swell direction is northeast while the southern extreme experiences southwesterly swells.

VI.2.1.12 December: As mentioned earlier the mean wave fields during the months of December and January are more or less similar. Wave activity is more during December (Fig.29A) compared to November. Wave height maxima ($H_s \geq 1.5$ m and $H_{sw} \geq 1.0$ m) are noticed in the southwestern Arabian Sea and off the southeast coast of India. The T_s and T_{sw} vary from about 4 to 6s and 6 to 9s respectively both in the Arabian Sea and Bay of Bengal. The wave measurements off Cochin using wave-rider buoy during December 1986 showed the variation of H_s from 0.5 to 1.0m and T_s from 4.0 to 6.7s (Swain and Ananth, 1992). To site one example of shallow water measurements here, directional wave measurements were carried out off the southeast coast (off Tamilnadu) during November–December 1995 (Sanil Kumar et al., 1996). During the period of measurement, the most probable significant wave height, significant wave period and mean wave direction varied from 0.4 to 1.6m, 3 to 5s, and 30 to 120 degrees respectively. Fig.29A indicate that the windsea direction is generally northeast during December except off the west coast and south of 5° latitude. Windseas south of 5° latitude move eastward while their directions off west coast varies from north of northwest to west of northwest. The H_{sw} remains low along the west coast (≈ 0.3 m). Swell direction remains northeast for a stretch of 5 degrees off the Arabian coast. The rest of the region in the Arabian Sea excepting 0° to 20° N and 70° to 80° E experiences northerly swells. In the Bay of Bengal the swell direction varies from north of northeast to east of northeast except in the southern extreme.

VI.2.2 Seasonal distribution

There are no deep water measurements available anywhere in the Indian Seas covering one full seasonal cycle. However, there are some shallow water measurements available at a few selected locations along the east and

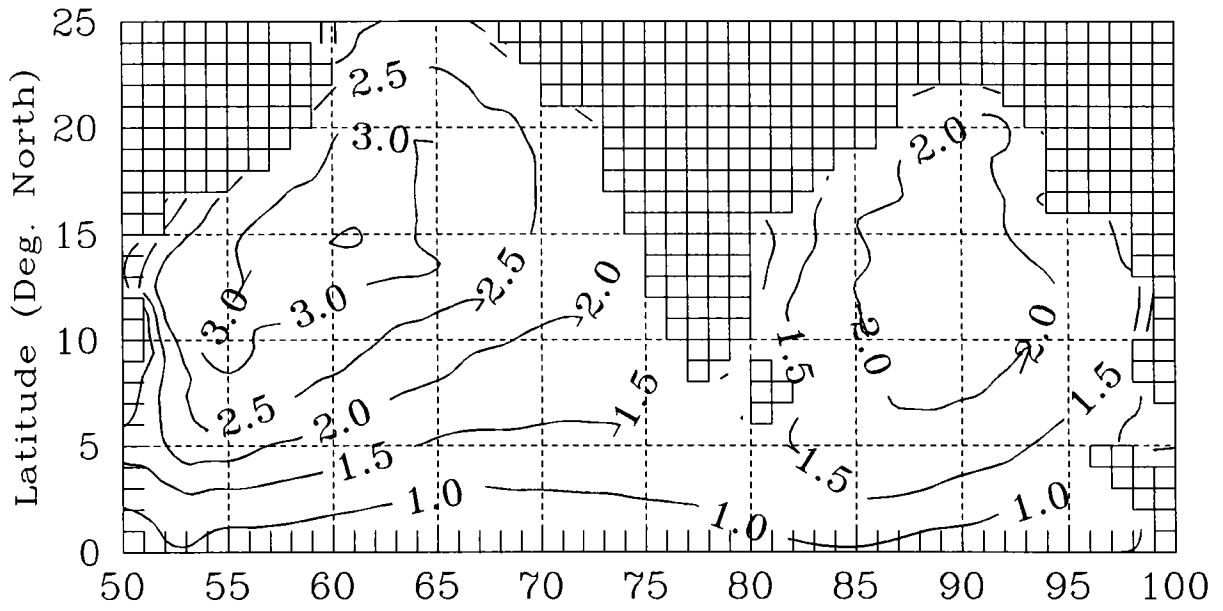
west coast of India and near Island stations. Deep water wave measurements were carried out off Trivandrum and Cochin for about a period of 40 days covering the months of May, June, and August 1984 during southwest monsoon (Baba and Joseph, 1988). They showed Hs and Ts variations from 0.6 to 2m and 3 to 10s respectively. In one of the shallow water measurements off Cochin during May-October 1986, Hs and Ts varied from 0.4 to 2m and 3.5 to 8.0s during the rough weather season (Swain et al., 1993). The observed Hs during this year was generally low due to the weak monsoon winds (Sharma et al., 1992). Although the observation site was in shallow waters, the mean Hs for the rough weather season May-September 1986 is found relatively low compared to the simulated mean shown in Fig.30.

As the wind pattern completely reverses between the boreal winter and the boreal summer monsoons over a large part of the Indian Ocean, the wave field over the Arabian Sea and Bay of Bengal also show significant seasonal variations (Fig.30 & 31). The mean Hs over the Arabian Sea and Bay of Bengal during the rough weather season (May-September) reach up to 3.5 and 2.5m respectively. The Hs minimum is around 1.0m for the whole of Indian Seas. Hs maxima are noticed around the north west Arabian Sea region and the central Bay of Bengal. However, during the fair weather season (October-April), the mean Hs in the Arabian Sea and Bay of Bengal reach up to 1.2 and 1.0m respectively. The minimum Hs is as low as ≤ 0.5 m over the Arabian Sea and Bay of Bengal. The Hs maxima in the Bay of Bengal shifts towards southwest and the same is noticed in the southwest extreme of the Arabian Sea. Ts varies from 6 to 9 and 5 to 7s respectively in the Arabian Sea and Bay of Bengal during the rough weather season while the same varies from 7 to 9 and 6 to 8s respectively during fair weather season. In general, the simulated wave heights for the rough weather season are about three times higher than those for the fair weather season.

VI.2.3 Annual distribution

Annual distributions of Hs and Ts for the Arabian Sea and Bay of Bengal are shown in Fig.32. The average Hs over the Arabian Sea and Bay of Bengal vary from about 0.7 to 2.0 and 0.6 to 1.6m respectively. Hs maxima appear in the western Arabian Sea (>1.8 m) towards the Arabian coast and the central Bay of Bengal (≥ 1.5 m). Average Hs in the south west coast is 1m which increases gradually towards north west coast. Average Ts varies from 5 to 8s for the Arabian Sea and Bay of Bengal. The Ts maxima follow the wave height distribution to a considerable extent.

May-September [a]



[b]

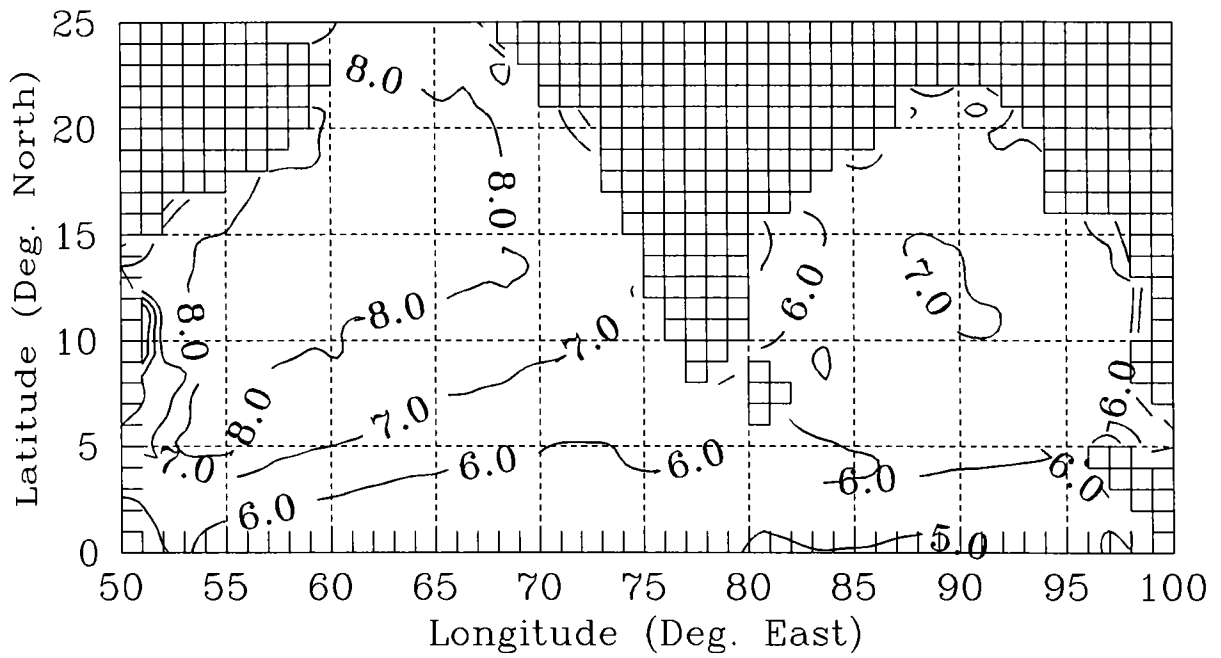
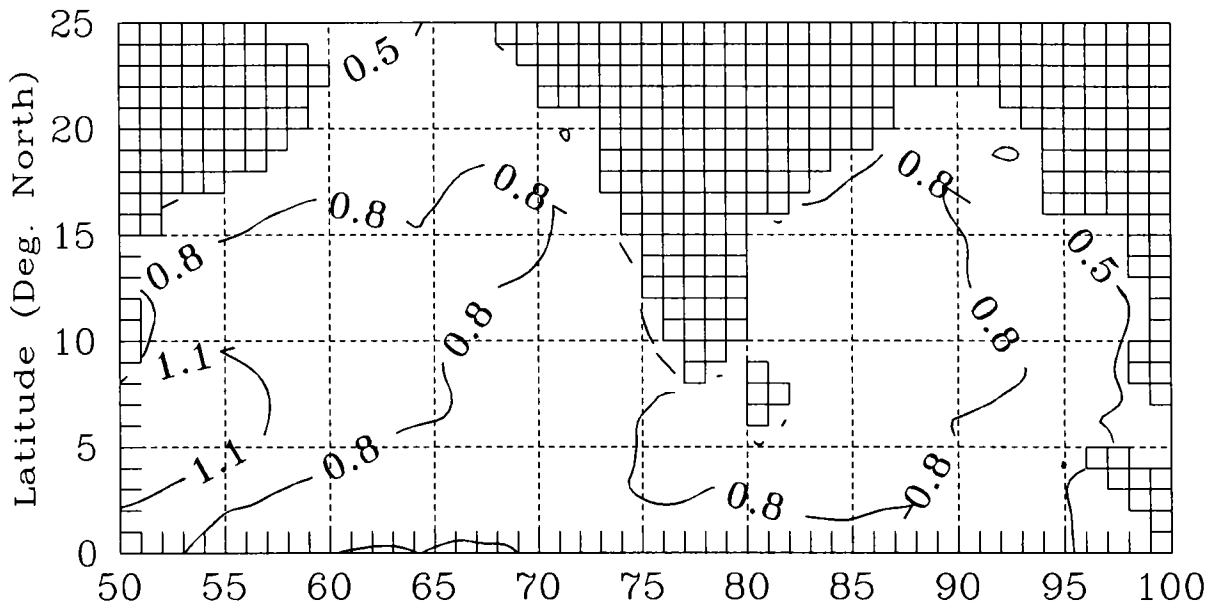


Fig.30 [a] The significant wave height (m), [b] Significant wave period (s).

October–April [a]



[b]

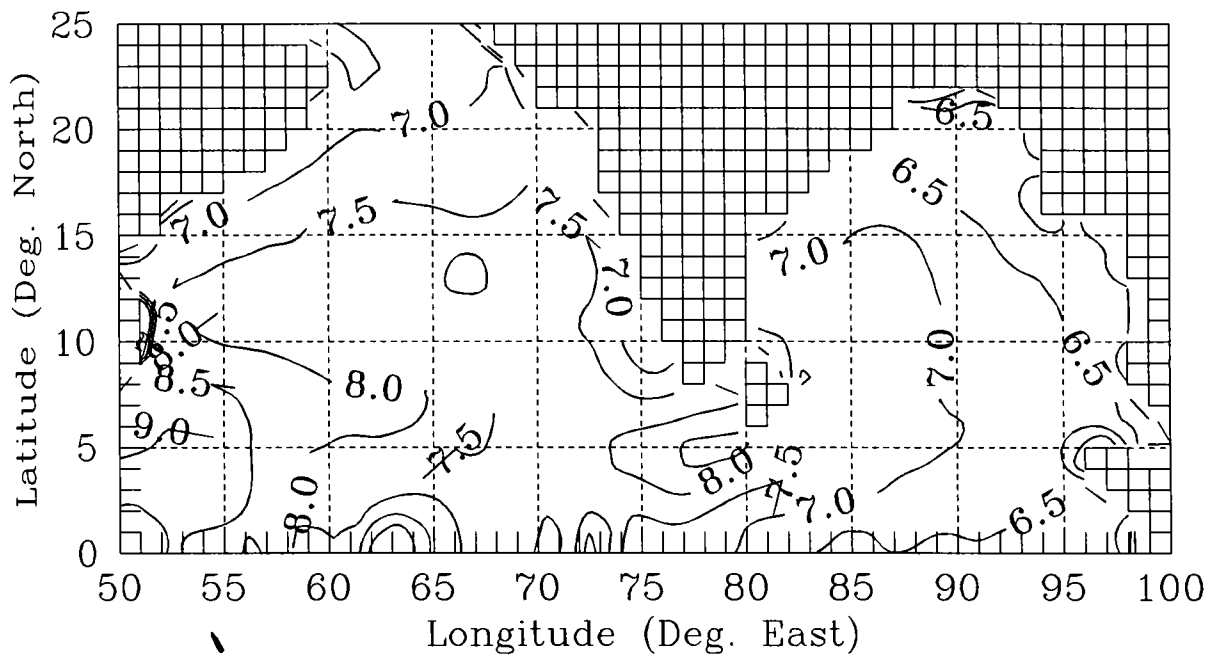
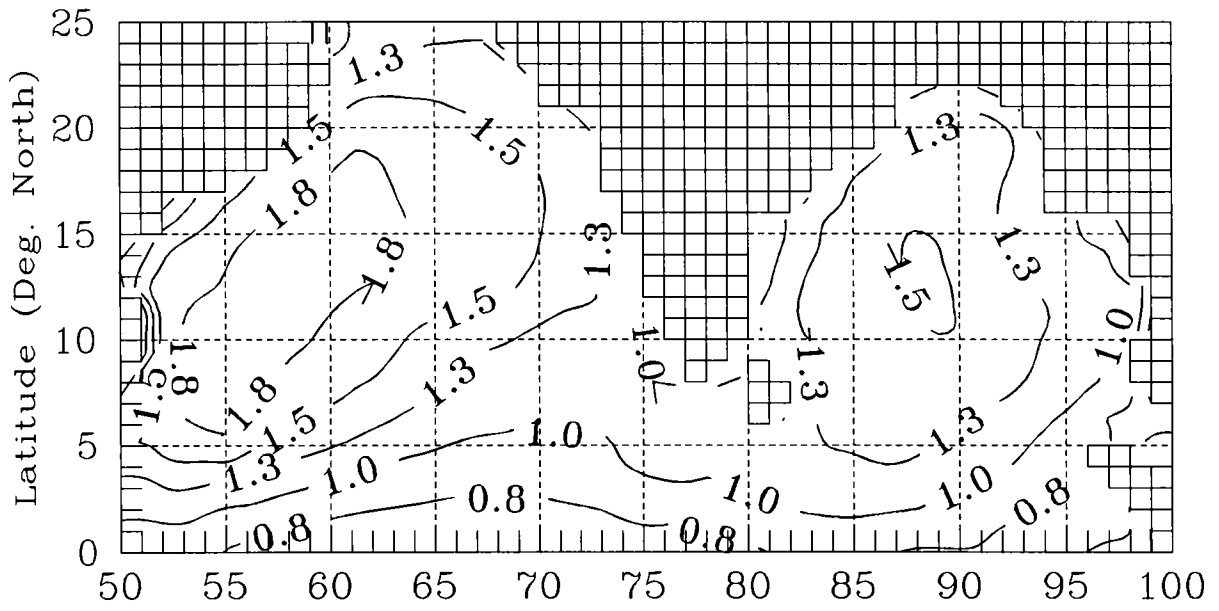


Fig.31 [a] The significant wave height (m), [b] Significant wave period (s).

January–December [a]



[b]

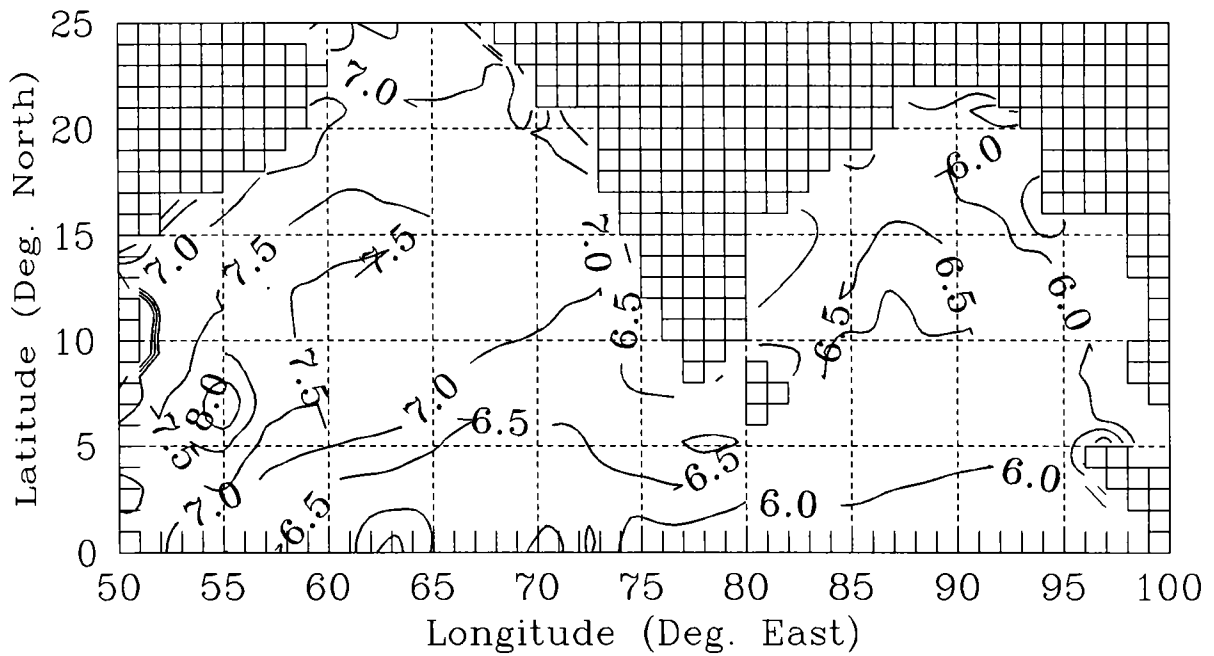


Fig.32 [a] The significant wave height (m), [b] Significant wave period (s).

VI.3 STATISTICAL DISTRIBUTION OF WAVE HEIGHT AND PERIOD

In this study, the monthly distributions of wave height and period for the different regions in the Arabian Sea and Bay of Bengal are not attempted. However, seasonal distributions of Hs and Ts for both the Arabian Sea and Bay of Bengal are brought out for both the rough weather and fair weather seasons.

VI.3.1 Bivariate distribution

The bivariate distributions of Hs and Ts give a detailed information on wave climate of a region. Fig.33 presents the number of occurrences out of 1000 for the respective ranks of wave heights (Hs at 0.5m interval) and periods (Ts at 1s interval) during the rough and fair weather seasons in the Arabian Sea and Bay of Bengal. Dotted lines in the figure show the significant wave steepness. The correlation between Hs and Ts is found to be insignificant for all the four cases as the wave climate in the Indian Seas is composed of windseas and swells. The correlation between Hs and Ts can be significant if the wave climate is dominantly governed by local wind waves. This is true in the case of enclosed water bodies (Goda, 1990). Fig.33 reveals that during fair weather season there are more number of waves occurring with relatively higher period compared to their height. It indicates that, the sea-state during the fair weather is generally dominated by swells. The Hs and Ts vary from 0.3 to 6.0m and 3 to 17s respectively for the Arabian Sea during the rough weather season. The wave activity drastically reduces during the fair weather period. Hs and Ts range from 0.2 to 3.5m and 2 to 14s respectively during the fair weather season. Similarly, in the Bay of Bengal during the rough weather season, Hs and Ts vary from 0.3 to 4.5m and 3 to 15s respectively. During the fair weather season, they vary from 0.2 to 3.0m and 2 to 13m respectively.

VI.3.2 Cumulative distribution

Fig.34A & B present cumulative distributions of Hs and Ts respectively for the Arabian Sea and Bay of Bengal during the rough and fair weather seasons. It may be noted that, the sea remains calm ($H_s < 0.5$ m) only for 5% of the time during the rough weather season. During the fair weather period the sea remains calm for about 20% of the time. The Hs exceeds 1m for 70% of the time in both the Arabian Sea and Bay of Bengal during the

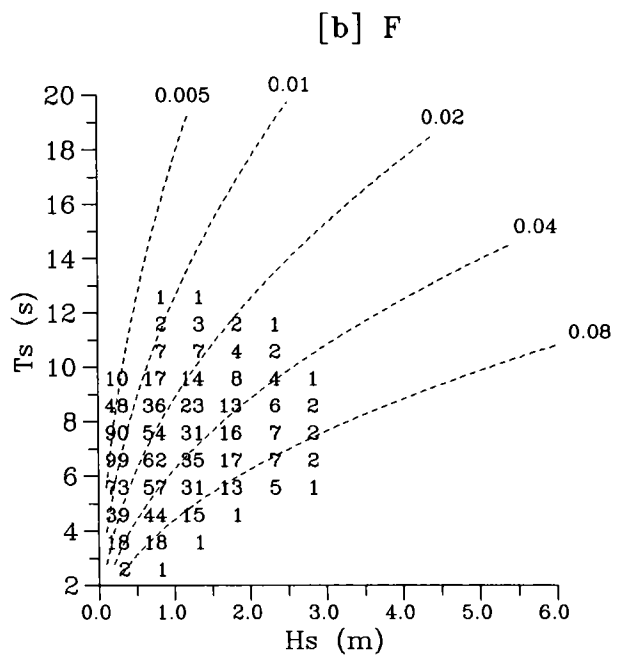
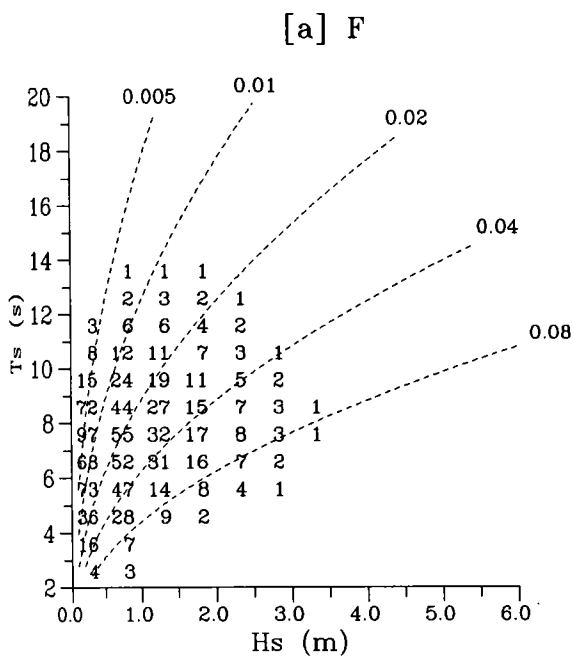
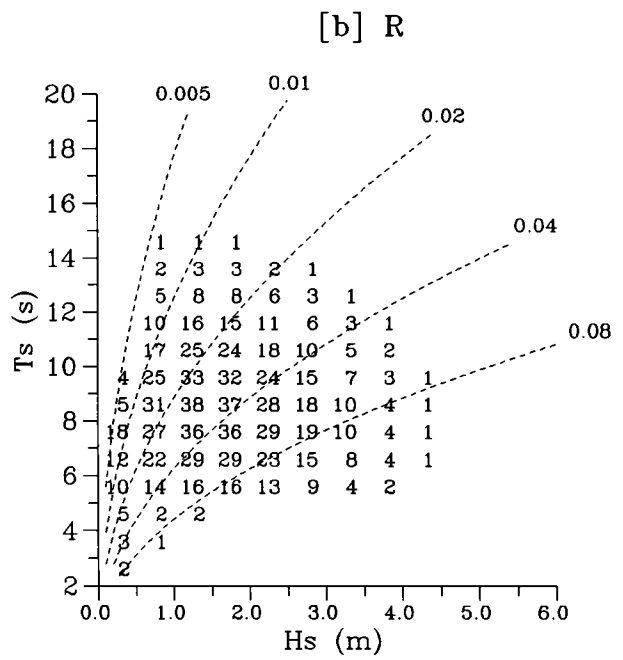
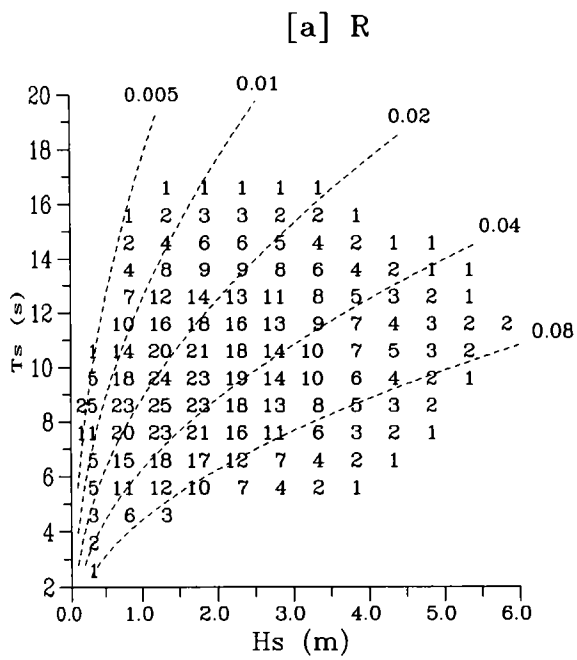


Fig.33 Bivariate distribution for Hs and Ts. [a] - Arabian Sea [b] Bay of Bengal, R - Rough weather, F - Fair weather.

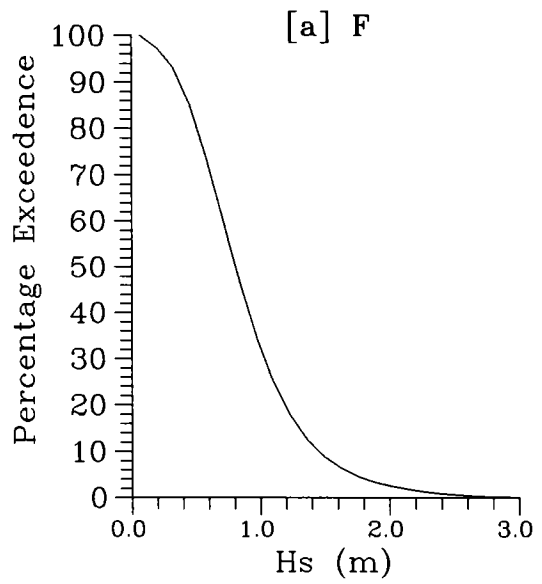
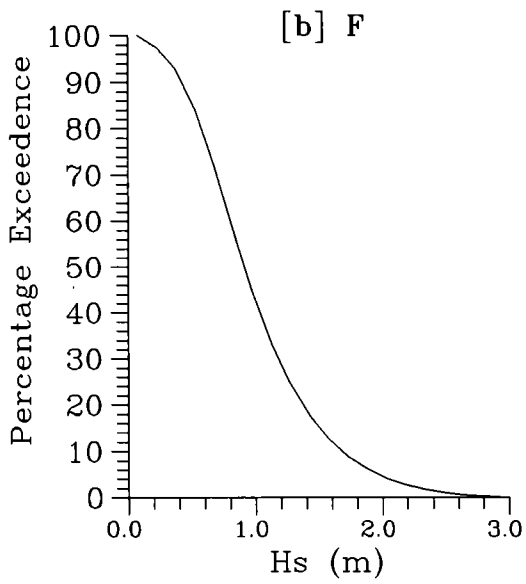
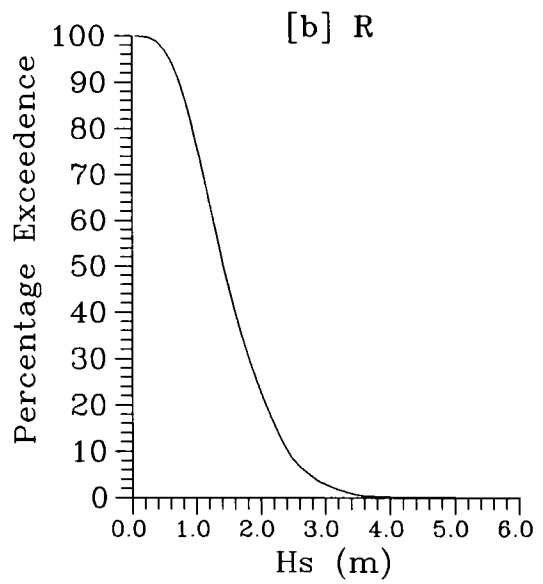
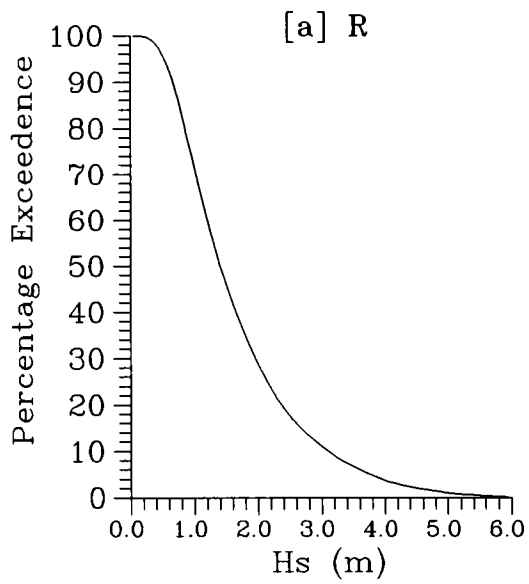


Fig.34A Cumulative distribution of Hs. [a] Arabian Sea, [b] Bay of Bengal, R - Rough weather, F - Fair weather

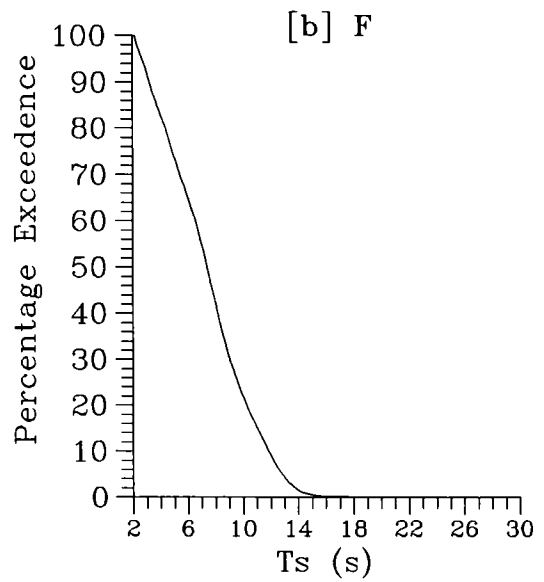
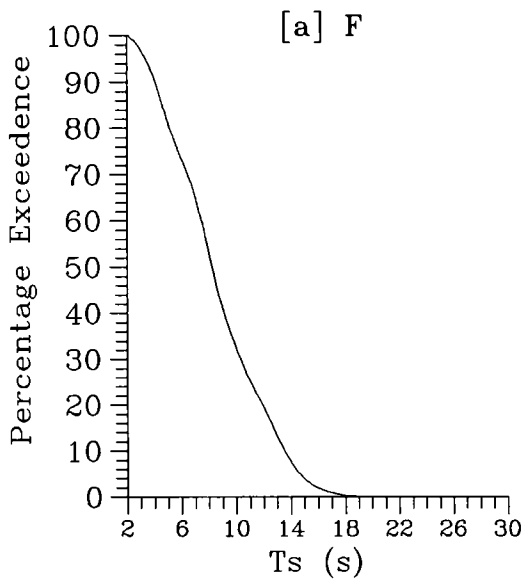
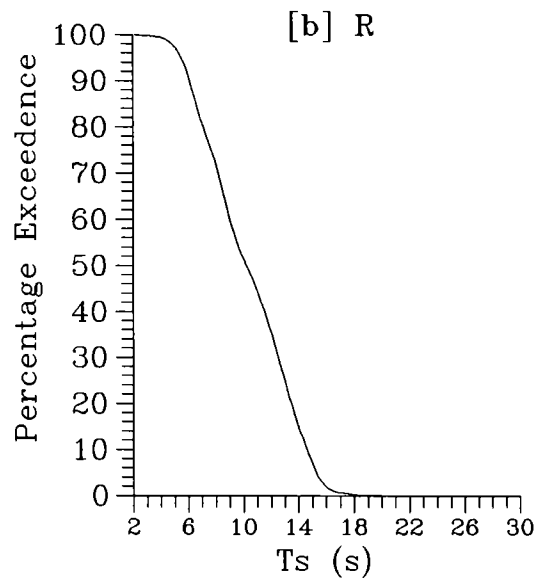
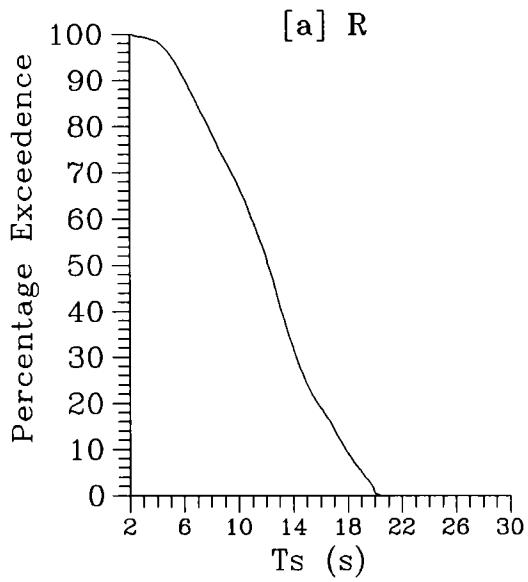


Fig.34B Cumulative distribution of Ts. [a] Arabian Sea, [b] Bay of Bengal, R - Rough weather, F - Fair weather

rough weather. During this period H_s exceeds 3m for 10% of the time in the Arabian Sea and 4% of the time in the Bay of Bengal. H_s exceeds 1m for 40% and 30% of the time in the Arabian Sea and Bay of Bengal respectively during fair weather season. During this period H_s exceeds 2m for about 3% of the time in both the seas.

The cumulative distributions of T_s for the Arabian Sea and Bay of Bengal during the rough and fair weather seasons are shown in Fig.34B. During the rough weather season T_s exceeds 5s over 95% of the time in the Indian Seas. During fair weather it exceeds for 80% and 70% of the time in the Arabian Sea and Bay of Bengal respectively. T_s exceeds 9s for 65% and 50% of the time in the Arabian Sea and Bay of Bengal respectively during rough weather. It exceeds the same value only for 30% and 20% of the time respectively in the Arabian Sea and Bay of Bengal during fair weather. Only in the Arabian Sea during rough weather, T_s exceeds 15s for 20% of the time.

VI.4 SPECTRAL CHARACTERISTICS

The average wave spectra for a selected site (67.5 E, 12.5 N) during the rough and fair weather seasons are shown in Fig.35A & B. During the rough weather period the spectra are single peaked with minimum directional spread. The average spectrum shown in Fig.35A belongs to the central Arabian Sea. The peak frequency and direction are 0.1 Hz and 270° respectively. Wave directions vary from around 210° to 360° . On the other hand, the spectra during the fair weather season (Fig.35B) show multiple peaks and the energy spreads over various directions. The peak frequency and direction are 0.14 Hz and 330° respectively. The total wave energy during rough weather is about four times higher than that during fair weather season for the above mentioned location. This gives an indication that the simulated spectral characteristics can be studied further in detail and compared with available data gathered during field measurements in deep waters.

VI.5 A COMPARATIVE STUDY OF WAVE CLIMATE

The prevailing wind and wave conditions in the Arabian Sea and Bay of Bengal show significant differences. Most of them were already brought out earlier in this chapter. A few other important features are brought out in the following sections.

67.5 E, 12.5 N

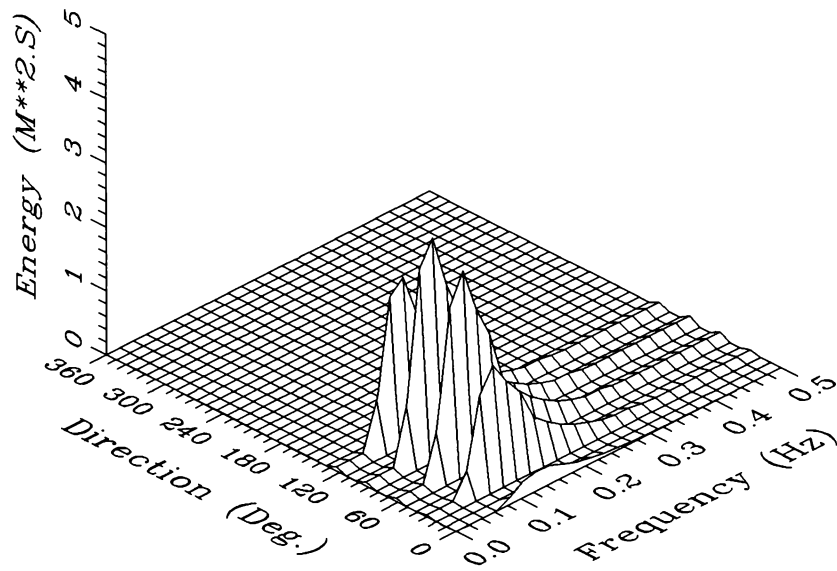


Fig.35A Average wave spectrum for a selected site in the Arabian Sea during rough weather season.

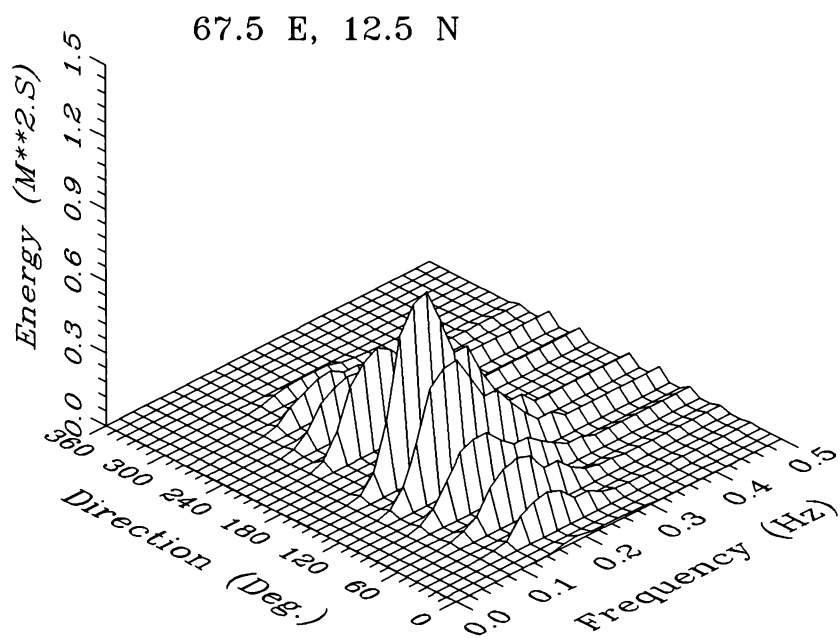


Fig.35B Average wave spectrum for a selected site in the Arabian Sea during fair weather season.

VI.5.1 Arabian Sea and Bay of Bengal

The assumed area for the Bay of Bengal is about 60% of the Arabian Sea. The annual mean wind field over the Arabian Sea is stronger than that over the Bay of Bengal. Therefore the annual mean wave field also show higher Hs and Ts values in the Arabian Sea. However, the average Hs over the Arabian Sea and Bay of Bengal during the fair weather period remains nearly the same but the Ts is higher in the Arabian Sea. During rough weather season the wave activity is higher (Hs and Ts) in the Arabian Sea compared with the Bay of Bengal. Higher waves are generally noticed towards the western Arabian Sea and the western Bay of Bengal during November to March. During October the southern Arabian Sea and the Bay of Bengal remain rough while the northern parts become rough during April. The general wave direction (mean windsea and swell) is northeast during November to February and southwest during May to September. However during May-September waves move towards east from the central Arabian Sea towards the west coast of India. Significant changes in wave direction are observed from February to March and April to May. Similar changes are also observed during the transition months of October-November.

VI.5.2 East and West coasts of India

There are remarkable differences between deep water wave conditions along the east and west coast of India which is mainly governed by the prevailing wind conditions and the advection of swell from other areas of wave generation. During the rough weather season Hs and Ts gradually increase from south to north along the west coast (Fig.30). There is marginal increase in Hs and Ts from south to north along the east coast. By and large wave activity is relatively high along the west coast compared to east coast. However, the reverse is the case during fair weather season as may be seen from the monthly and seasonal distributions. Hs and Ts increase from north to south along the east coast of India except during the month of April. However, they remains more or less constant along the west coast. Wave directions along the east and west coast of India also show remarkable differences. During the rough weather season waves off the east coast are from south to southwesterly direction. On the other hand, the waves approach the west coast from directions which vary from southwest to north of northwest. The general wave direction along the west coast of India is around northwest during fair weather season. Along the east coast, the wave

direction is around northeast during November-January. Wave directions vary along the coast for the rest of the period during fair weather season (October-April).

VI.6 LIMITATIONS OF SIMULATED WAVE CLIMATE

It was mentioned in Chapter-V that, sufficient wind measurements are not available in the Indian Seas for carrying out long-term wave hindcasts for establishment of wave climate. The present simulation experiment cannot replace the hindcast wave climate although care has been taken to predict wave variability in terms of mean monthly fields of significant wave parameters. Ideally, wave climate based on long-term wave measurements using standard equipment is superior to all other methods of wave climate estimation. It may be possible to utilize measured data for this purpose at some specific sites of interest but not over very large areas such as the Arabian Sea and Bay of Bengal. A most promising method is the satellite remote sensing, which provides large coverage of the ocean surface. For example, Young and Holland (1996) have published "the atlas of the oceans: Wind and wave climate" based on GEOSAT altimeter data ($4^{\circ} \times 4^{\circ}$ resolution) covering about 3 and a half years. However, the average data density for each grid (4x4 degrees) in this atlas varies from about 17 to a maximum of 32 per month. If such data are gathered over several years, long-term wave climate for the regions of interest can be established over a finer grid resolution. As for as the Indian Seas are concerned, it is clear that wave climate based on a simulated database is the only solution as there are limitations for the available visually observed wave database.

The basic wind data utilized for the establishment of a mean climatic year of winds are reported by ships of opportunity. Ship reported data are mostly restricted to shipping routes. Hence data density is low for the rest of the areas. Also ships have the tendency to avoid rough weather. Therefore ship-reported wind data do not include such observations which are considerably higher compared to those under normal wind conditions although they occur less frequently. The basic wind data supplied by IMD for a ten-year period was utilized for the estimation of probability density for a given u and v component of wind. The same was utilized along with the sixty-year mean monthly wind fields of Hastenrath and Lamb (1979) for deriving a "mean climatic year of wind". Confidence limits for the estimated mean climatic year of winds would have improved if the basic wind data were available for the full sixty-year period. Finally the simulated

wave database could not be validated thoroughly as long-term wave measurements are not available in the deep waters at least for a few selected locations around the Indian Seas.

VI.7 FUTURE OUTLOOK

The present study discussed only about the most commonly used wave parameters such as significant wave height, significant wave period, windsea direction, swell wave height, swell wave period and direction. However, there are six other gridded outputs of the wave model (Chapter-II). These outputs, namely the mean wave frequency, mean wave direction, friction wind speed, friction wind direction, sea-state dependent drag coefficient, and normalized wave stress can also be studied to meet several requirements. Detailed analysis of the spectral outputs (total sea and swell) is beyond the scope of the present study. Characteristics of the average wave spectrum for a selected site during fair as well as rough weather seasons were discussed as typical examples. Therefore, the spectral characteristics using the simulated database can be studied further along with available measurements around the Indian Seas.

The climatic database obtained from the present simulation experiment can be put to use for several practical applications. It is proposed to bring out a climatic atlas using this simulated database which can be a useful reference for all those who are concerned with coastal and offshore activities. Further, the mean monthly wave power potential along the east and west coast of India can be estimated based on the mean monthly fields of significant wave parameters incorporating the shallow water effects into account. Moreover, specific requirements for the establishment of wave climate for selected areas can be met making use of the simulated database. Finally, it may be seen from Appendix-D (PREPROC.DAT) that the spectral information were generated at the boundaries of a fine grid system bounded by 7° to 21° N and 71° to 78° E with an aim to simulate shallow water wave climate later. Similar fine grid simulation can be carried out for any area of interest if required.

Presently, long-term wave climates are established through model hindcasts using past wind fields as input to the model at selected time-steps. Model outputs for the hindcast period are finally analyzed for establishing the wave climate. Accuracy of the hindcast depends on the quality of wind input, performance of the model, and duration of the

hindcast. Such hindcast wave climates may be verified by conducting simulation experiments as in the present study. If the comparison is satisfactory, a large amount of computer time can be saved since it is easier to establish a mean climatic year of winds based on the long-term wind database and execute the wave model accordingly. Such a study can bring out the reliability and long-term representativity of the wave climate for regions where wind data are insufficient to conduct long-term wave hindcasts.